STUDIES ON IN-SITU DEPOSITION OF LEAD ZIRCONATE TITANATE (PZT) BY ELECTROLYTIC AND ELECTROPHORETIC METHODS

Thesis submitted to the

COCHIN UNIVERSITY OF SCIENCE AND TECHNOLOGY

in partial fulfilment of the requirements for the degree of

DOCTOR OF PHILOSOPHY

Under the Faculty of Technology

by

SHERIN JOSEPH

(Reg. No. 4276)

NAVAL PHYSICAL AND OCEANOGRAPHIC LABORATORY

Defence Research and Development Organisation

Kochi, Kerala, India, 682021

JANUARY 2018

CERTIFICATE

This is to certify that the thesis entitled, "**Studies on in-situ deposition of lead zirconate titanate (PZT) by electrolytic and electrophoretic methods"** is an authentic record of research work carried out by Smt. Sherin Joseph, under my supervision and guidance at Naval Physical & Oceanographic Laboratory, Kochi – 21, in partial fulfilment of the requirements for the award of Ph.D. degree of the Cochin University of Science and Technology in the Faculty of Technology and no part of it has previously formed the basis for the award of any degree in any university. All the relevant corrections and modifications suggested by the audience during the pre-synopsis seminar and recommended by the Doctoral Committee have been incorporated in the thesis.

Kochi-21
19 January, 2018

Dr. Reji John
(Research Guide)
Scientist 'G'
Naval Physical and Oceanographic Laboratory
Kochi- 21

DECLARATION

I hereby declare that the thesis entitled "**Studies on in-situ deposition of lead zirconate titanate (PZT) by electrolytic and electrophoretic methods"** is an authentic research work carried out by me and no part thereof has been presented for the award of any degree or diploma in any University or Institution.

Kochi – 21
19 January 2018

Sherin Joseph
Reg. No. 4276

ACKNOWLEDGEMENTS

I would like to express my heart felt gratitude to each and every one who had helped me with this research work. First and foremost I thank God Almighty for the successful completion of thesis.

I take this opportunity to sincerely thank my thesis supervisor and guide Dr. Reji John, Sc 'G', NPOL for his valuable guidance and unconditional support throughout the period of my research work.

I am greatly indebted towards Dr. A. V. Ramesh Kumar, Sc 'F', NPOL, for his help and consistent encouragement in my research work. Without his support, advice and suggestions successful completion of this thesis would not have been possible.

I would like to express my gratitude to Shri. S. Kedarnath Shenoy, Outstanding Scientist and Director, NPOL for providing requisite facilities and encouragement during the work. I would also like to thank Shri. S. Ananthanarayan, former Director, NPOL for his support and encouragement.

I sincerely thank all my Doctoral Committee Members, Dr. K. Sudarsan, former Chairman HRD Council, NPOL; Dr. R. Ramesh, Sc 'F', NPOL; Dr. Sunil. K. Narayanankutty, Professor, Department of PS & RT, CUSAT.

I am extremely grateful to Dr. T. Mukundan, Sc 'G, Group Head, Material Science & Materials Engineering (MS & ME), NPOL and Dr. V. Natarajan, Sc 'G', former Group Head MS & ME, NPOL for their encouragement for the successful completion of this research work.

My heartfelt thanks to Dr. Jayakumari, Sc 'F'; Dr. Rahna. K. Shamsudeen, Sc 'E'; Smt. Shiny Nair, Sc 'E'; Dr. Sandhya Songara, Sc 'D'; Dr. P. N. Vinod, Sc 'D'; Mr. K. A. Thomas, Sc 'D'; Smt. Kusumakumari, TO 'D' (Retd.); Smt. Rajeswari. R, TO 'A'; Shri. Jayesh. P, TO 'A'; Shri. Arun Sundar, TO 'A' all from NPOL for their consistent help and suggestions. I also extend my gratitude towards each and every one of MS & ME Group of NPOL who have directly or indirectly helped me in my research work.

I am thankful to Smt. Resmi, Sc 'C'; Shri. Linthish. P, Sc 'C'; Shri. Rajesh, TO 'A'; Shri. Manoj. N. Unni, TO 'A' all of NPOL for their kind help for carrying out the underwater studies required for the thesis. I also acknowledge the help given by Mr.

Varadarajan, Sc ‘E’, RIC Chennai and Mr. Martando Rath, Research Scholar, IIT Madras for their assistance in conducting the piezoelectric characterization.

Special thanks to Ms. Anoopa Prasad. C, Mr. Kiran Booby, Mr. Vaisakh. R. Pillai, Mr. Rohith. K. R, Mr. Rithul Mohan, Smt. Bijitha for their help and support during my research period at NPOL.

Last but not the least, I thank my family members for their immense support and constant encouragement. I take this opportunity to express heartfelt thanks to my husband Mr. Mithun Thomas, my sons Master David and Master Daniel for being my strength and support which had contributed in a great way, in making this thesis a reality. I am indebted to my mother-in-law Smt. Valsa Irene, my father-in-law Mr. N. M. Thomas for their support and help. I am extremely fortunate to have the most loving parents and express my gratitude to my mother Smt. E. A. Mary, who has been my inspiration and my father Mr. T. A. Josey. I also greatly acknowledge my sister, my brothers-in-law and my sister-in-law for their help and support.

SHERIN JOSEPH

ABSTRACT

Piezoelectric materials are mainly used for underwater electroacoustic transduction where electrical energy is converted into acoustic energy or vice versa. Lead based piezoelectric ceramics such as lead zirconate titanate (PZT) have emerged as one of the most significant piezoelectric materials due to its very strong and stable piezoelectric effects. Therefore, PZT has been used in underwater transducers and other applications such as sensors (microphones), actuators (loudspeakers), frequency standards (quartz clocks), piezoelectric motors (cameras), ultrasonic transducers for medical purposes, high voltage sources etc.

PZT is the most preferred and commonly used piezoceramic for most of the piezoelectric applications and other flexible piezoelectric materials like polyvinylidene fluoride (PVDF) and other piezoceramic-polymer composites do not match up to the properties of PZT. But PZT has certain limitations. Due to the hard and brittle nature of PZT, it has restricted use in large area conformal array applications where material flexibility is one of the main criteria. Moreover, the current trend of miniaturisation of various sensor systems has resulted in an increased interest among researchers for developing thin/thick films of PZT which can offer many advantages over bulk PZT. A great deal of studies have reported PZT film fabrication using other techniques such as sputtering, pulsed laser deposition (PLD), sol gel method, chemical vapour deposition (CVD), etc. However, the electrodeposition techniques are not much utilised. Electrodeposition is a simple, fast and cost effective process which can provide films or deposits with effective control on the structural and morphological characteristics.

The present work highlights the development of PZT films on flexible metallic foil substrates using electrodeposition methods such as electrolytic deposition (ELD) and electrophoretic deposition (EPD). Development of PZT films by ELD and EPD for piezoelectric applications are considered a grey area and not much research has been done in this area. A few publications can be found on the synthesis of ceramic films by electrodeposition, however optimisation of process parameters, detailed material characterisation, dielectric and piezoelectric studies of electrodeposited PZT films have not been reported. In this work, the process optimisation and material characterisation were also carried out in detail. In addition dielectric properties, ferroelectric characteristics of the PZT films were studied.

Electrolytic deposition (ELD) was extensively used to deposit PZT films on two different substrates viz. (1) titanium foil and (2) stainless steel (SS) foil. The medium for deposition also varied viz. (i) aqueous and (ii) non-aqueous, to evaluate the influence of electrolyte on the deposition. PZT films were deposited in aqueous medium containing salts of Pb, Zr, Ti in the presence of hydrogen peroxide. In non-aqueous deposition, DMSO based electrolyte containing the salts of Pb, Zr and Ti were used for PZT deposition. Electrodeposition of PZT was carried out using regulated power supply. The effect of various parameters such as (i) electrolyte medium, (ii) current density, (iii) time of deposition, (iv) sintering temperature and (v) heating time were studied. For aqueous PZT films, the current density and time of deposition were optimized as 15 mA/cm^2 and 5 minutes respectively with a faradaic efficiency of 17 %. However, for non-aqueous films, it was found that a current density of 25 mA/cm^2 for a deposition time of 5 minutes gave a good film. The faradaic efficiency of non-aqueous PZT electrodeposition was found to be 22 %. Sintering temperature and time were optimized as 500 °C and 1 hour respectively for the PZT films prepared by aqueous and non-aqueous methods. PZT films of thickness 100 – 140 µm were obtained for aqueous and non-aqueous ELD method. The morphology and topography examination of the films were carried out using Scanning Electron Microscopy (SEM), Transmission Electron Microscopy (TEM) and Atomic Force Microscopy (AFM). It was observed that PZT films prepared by non-aqueous ELD had more or less uniform morphology, continuous and crack free microstructure with a surface roughness of 2 nm. Adhesion to the substrate was also found to be more for non-aqueous films. The perovskite phase formation of the PZT films were confirmed using XRD (X-ray diffraction) and Raman spectroscopy. In this work, the dielectric and piezoelectric characterisation of PZT films prepared by ELD are reported, for the first time. Dielectric constant and dielectric loss (tan δ) for the ELD PZT films were obtained as 452.9 and 0.0469 respectively. Ferroelectric hysteresis measurements were also carried out for the PZT films.

Electrophoretic deposition (EPD) using an acetic acid based suspension was employed in this work for the deposition of PZT films. The deposition was carried out on two different substrates viz. (i) titanium foil and (ii) SS foil. The deposition was carried out on the above mentioned substrates immersed in a PZT suspension in acetic acid using a regulated power supply. A detailed study of EPD reaction mechanism, suspension stability, the effect of process parameters viz. (i) voltage, (ii) time of

deposition, (iii) PZT concentration, (iv) film thickness on the properties of the prepared PZT films were carried out. It was found that acetic acid based suspension containing 3 wt. % PZT for a voltage range 200 – 300 V/cm and time of deposition ≥1 minute gave superior quality PZT films by EPD technique. PZT films of thickness ranging from 15 – 160 µm were deposited using EPD technique, having bulk density up to 67 %. Moreover, this work aimed to carry out low temperature sintering (≤ 600 °C) of EPD PZT films. The morphology and topography examination of the films were analysed by SEM, TEM and AFM. It was found that, uniform and continuous PZT films having surface roughness value of 25 nm were obtained by EPD technique. Perovskite PZT phase formation was studied using XRD and Raman spectroscopy and also the dielectric constant, dielectric loss, piezoelectric hysteresis and leakage current characteristics of the films were evaluated. Dielectric constant and tan δ values at 1 kHz was obtained as 189 and 0.0686 respectively. Hysteresis plots gave a saturation polarisation of 5.1 µC/cm^2 and the leakage current density was measured as ± 2.85x10^{-7} A/cm^2.

The use of the PZT film developed is for underwater acoustic sensing applications. In this regard, acoustic sensor was fabricated using PZT film deposited by EPD technique. The sensor assembly included poled and electroded PZT film as the base material. In order to make the sensor water worthy, it was encapsulated with acoustically transparent epoxy resin. Underwater acoustic evaluation of the fabricated sensor was conducted. The evaluation consisted of measurement of underwater receiving sensitivity and directivity pattern. The underwater acoustic receiving sensitivity obtained was – 194 to – 193 (dB re 1V/µPa) in the frequency range 20 – 35 kHz. The directivity pattern showed increased sensitivity in all directions with maximum values obtained at angles of 90° and 270°. The fabricated sensor could be used for high frequency underwater sensing applications. Sensor fabrication using EPD PZT film and its underwater characterization were reported for the first time to the best of our knowledge.

Two international and one national journal papers have been published based on this work.

STUDIES ON IN-SITU DEPOSITION OF LEAD ZIRCONATE TITANATE (PZT) BY ELECTROLYTIC AND ELECTROPHORETIC METHODS

TABLE OF CONTENTS

LIST OF FIGURES

LIST OF TABLES

Chapter – 1

INTRODUCTION

1.1 PIEZOELECTRIC MATERIALS FOR UNDERWATER SENSOR APPLICATIONS

The most widely used underwater detection technique is based on the transmission of sound energy of various frequencies, receiving the echo and processing it to get the desired information about the targets of interest. Acoustic energy commonly used for the underwater detection is due to its ease of transmission in water without much attenuation. Piezoelectric materials are mainly used for electroacoustic transduction [1] where electrical energy is converted into acoustic energy or vice versa. The initial forms of transducers were based on piezoelectric crystals mainly quartz, Rochelle salt, tourmaline etc. but they have certain limitations such as high processing cost, size restrictions and low piezoelectric properties and so they were then replaced by magnetostrictive materials in the 1940s and 1950s. Magnetostrictive transducers were robust and depended on the interaction between mechanical stress and magnetic field in some metallic materials. Piezoelectric ceramics such as barium titanate were introduced due to their effective piezoelectric properties and ease of manufacture in a variety of shapes and sizes. Also, the first piezoceramic based transducer using barium titanate was developed in 1947. Until 1957 barium titanate was the most prominent piezoelectric ceramic used for majority of applications. However, lead zirconate titanate (PZT) progressively replaced barium titanate, owing to its very strong and stable piezoelectric effects and has now emerged as the most commonly used material for underwater transducers as well as for various other applications. When a transducer is used as a receiver it is known as a hydrophone. A hydrophone converts acoustic pressure variations to electrical output signals. A transducer can also be used as an acoustic source to generate sound, which converts electrical energy into acoustic energy and is referred to as a projector. An underwater sonar system consists of hydrophones, projectors and associated electronics such as amplifiers and data acquisition systems.

In this thesis, attempts are made to develop PZT using electrochemical methods. Although much studies are carried out in wet and other dry physical methods of PZT synthesis, detailed studies were not carried out using electrochemical techniques.

1.2 EVOLUTION OF PIEZOELECTRICITY

"Piezo" is a Greek term meaning "to press", and hence the term "piezoelectricity" which stands for electricity generated from pressure. Piezoelectric effect [2-10] was discovered in1880 by Jacques and Pierre Curie, who found that certain crystals when subjected to mechanical strain, become electrically polarised and the degree of polarization is proportional to the applied strain. This is called the direct piezoelectric effect. Conversely, when the materials are exposed to an electric field, they undergo deformation and this phenomenon is called inverse piezoelectric effect. In 1890, Voigt established the relation between piezoelectricity and crystal symmetry. Some of the earliest reported piezoelectric materials include Rochelle salt, quartz, zincblende, tourmaline, sodium chlorate, boracite, calamine, topaz, tartaric acid and cane sugar. Piezoelectricity remained a scientific curiosity for about 30 years after the discovery until World War I, when Paul Langevin and his team tried to develop an ultrasonic submarine detector using quartz crystal plates. This was one of the first forms of sonar transducers using the "echo method" which was used to detect immersed objects and exploring ocean bottom by sending a high frequency signal into water and measuring its time of return. The exigency situation during the world war had led to extensive research in this area resulting in different practical applications of piezoelectric crystals such as piezoelectric resonators, oscillators, ultrasonic transducers, microphones, telephone receivers, phonograph pickups, record cutters etc. A major milestone in the field of piezoelectricity took place with the discovery of ferroelectricity in single crystal Rochelle salt by Joseph Valasek in 1921 [11]. Ferroelectric materials are characterised by a spontaneous electric polarisation or dipole moment whose direction can be reversed by the application of an external electric field. Until 1940, only Rochelle salt and potassium dihydrogen phosphates were known as the prominent ferroelectric materials.

A new era in the history of ferroelectric materials began with the birth of ferroelectric ceramics in the 1940s during the World War II. The discovery of ferroelectric ceramics resulted from the mounting demand for a high dielectric constant material for ferroelectric capacitor applications. Barium titanate (dielectric constant > 1200) was the first ferroelectric ceramic developed and commercially used in

ferroelectric capacitors and also in piezoelectric transducer applications. Piezoceramics such as lead zirconate titanate (PZT) solid solutions came into picture in 1952 and have since emerged as the most significant piezoelectric material with the highest performance for practical applications. The synthesis of relaxor ferroelectrics such as lead magnesium niobate (PMN) ceramics were reported in 1961. Another class of piezoelectric materials are piezoelectric polymers which offer advantages such as flexibility, toughness, light weight properties etc., and have their own established area of technical device applications. Piezoelectric effect in polymers such as polyvinylidene chloride (PVDF) was first observed by Kawai in 1969 [12]. PZT substituted with lanthanum generally known as PLZT ceramics gained interest in the late 1960s due to its optical transparency and various electro optic properties. Other research activities includes the development of ferroelectric ceramic – polymer composites in 1970s, electrostrictive relaxor PMN devices in the 1980s and the synthesis of relaxor single crystals for ferroelectric transducer applications by Park and Shrout in 1997 [13]. Lead oxide based ferroelectric ceramics PZT, being its most prominent member are the most widely used materials for electronic devices, such as actuators, sensors and transducers, because of their excellent piezoelectric properties. Recently, lead-free piezoelectric materials have also been attracting attention worldwide as new materials to replace PZT based piezoelectric ceramics, due to the environmental issues and health hazards posed by the toxicity of lead. However PZT is the most sought after piezoelectric material till date and no other material is able to take its place in the present scenario of diverse piezoelectric applications.

1.3 PIEZOELECTRICITY AND CRYSTAL SYMMETRY

Following the discovery of piezoelectricity much more work have been done to define the crystallographic principles [7] of the effect as it was understood from the beginning that crystal symmetry plays a decisive role in the piezoelectric phenomena.

A body or any one of its physical properties may be symmetrical with respect to a point, a line, a plane or any combination of these. If symmetrical with respect to a point, the body is centrosymmetric and can possess no piezoelectric properties; hence no piezoelectric crystals are found in any of the 11 centrosymmetric classes out of the 32 crystal point groups. In the remaining 21, with one exception, all are devoid of a centre of symmetry and are piezoelectric. The exception is group 29 (cubic class 432), which although lacking a centre of symmetry, however has other symmetry elements that

combine to exclude the piezoelectric property. Statistically, out of all the total materials known only 30% are non-centrosymmetric, and within those, significant piezoelectric properties are reported only in very few compounds for practical applications. Therefore, it can be understood that the absence of centre of symmetry is one of the necessary but not the only criteria for piezoelectricity in a material.

Among the 20 piezoelectric crystal classes, there are ten pyroelectric point groups that possess a unique polar axis. Pyroelectric crystals contain a built-in polarization, which manifests itself in temperature-induced changes of the total dipole moment of the unit cell (in the absence of applied fields). If such spontaneous polarization can be reversed by an external sufficiently high electric field, the crystal is called ferroelectric. So by default, all ferroelectric materials are simultaneously pyroelectric and piezoelectric. Similarly, all pyroelectric materials are by default piezoelectric but not all of them are ferroelectric. The schematic classification of piezoelectric, pyroelectric and ferroelectric materials are shown in Fig 1.1

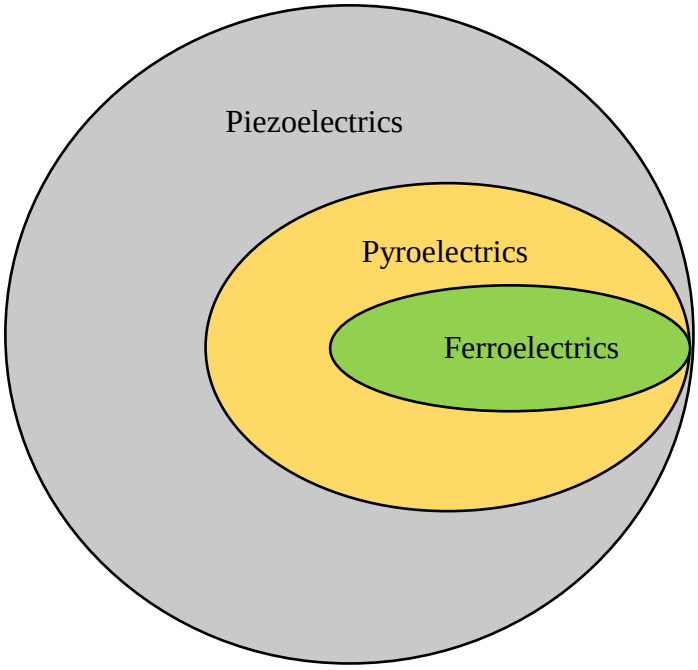

Fig 1.1 Venn diagram classification of piezo-, pyro- and ferroelectrics

As a piezoelectric material approaches a certain temperature T_C (often termed the Curie point) [14] the piezoelectric activity maximises and the piezoelectric coefficients show a drastic increase. However, in the case of a piezoelectric material subjected to higher temperatures above T_C, the spontaneous polarization vanishes, and the ferroelectric crystal transforms into the paraelectric state. Many ferroelectrics lose their

piezoelectric properties above T_C completely, because their paraelectric phase has centrosymmetric crystallographic structure.

The dipoles in a ferroelectric material are not randomly oriented throughout the material. Neighbouring dipoles align with each other to form regions of local alignment known as Weiss domains. Within a Weiss domain, therefore, all the dipoles are aligned giving a net dipole moment to the domain and hence a net polarization (dipole moment per unit volume). In the case of single-domain ferroelectric crystals, the spontaneous polarization is constant everywhere. Another technologically important class of materials is represented by piezoelectric ceramics, which consist of randomly oriented crystallites (grains), separated by grain boundaries. Ceramics are much less expensive in processing than single crystals and frequently offer comparable piezoelectric and electrostrictive properties. It should be emphasized that, in non-ferroelectric ceramics, the piezoelectric responses of individual crystallites are cancelled out after averaging over the entire sample. Hence, on the macroscopic level, the polycrystal has a centre of symmetry and negligible piezoelectric properties.

Ferroelectric materials are found to exhibit spontaneous polarisation below the Curie point. They are characterised by the presence of polarisation along a unique crystallographic direction leading to a dipole moment in that particular direction. Depending on the crystal system there may be few or many possible axes and the dipole moments of the unit cells in one region may lie along any one of the six directions. Each of these regions are known as domains. A domain is a homogenous region of a ferroelectric, where all the dipoles have the same orientation. However, in a ferroelectric material or crystal, there are many domains having different orientations, with a result that there is no net polarisation.

A major milestone in the history of ferroelectrics is the discovery of the poling process. It is the application of a high voltage sufficient to reverse electric moments of spontaneously polarized regions of the ferroelectric into a particular direction (same as that of the applied field). The poling process is clearly shown in Fig1.2.

The domains in a ceramic material are aligned by exposing it to a strong, DC electric field, usually at a temperature slightly below the Curie temperature and this is referred to as poling. After the poling treatment, domains most nearly aligned with the electric field expand at the expense of domains that are not aligned with the field, and

the material expands in the direction of the field. When the electric field is removed most of the dipoles are locked into a configuration of near alignment. The element now has a permanent polarization and a remnant polarization. The first reported poled piezoceramic was barium titanate.

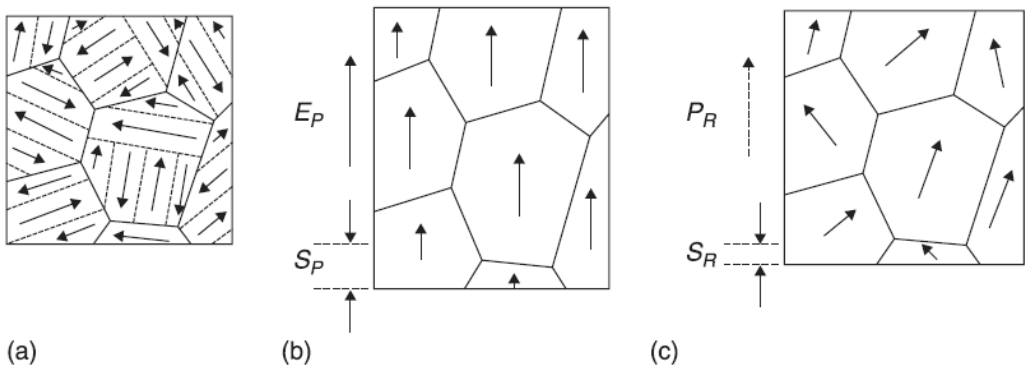

Fig 1.2 Different stages during poling of a piezoelectric ceramic [15]: (a) in its natural condition, (b) during poling (poling field E_P, poling strain S_P) and (c) after poling (remnant polarisation P_R, remnant strain S_R)

1.4 PIEZOELECTRIC EFFECT AND CONSTITUTIVE EQUATIONS

The constitutive equations [15] describing the piezoelectric property are based on the assumption that the total strain in the transducer is the sum of mechanical strain induced by the mechanical stress and the controllable actuation strain caused by the applied electric voltage. The axes are identified by numerals rather than letters. In Figure 1.3, 1 refers to the x axis, 2 corresponds to the y axis, and 3 corresponds to the z axis. Axis 3 is assigned to the direction of the initial polarization of the piezoceramic, and axes 1 and 2 lie in the plane perpendicular to axis 3.

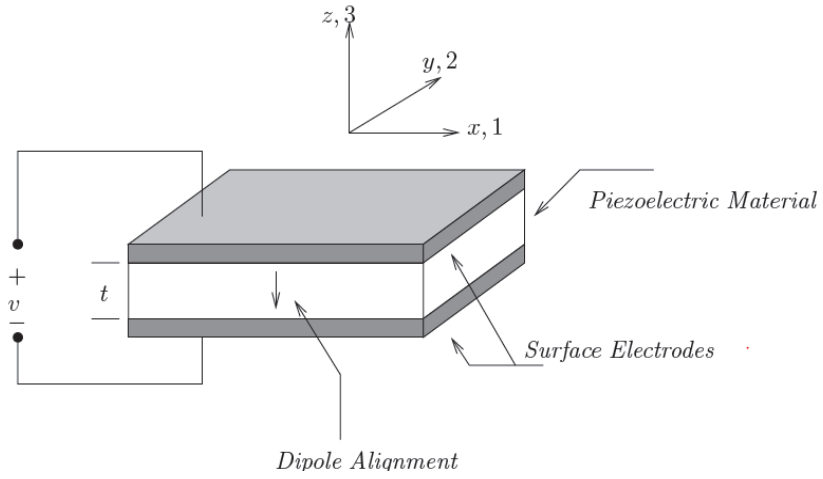

Fig1.3 Schematic diagram of a piezoelectric transducer

When a poled piezoelectric ceramic is mechanically strained it becomes electrically polarized, producing an electric charge on the surface of the material. This property is referred to as the "direct piezoelectric effect" and is the basic working principle of sensors. Piezoelectric sensors, like acceleration sensors and pressure sensors, also exploit the direct piezoelectric effect. The direct piezoelectric effect can be expressed by equation (1.1)

$$e_i = S^E_{ij}\sigma_j + d_{mi}E_m \quad \text{or} \quad e_i = S^D_{ij}\,\sigma_j + g_{mi}D_m \tag{1.1}$$

In the inverse piezoelectric effect the same materials become strained when an electric field is applied, the strain again being proportional to the applied field. Piezoelectric actuators which can be used for micro-positioning, and acoustic projectors rely on the inverse piezoelectric effect and it can be shown as in equation (1.2)

$$D_m = d_{mi}\sigma_i + \xi^\sigma_{ik}E_k, \quad \text{or} \quad E_i = g_{mi}\sigma_i + \beta^\sigma_{ik}D_k \tag{1.2}$$

Where

σ . . . stress vector (N/m^2)

e . . . strain vector (m/m)

E. . . vector of applied electric field (V/m)

ξ . . . permittivity (F/m)

d . . . matrix of piezoelectric strain constants (m/V)

S . . . matrix of compliance coefficients (m^2/N)

D. . . vector of electric displacement (C/m^2)

g . . . matrix of piezoelectric constants (m^2/C)

β . . . impermittivity component (m/F)

1.5 PIEZOELECTRIC PROPERTIES

A piezoelectric material is usually characterised by its important properties [16, 17] like dielectric constant, compliance, piezoelectric coefficients, coupling factor etc.

(i) Permittivity (ε)

The (absolute) permittivity (or dielectric constant) is defined as the dielectric displacement per unit electric field [4]. The permittivity can be expressed by the equation (1.3).

$$\varepsilon = \begin{bmatrix} \varepsilon_{11} & 0 & 0 \\ 0 & \varepsilon_{22} & 0 \\ 0 & 0 & \varepsilon_{33} \end{bmatrix} \tag{1.3}$$

The first subscript gives the direction of the dielectric displacement, the second gives the direction of the electric field. For example, $\varepsilon^{\sigma}_{11}$ is the permittivity, for the dielectric displacement and electric field in direction 1 under constant stress, we can define the same under the condition of constant strain also.

(ii) Compliance (s)

The compliance (s) of a material is defined as the strain produced per unit stress. It is the reciprocal of the modulus of elasticity. The compliance can be expresses by the equation (1.4).

$$s = \begin{bmatrix} s_{11} & s_{12} & s_{13} & 0 & 0 & 0 \\ s_{12} & s_{22} & s_{23} & 0 & 0 & 0 \\ s_{13} & s_{23} & s_{33} & 0 & 0 & 0 \\ 0 & 0 & 0 & s_{44} & 0 & 0 \\ 0 & 0 & 0 & 0 & s_{55} & 0 \\ 0 & 0 & 0 & 0 & 0 & s_{66} \end{bmatrix} \tag{1.4}$$

The first subscript refers to the direction of strain, the second to the direction of stress. For example, S^{E}_{11}--is the compliance for a stress and accompanying strain in direction 1 under conditions of constant electric field. S^{D}_{36}--is the compliance for a shear stress about axis 3 and accompanying strain in direction 6 under conditions of constant electric displacement.

(iii) Piezoelectric charge constants (d)

The piezoelectric charge constant is defined as the electric polarization generated in a material per unit mechanical stress applied to it. Alternatively, it is the mechanical strain experienced by the material per unit electric field applied to it. The first subscript refers to the direction of polarization generated in the material (at E = 0) or to the applied field strength, the second refers respectively to the direction of the applied stress or to the direction of the induced strain. For example, d_{33} is the induced polarisation in direction 3 when the stress is applied in 3 directions. Piezoelectric charge constant can be expressed by the equation (1.5).

$$d = \begin{bmatrix} 0 & 0 & 0 & 0 & d_{15} & 0 \\ 0 & 0 & 0 & d_{24} & 0 & 0 \\ d_{31} & d_{32} & d_{33} & 0 & 0 & 0 \end{bmatrix} \quad (1.5)$$

(iv) Piezoelectric voltage constants (g)

The piezoelectric voltage constant is defined as the electric field generated in a material per unit mechanical stress applied to it. Alternatively, it is the mechanical strain experienced by the material per unit electric displacement applied to it. The first subscript refers to the direction of the electric field generated in the material or to the applied electric displacement; the second refers respectively to the direction of the applied stress or to the direction of the induced strain. A brief description of definitions for piezoelectric constants are given in the table 1.1. "d" and "g" are piezoelectric constants, related by the general expression, $d = \varepsilon_0 \varepsilon_r g$.

Table 1.1 Definitions for piezoelectric constants

Equations	Units
$d=(dD/dX)_E=(dD/dX)_X$	(C/N or m/V)
$e=(dD/dX)_E=-(dD/dX)_S$	(C/m or N/Vm)
$g=(dD/dX)_D=(dD/dX)_X$	(Vm/N or m^2/V)

(v) Electromechanical coupling factor (k).

The electromechanical coupling factor, which measures the ability of a material to interconvert electrical and mechanical energy, is expressed by the equation (1.6).

$$k^2 = \frac{Converted\ Electrical\ Energy}{Input\ Mechanical\ Energy}$$

Or (1.6)

$$k^2 = \frac{Converted\ Mechanical\ Energy}{Input\ Electrical\ Energy}$$

The coupling factor k is a measure of the extent of the piezoelectric effect (not an efficiency factor). It describes the ability of a piezoelectric material to convert electrical energy into mechanical energy and vice versa. At resonance, k is a function of the corresponding form of oscillation of the piezoelectric body.

Examples:

k_{33} --Coupling factor for longitudinal oscillation

k_{31} --Coupling factor for transverse oscillation

k_P --Coupling factor for radial oscillation (planar) of a round disk

k_t --Coupling factor for the thickness oscillation of a plate

k_{15} --Coupling factor for the thickness shear oscillation of a plate

(vi) Mechanical Quality Factor (Q_m)

The mechanical quality factor Q_m characterizes the "sharpness of resonance" of a piezoelectric body or resonator and is primarily determined from the 3 dB bandwidth of the series resonance of the system which is able to oscillate. The reciprocal value of the mechanical quality factor is the mechanical loss factor, the ratio of effective resistance to reactance in the equivalent circuit diagram of a piezoelectric resonator at resonance.

(vii) Piezoelectric hysteresis

Since ferroelectric materials show a hysteresis loop and remnant polarization ± P_r at zero field, these two polarization states can be used as '0' and '1' states of binary data storage in memory devices. The Fig 1.4 indicates hysteresis loop of a poled piezoelectric ceramic material showing remnant polarisation (Pr) and coercive field (Ec). The definitions of various terms are as follows:

Saturation polarisation- Maximum level of polarisation can be achieved in a material by the application of electric field. Further application of electric field doesn't cause any effect in polarisation of material, i.e. dipoles are aligned in best possible order.

Remnant polarisation- Electric charge stored per unit area in the material when magnitude of applied field is zero

Coercive field- Value of reverse electric field that must be applied to the material for bringing it to zero polarisation

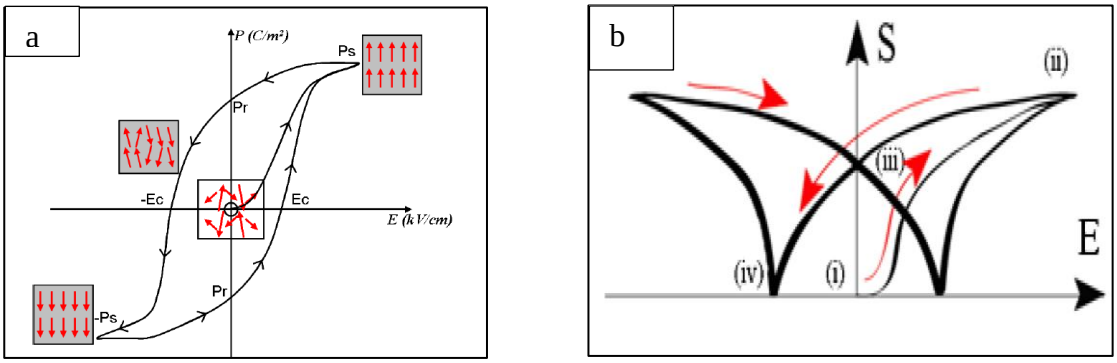

Fig 1.4 (a) Hysteresis loop of a poled piezoelectric ceramic material, (b) Butterfly loop observed in converse piezoelectric measurements [8].

The advantages of using piezoelectrics are that the data will be stored when power is lost during operation leading to non-volatile data storage. Other advantages are that ferroelectric switching is a very fast phenomenon and hence memories can operate very fast. Many of these materials tend to be radiation resistant and hence can be used in space applications. The voltage-dependent displacement curves of piezo actuators have a strongly nonlinear course that is subject to hysteresis due to the extrinsic domain contributions. It is therefore not possible to interpolate linearly from the nominal displacement to intermediate positions with a particular driving voltage. The electromechanical and dielectric large-signal curves of piezoceramics illustrate the characteristics. The origin of each graph is defined by the respective thermally depolarized condition. The shape of both bipolar large-signal curves is determined by the ferroelectric polarity reversal process when the coercive field strength E_C is achieved in the opposing field. The dielectric curve shows very large polarization changes at these reversal points. At the same time, the contraction of the ceramic after reversing the polarity turns into expansion again, since the polarization and the field strength have the same orientation once more. This property gives the electromechanical curve its characteristic butterfly shape.

1.6 COMPARISON OF DIFFERENT PIEZOELECTRIC MATERIALS

Generally piezoelectric materials can be divided into four groups: (1) naturally occurring piezo crystals, (2) piezo ceramics, (3) piezo polymers [18] and (4) piezoelectric-polymer composites.

1.6.1 Piezoelectric crystals

Piezocrystals [15] were the first piezoelectric materials but they were largely superseded by piezoelectric ceramics. However, lithium niobate ($LiNbO_3$), and aluminium nitride (AlN) are two piezocrystals with properties that make them attractive for specific applications. In crystallographic terms, $LiNbO_3$ has lower symmetry than PZT but higher symmetry than PVDF. Lower losses and high longitudinal propagation speed makes it particularly appropriate for high-frequency applications, the propagation speed leading to a relatively large thickness for a given operating frequency. $LiNbO_3$ has also been selected for applications with elevated temperatures because of its very high Curie temperature, $T_c \approx 1200$ °C. AlN has the same crystallographic symmetry as PZT and somewhat similar behavioural characteristics to $LiNbO_3$. However, it is distinguished by its realisation as a highly inert, crystalline thin film. This has led to its

use in surface acoustic wave devices and in the exploration for applications where it can be integrated with test objects for NDE or with circuitry for minimally invasive sensing. A much newer family of single-crystal piezoelectric materials is represented by lead magnesium niobate doped with lead titanate, $_{(x)}Pb(Mg_{1/3}Nb_{2/3})O_3 - _{(1-x)}PbTiO_3$ (PMN-PT). It is similar to PZT in many behavioural characteristics, its particularly attractive properties are its very high bar-mode coupling coefficient, $k_{33} \approx 0.9$, and piezoelectric strain coefficient,$d_{33} \approx 1400$ pm.V^{-1}, combined with a relatively high value for the piezoelectric voltage coefficient, $g_{33} \approx 30$ mV.m.N^{-1}. Its significant application is in biomedical imaging. Being a relaxor material, PMN-PT has lower Curie temperature ($T_c \approx 120$ °C) and an even lower temperature phase transition zone. With relatively high mechanical losses, this significantly limits its potential applications where elevated temperatures or high average output ultrasound intensities are required. To overcome this problem, research is under way to extend the binary PMN-PT material system to ternary systems and doped ternary systems.

1.6.2 Piezoelectric polymers

Polyvinylidene fluoride (PVDF) [14, 19] is the most widely reported piezoelectric polymer. Crystallographically, it has very less symmetry and poling is achieved by uniaxial or biaxial stretching rather than the application of an electric field. The properties that make it attractive are its low acoustic impedance, Z = 3.9 MRayl, its low Q_m, its high piezoelectric voltage constant, $g_{33} = 0.23$ V.m.N^{-1} and high flexibility. It finds use as a broadband receiver for underwater sonar and also in biomedical imaging applications, where the ultrasonic medium has an acoustic impedance, Z ≈ 1.5 MRayl. Disadvantages of PVDF includes low d coefficient when compared to piezoceramics, variation of properties with manufacturing techniques and ageing, and lower working temperature range (below 80 °C). In order to pole PVDF, an extremely high electric field is necessary, which limits the thickness of the material. The properties of PVDF can be improved by forming copolymers with trifluoroethylene, tetrafluoroethylene, and hexafluoropropylene. The recent development of copolymers consisting of vinylidene fluoride (VDF) and trifluoroethylene (TrFE) has resulted in piezopolymers with properties superior to those of PVDF homopolymer. Reduced poling fields (0.7 MV/cm) can be used and also its hydrostatic charge constant, d_h is larger than that of PVDF. However, the most significant improvement was observed in the k_t (0.3) value of the copolymer. The PVDF-trifluoroethylene copolymer also have some drawbacks such as

large tan δ value, lower d_{33} and d_h coefficients and its 'k_t' value, when compared to materials like PZT.

1.6.3 Piezoelectric composite materials

Piezocomposites [20 – 24] typically comprise pieces of a piezoelectric ceramic or single-crystal phase bound together with a polymer matrix. They are usually defined by their dimensional connectivity. In general, an m-n connectivity composite has its piezoelectric phase connected in m dimensions and its polymer phase in n dimensions. Even though they do not match up to the piezoelectric properties of the like of PZT, many studies have focused on the development and characterization of piezoelectric ceramic-polymer composites. It was found that such composites have high hydrostatic coefficients and reduced stiffness and can be utilised to fabricate piezoelectric materials which are flexible and suitable for covering large areas and can be made use in large hydrophone arrays. Piezocomposite materials [3, 20, 25] increase the performance of ultrasonic transducers for applications in biomedical imaging, underwater sonar etc.

1.6.4 Piezoelectric ceramics

Piezoceramics are, presently, the most widely used piezoelectric materials. Barium titanate was the first piezoelectric ceramic to be developed commercially and widely used due to its properties like high coupling coefficient and ease of manufacture. At temperatures between 130 ℃ and 1460 ℃, barium titanate has a cubic perovskite structure. Below 130℃ (Curie temperature), the unit cell becomes elongated along one edge, thus becoming tetragonal, and this distortion from cubic symmetry gives rise to a spontaneous polarisation along the longer (c) axis making the material ferroelectric. The important differences in properties of barium titanate compared with PZT are its lower coupling coefficients, its higher Young's modulus and its lower density. Because of the difference in coupling coefficients, barium titanate ceramics have been largely replaced by PZT in most of the commercial applications, but they are still used in some underwater transducers. After the discovery of piezoceramics in the 1950s, lead-based materials emerged with the highest performance for practical applications with PZT leading from the front. The properties of various piezoelectric materials are summarised in Table 1.2.

Table1.2 Properties of selected piezoelectric materials [15]

Type of material			PZT-4	PZT-5H	$PbNbO_3$	PVDF	$LiNbO_3$	AlN	PMN-PT
			'Hard' ceramic	'Soft' ceramic	High-temperature ceramic	Polymer	Traditional single crystal	Crystalline thin film	New, high-performance single crystal
Thickness-mode coupling coefficient	k_t		0.47	0.52	0.33	0.19	0.16	0.24	0.57
Length-extensional coupling coefficient	k_{33}		0.69	0.75	0.33	0.13	0.16	0.31	0.90
Piezoelectric strain constant	d_{33}	$pm.V^{-1}$	290	590	85	25	5.9	5.5	1400
Piezoelectric voltage constant	g_{33}	$mV.m.N^{-1}$	26	20	32	230	22	52	30
Piezoelectric figure of merit	FOM = $d_{33}.g_{33}$	$pm.N^{-1}$	7.5	12	2.7	5.8	0.13	0.29	43
Stiffness	c_{33}^D	$GN.m^{-2}$	150	160	68	8.5	250	420	140
Density	ρ	$kg.m^{-3}$	7700	7500	6200	1800	4600	3300	8000
Longitudinal speed	v	ms^{-1}	4600	4600	3100	2200	7400	11400	4040
Acoustic impedance	$Z = \rho v$	MRayl	35	34	19	3.9	34	37	32
Electrical loss tangent	$\tan \delta$		0.004	0.02	0.01	0.3	0.001	0.0005	0.01
Mechanical quality factor	Q_m		High	Medium	Low	Low	Very high	Very high	Low
Relative permittivity at constant stress	ε_{33}^T		1270	3430	300	8.4	29.8	12.0	3950
Relative permittivity at constant strain	ε_{33}^S		640	1470	270	10–12	29	10.7	818
Curie temperature (*usable temperature, **phase transition temperature)	T_c	°C	Medium / High (~350 °C)	Medium (~200 °C)	High (~400 °C)	Low (~150 °C)	Very high (~1200 °C)	Very high (~1150 °C*)	Low (~90 °C**)
Usual physical form			Bulk ceramic	Bulk ceramic	Bulk ceramic	Thin film	Bulk crystal	Thin crystal film	Bulk crystal

1.7 LEAD ZIRCONATE TITANATE (PZT)

Lead zirconate titanate ($Pb[Zr_{0.52}Ti_{0.48}]O_3$) or PZT is one of the most significant and widely used piezoceramics. High stiffness of PZT material permits them to function as good actuators and high strain coefficients makes them suitable as good sensors. It is widely used in deformable mirrors, mechanical micro positioners, impact devices and ultrasonic motors, sonic and ultrasonic sensors, filters and resonators, signal processing devices, igniters and voltage transformers etc.

PZT is a polycrystalline ferroelectric material with a perovskite crystal structure i.e. a tetragonal/rhombohedral structure very close to cubic. Moreover, it is a solid solution formed by orthorhombic phase of $PbZrO_3$ (PZ) and tetragonal phase $PbTiO_3$ (PT) with a special narrow phase boundary region at a ratio of about 52:48. This boundary separates rhombohedral and tetragonal phases of PZT and multiple phases coexist within this region, so it is called Morphotropic Phase Boundary (MPB). The curie temperatures Tc for $PbTiO_3$ and $PbZrO_3$ are 490 ºC and 235 ºC respectively and T_C of PZT, the solid solution formed by the above two components lie between these temperatures. For most of the compositions of PZT, the Tc is >300 ºC which permits them to be used at high operating temperatures. Another important property of the lead-

zirconate-titanate system, is the occurrence of a morphotropic phase transition, i.e., a composition-dependent phase transition from a ferroelectric tetragonal structure in the Ti-rich region to a ferroelectric rhombohedral structure in the Zr-rich region. It is found that the MPB (Fig 1.5) maximises the dielectric constant, piezoelectric coefficient and relative properties. Most of the compositions of interest for transducer applications lie near the MPB [25].

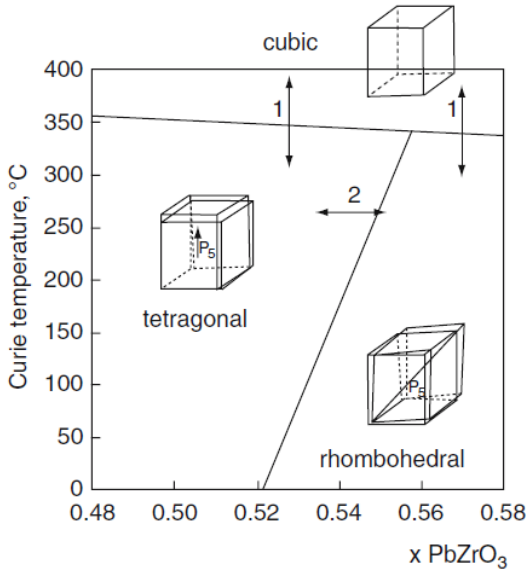

Fig 1.5 Phase transitions of lead zirconate titanate ceramics [25]

PZT is a very versatile and smart material and it is chemically inert, has high elastic modulus and exhibits high sensitivity. It exhibits large range of linearity, fast response, long term stability and high energy conversion efficiency. Limitations of PZT are its low hydrostatic sensitivity, high density, brittleness and low tensile strength. Permanent polarization of dipoles in PZT can be achieved by poling process. PZT has negative 'd_{31}' i.e. when an electric field in the direction of polarization (positive electric field) is applied, a compressive strain is found in the PZT material. Above Curie temperature, piezoelectric effect disappears. Strong electric fields can break down electric dipoles and depolarise a piezoelectric material. Maximum operating temperature is approximately 50 – 60 % of Curie temperature.

Piezoelectric properties of PZT can be further improved by the incorporation of certain additives (or dopants). A dopant is a substance which is added in smaller amounts to a piezoelectric material to alter its conductive properties. Calcium, strontium or barium may be substituted for a fraction of the lead and tin for zirconium resulting in lowered Curie point and increased permittivity. PZT-4 is such a composition where the substituent atom has the same valence as the replaced one and is known as hard PZT.

More profound changes in physical properties occur when a substituent of higher valence is introduced in the amount of 1 atom% or less, such as pentavalent niobium replacing tetravalent titanium, or trivalent lanthanum replacing bivalent lead. The PZT-5 compositions are such electron-donor doped lead zirconate titanates, characterized by enhanced permittivity and compliance with increased loss tangent, increased dc resistivity, and reduced aging rates and is referred as soft PZT.

Because of the wide variety of PZT compositions, their properties also show considerable variation, but they generally fall into two main groups. One of the groups is intended for high power transmitter (projector) applications and the other is meant for use in hydrophones. The first group meant for transmitter applications show properties like low dielectric loss maintained up to high fields, and low internal mechanical losses. PZT compositions include PZT-4 (US Navy Type I) and PZT-8 (US Navy Type III). These materials show high stability under high electric fields and high operating pressures but with slight reduction in piezoelectric properties. The other main category which is intended for hydrophone applications show high permittivity and sensitivity at the expense of some degradation in high field characteristics. The main PZT compositions include PZT-5 (US Navy Type II) and PZT-5H (US Navy Type IIH) and they achieve high relative dielectric constants without sacrificing sensitivity and have high values for hydrophone figure of merit.

1.7.1 Processing of PZT Films

Although renewed interest in ferroelectric films has existed since the mid-1970s, it has significantly increased during the early 1990s for two principal reasons. First, the techniques and equipment for producing high-quality films are more advanced than in the previous years. Second, the need for such films has become more acute as the trend toward miniaturisation and integration continues. In addition, owing to breakthroughs in the fabrication of thin films of PZT materials, research in this field has gathered greater momentum. The advantages which ferroelectric thin and thick films offer in comparison to bulk materials include: (1) lower voltage operation with thinner structures, (2) higher speed/less power with smaller areas and greater integration, (3) multi-layer/planar structures for simplicity of processing, (4) lower cost with fewer processing steps at lower temperatures, (5) larger areas possible with a minimal cost penalty, and (6) unique/multifunction structures that are relatively simple to incorporate.

1.7.2 PZT film processing techniques

A variety of techniques are available today for the fabrication of PZT films [26 – 29]. In general, they can be divided into two major categories: i.e. dry and wet processes (Table 1.3). The dry process includes physical vapour deposition (PVD) and chemical vapour deposition (CVD). The wet process includes chemical solvent deposition and chemical melt deposition.

Table 1.3 PZT film deposition techniques

Dry Process	Wet Process
1. Physical Vapour Deposition (PVD)	1. Chemical Solvent Deposition
(i) Sputtering (ii) Evaporation (E-beam, resistance, molecular beam epitaxy	(i) Sol-gel (ii) MOD (metallo-organic deposition) (iii) Electrochemical method (iii) Hydrothermal growth
2. Chemical Vapour Deposition (CVD)	2. Chemical Melt Deposition
(i) MOCVD (metallo-organic CVD) (ii) PECVD (plasma enhanced CVD) (iii) LPCVD (low pressure CVD)	(i) LPE (liquid phase epitaxy)

Generally, the PVD techniques requires a high vacuum, usually better than 5 – 10 torr, in order to obtain a sufficient flux of atoms or ions capable of depositing onto a substrate. The advantages of the PVD techniques are: (1) high purity and cleanliness, (2) compatibility with semiconductor integrated circuit processing, and (3) epitaxial/single crystal film growth is possible. However, these are offset by disadvantages such as (1) slow deposition rates, (2) difficult stoichiometry control in multi-component systems where evaporation or sputtering rates differ considerably, (3) high temperature post deposition anneal is often required for crystallisation, and (4) high capital equipment acquisition and maintenance costs are required. Sputtering and evaporation are examples of well-established and successful PVD techniques. Ion-beam assisted evaporation and sputtering are continuing to become more popular in order to increase film uniformity and deposition rates. Laser ablation, a technique which is similar in concept to low energy

thermal evaporation, seems to be more advantageous, for example, it allows congruent transfer of target material, with high deposition rate and lower processing temperature.

The CVD techniques when compared to other dry deposition methods, are usually characterised by (1) higher deposition rates, (2) good stoichiometry control, (3) large area, pin-hole free films, and (4) lower initial equipment costs. However, the limited availability and toxicity of some of the precursors for the ferroelectric compositions has posed a real problem for this method.

Combining the advantages of excellent composition control, spin-on/spray-on/dip-coating capability, low deposition/pyrolysis temperatures and very low equipment costs, the wet chemical techniques, e.g. sol-gel and metallo-organic decomposition (MOD), have already been quite successful and considered the most promising techniques for producing ferroelectric thin films. The sol-gel method involves the preparation of a sol with polymerizable oligomer species which polymerise during spin- or dip-coating deposition. The formation of such networks can be very important for microstructure and crystalline phase development when the films are heat-treated to obtain the crystalline ceramics. The MOD method is a similar technique as sol-gel. It involves the synthesis of a solution containing high molecular weight precursors such as carboxylates which are deposited onto the substrate for further heat treatment causing densification and crystallisation. The difference is that the solution does not form complexes or networks.

The common limitations for the wet chemical techniques are, for example, that film cracking occurs during the drying/firing process because the loss of volatile organic tends to lead to film shrinkage, and further heat treatment is normally required to obtain the desired crystal structure.

Nevertheless, thick films with thickness in the range of 5 to 50 μm remains a fruitful area of research and development because certain phenomena, including dielectric (capacitors), electromechanical (piezoelectrics), pyroelectric and electrooptical (optoelectrics) effects can be utilised profitably in materials and devices within this thickness range. For example, multilayer components, such as multilayer actuators, the most frequently used forms of ferroelectric ceramics in the marketplace nowadays, normally consist of layers of one or more ceramic compositions, of thickness in the range of 5 to 500 μm, separated by metallic layers acting as electrodes.

Currently, however, there are no inexpensive thick film fabrication methods available that provide the required quality. A variety of approaches have been investigated to prepare PZT thick films. Hydrothermal process has been directly applied to fabricate PZT thick films from solution but it is difficult to get stoichiometric PZT compositions because of the large difference between the solubility of each of the components and the unique nucleation and growth mechanism [31]. Plasma spraying technology has been used to deposit PZT thick films but it was found that it suffered from the problem of the incongruent melting of the PZT during deposition [32]. Therefore, thick-film technologies mostly rely on the densification of powder films instead of deposition with regard to their costs and properties. The powder layer is formed on the substrate as a powder slurry by, e.g. tape casting [33], screen printing [34] and jet printing [35]. As the liquid phase is removed by evaporation, capillary pressure exerted on the particle network causes the particles to rearrange and increase their pack density. However, sintering was found to be a major problem due to the large ratio of surface to film thickness and relatively high sintering temperatures required. On one hand, large lead loss occurred owing to the large surface area and the evaporation of PbO at temperatures above 800 °C. On the other hand, an increase of the sintering temperature was necessary to get the dense PZT film because the lateral shrinkage of the green film applied on a substrate was suppressed [36]. To reduce the sintering temperature, melt processing was used to fabricate PZT thick films by combining PZT ceramic powders with some low melting crystalline or glass phases (e.g. $Pb_5Ge_3O_{11}$ or $Pb_5(Ge_{1-x}Si_x)_3O_{11}$) to allow the densification at lower temperatures [37].

1.8 PZT FILMS BY ELECTRODEPOSITION TECHNIQUES

Electrochemical methods are increasingly being used for the preparation of thin and thick films and coatings. Recently, electrodeposition of metals attracted renewed attention, due its adoption by major companies for the processing of advanced microelectronic components. Electrodeposition has been widely investigated to obtain polymer films. In the recent past, rapid progress has been made in electrochemical deposition of ceramic materials. Electrodeposition [38, 39] is also being recognized as an effective technique for the fabrication of organoceramic films. Ceramic and organoceramic thin films are important functional materials in various devices. The rapidly increasing scientific interest in electrodeposition of ceramic and organoceramic

materials has opened new opportunities in the development of advanced thin films for novel applications.

Electrodeposition is the process of depositing a material on to a conducting surface from a solution containing ions or charged particles under the application of an electric field. This technique can be used to apply thin films of material on to the surface of an object. The set up consists of two electrodes such as a working electrode and a counter electrode connected to a dc power supply where the working electrode is the surface on to which the material is to be deposited. The electrodes are kept dipped in an electrolyte solution which contains the material to be deposited, in solution or as dispersion. Electrodeposition of ceramic materials can be performed by cathodic or anodic methods. However, anodic deposition has limited utility regarding possible materials to be deposited by this method and substrates used for deposition. Cathodic deposition has important advantages for industrial applications. There are two main electrodeposition techniques used which are electrolytic deposition (ELD) (which starts from solutions of metal salts) and (EPD) electrophoretic deposition (which is based on the use of suspensions of ceramic materials). A schematic of EPD and ELD is shown in Fig 1.6.

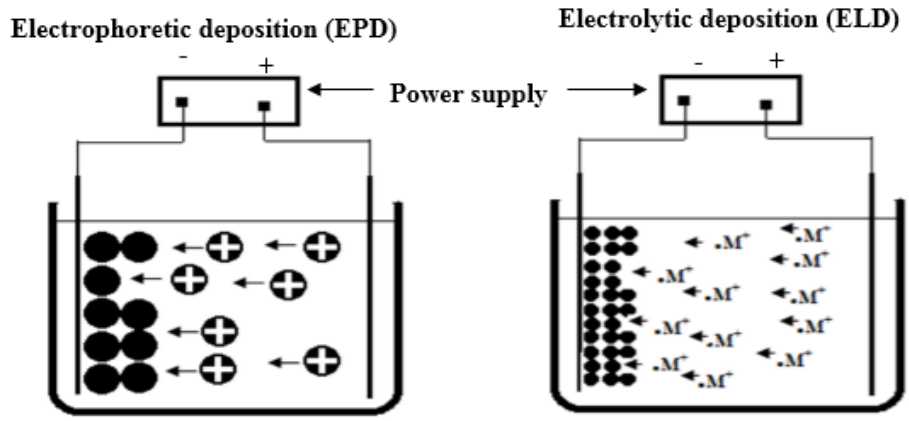

Fig 1.6 Schematic of electrophoretic deposition (EPD) & electrolytic deposition (ELD)

PZT as thin films or coatings can be obtained by both electrolytic and electrophoretic deposition. These methods have gained attention due to their versatility to be used with different materials and combinations of materials and are simple, rapid and low cost techniques which allows flexibility in substrate shapes. EPD produces thick films whereas ELD is used to obtain micro or nanostructured thin films.

1.9 LITERATURE REVIEW

Exclusive literature review on PZT films deposited using electrodeposition techniques such as ELD and EPD was carried out using Wiley, Science direct, IEEE journals, Sringer Science, Web search. It has been found that the majority of reported literature concentrates on development of PZT films using techniques like PLD, CVD, sol-gel etc. And only few studies are available on electrodeposition techniques for PZT deposition.

Zhitomirsky has carried out an exhaustive review on the fundamental aspects of electrodeposition (both ELD & EPD) of ceramic and organoceramic materials [38, 39]. The difference in mechanisms of both electrolytic and electrophoretic deposition techniques and its theoritical aspects was explained. Electrodeposition using organoceramic precursors for the deposition of CeO_2, ZrO_2, Y_2O_3 etc. using polyelectrolytes was reported. Moreover, codeposition of different compounds (e.g. RuO_2-TiO_2) using electrolytic deposition were also studied.

1.9.1 Electrolytic deposition of PZT films

Cathodic electrodeposition using peroxoprecursors is the method used by different researchers for the formation of PZT deposits. The method of ELD or electrolytic deposition is favoured due to its many advantages over other methods. Electrolytic deposition provides uniform deposits over flat as well as on curved shapes and also on selected areas of a substrate. It offers rigid control of film thickness and stoichiometry of the deposit. ELD does not require very high initial investment and can be converted from laboratory to manufacturing scale very easily.

Gal-Or et al. [40, 41] studied the electrosynthesis of zirconium, lanthanum and lead oxides from aqueous solutions. The deposits were characterised by X-ray diffraction (XRD), Thermogravimetric analysis (TGA) and Differential thermal analysis (DTA) techniques. Crystallite size determination as well as the studies on the effect of hydrogen peroxide on electrosynthesis process were also carried out.

Aghazadeh et al. carried out many studies [42, 43, 44] on synthesis of nanoscale zirconia powders by electrochemical techniques. Low temperature electrodeposition was proposed in these works for the cathodic electrolytic deposition of ZrO_2. They also utilised pulsed current electrodeposition as an effective route in the electrodeposition of

ZrO_2 and studied the effect of pulse current on the crystal structure, morphology and composition of the prepared nano powders.

Earlier, Yen [45] had also reported the preparation of electrolytic ZrO_2 coatings on titanium substrates. He studied the mechanism of electrolytic deposition and also determined the faradaic efficiency of the process. Espitia-Cabrera et al. [46] also studied the deposition of nanostructured zirconia films on stainless steel surfaces by electrolytic deposition and also analysed the effectiveness of zirconia coatings to be used as a protection against pitting corrosion of AISI 316L stainless steels. All these works had used aqueous electrolytes for zirconia electrosynthesis. But Pang et al. [47] reported electrodeposition of composite zirconia – poly diallyl dimethylammonium chloride (PDDA) films using a mixed methanol – water solvent. Here the mechanism of deposition involves electrosynthesis of zirconia and electrophoresis of PDDA in order to obtain zirconia nanoparticles in a polymer matrix.

Zhitomirsky et al. [48, 49, 50] had reported the electrosynthesis of PZT films using aqueous electrolyte solutions. They had carried out PZT deposition on various substrates such as platinum, graphite and carbon fibres using an aqueous hydrogen peroxide based peroxoprecursor technique. Later Lin et al. [51] had carried out the electrolytic deposition of PZT on carbon fibers for the development of multifunctional piezoelectric fiber composites for use as actuators in structural applications. Here ELD is employed for coating PZT films on to carbon fiber which are then embedded in a polymer matrix resulting in an active piezocomposite which possesses effective coupling coefficient and improved multifunctionality.

Ren et al. and Matsumoto et al. [52, 53] have utilised the electrochemical reduction technique for the preparation of PZT films. They found that the atomic ratio of the elements in the films depends on the molar concentration of the solutions, reduction current and reaction time. An optimum current density range was also suggested for the synthesis of PZT films by electrochemical reduction method.

All the above stated studies discuss the electrolytic deposition method using aqueous electrolytes for the synthesis of PZT or other ceramics such as zirconia, titania etc. But some limitations were also reported [48 – 50] for these aqueous deposits. Aqueous electrolytes result in adsorbed water in the deposits which can cause problems such as porosity and cracks which can seriously degrade the film performance in various

applications. As a result, researchers have also attempted non-aqueous ELD in order to improve the quality of the films.

Hennicke et al. [54] had reported the preparation of ceramic films such as titania, zirconia and lead zirconate using N, N-dimethyl formamide (DMF) based non-aqueous electrolyte. Further, trials using mixed water – DMF solutions were also successfully carried out. The morphology of the non-aqueous films were studied using electron microscopy and the properties of the non-aqueous films were compared with aqueous and mixed electrolytes and the advantages of using non-aqueous electrolytes were discussed in detail. Gheorghies [55] had described an electrolytic method for the preparation of $ZrTiO_4$ ceramic coatings on graphite substrates using a mixed methanol – water solvent. The properties of the deposition solution were studied by calorimetry nuclear magnetic resonance (NMR) techniques. In this, a programmed thermo-desorption analysis was carried out for coating which showed that the compactness of the coating depends strongly on the electrolyte concentration and deposition time. The role of OH^- groups in deposition were also confirmed by NMR analysis.

Bhattacharya et al. [56, 57] have reported the deposition of lead zirconium titanate powders by electrodeposition techniques by a non-aqueous route using a dimethyl sulphoxide (DMSO) solvent. The study demonstrates the feasibility of producing electrodeposited PZT films or powders from a DMSO based electrolyte and proves that the precursor components of PZT can be deposited simultaneously while providing atomic scale mixing, reducing reaction time to minutes and obtain the desired phase easily. Results from various studies have shown that electrolytic deposition can be used to obtain PZT depositions on flexible substrates such as carbon fibers [58, 59], metal plates, foils etc. PZT deposits on flexible substrates can be used to develop flexible PZT based sensors which can be attached to surfaces irrespective of their shapes (flat or curved surfaces). The PZT deposits can be used in sensors, actuators, structural health monitoring, energy harvesting, storage etc. ELD can be used to obtain PZT films with thickness in several microns in very short durations of time. This method also facilitates low temperature crystallisation (500 ^oC) of PZT deposits when compared to other commercially used methods for PZT fabrication.

1.9.2 Electrophoretic deposition of PZT

Electrophoretic deposition (EPD) [60, 61] is essentially a combination of two processes i.e. electrophoresis and deposition. Electrophoresis is a process by which charged species

or particles suspended in a liquid migrate towards oppositely charged electrode under the influence of an electric field. During deposition the particles undergo coagulation and get deposited at the electrode forming a dense and compact film. Heat treatment or sintering is required for further densification of the deposit and to eliminate porosity. In general EPD can be applied to any material that is available in powder form and can form a colloidal suspension. EPD can be performed for metals, ceramics, polymers, glasses etc. Depositions can be obtained on metals as well as on non-metals (graphite, carbon fibres etc.). EPD produces deposits on planar as well as on non-planar (individual fibres, fibre meshes etc.) substrates.

EPD process can be used to obtain depositions of a wide variety of ceramics and many review papers on the EPD technique have been published over the years. Earlier, Sarkar and Nicholson [62] have discussed in detail, the different mechanisms and kinetics of EPD. Here, a deposition mechanism was proposed based on the DLVO theory and the effects of suspension stability and zeta potential on EPD were explained. Ilaria Corni et al. [61] have given a chronological summary of the various historical developments that have occurred in the EPD field. Boccaccini and Zhitomirsky [63] have reviewed the potential of EPD process for use in different futuristic ceramic processing applications. Liang Yao et al. [64] have explained the basic principles and steps involved in the EPD process for coating purposes and porous materials applications. Van Tassel et al. [65] have listed out the various mechanisms by which electrophoretic deposition can occur. They have also explained how to distinguish EPD from other processes like ELD, electrostatic process, electro casting etc.

Kaya et al. [66] carried out EPD studies to prepare ceramic coatings for biomedical applications using both high solid loading as well as low solid loading suspensions. They also did work on preparation of PZT powders by hydrothermal process which was then electrophoretically deposited to produce PZT films. Titania coatings were also successfully obtained on stainless steel as well as on fibre mesh substrates by EPD technique.

Anne et al. [67] had studied the electrophoretic deposition behaviour of Al_2O_3 powder from different organic suspensions using solvents such as ethanol, methyl ethyl ketone (MEK) etc. They also studied the influence of the suspension composition on the electric field and deposition rate. It was then found that the electrophoretic behaviour of

one well defined suspension cannot be generalised to other powder – solvent suspension systems.

Zhitomirsky et al. [68] reported the electrophoretic deposition of ceramic materials for fuel cell applications. Ceramics such as $La_{0.8}Sr_{0.2}Ga_{0.875}Mg_{0.125}O_{3-x}$ (LSGM), $La_{0.8}Sr_{0.2}Co_{0.2}Fe_{0.8}O_{3-\delta}$ (LSCF), yttria stabilised zirconia (YSZ) and $(Ce_{0.8}Gd_{0.2})O_{1.9}$ (CGO) were electrophoretically deposited on Ni foils and Ni – yttria stabilised zirconia substrates prepared by tape casting. Ethyl alcohol – phosphate ester – poly vinyl butyral (PVB) combination was used as the effective solvent – dispersant – binder system.

Earlier Sweeny et al. [69] had reported the electrophoretic deposition of PZT films from acetone based suspensions with additions of nitric acid and nitrocellulose. Films up to 32 µm thickness were deposited using this technique and dielectric coefficients as well as pyroelectric coefficient and pyroelectric figure of merit were determined. The effect of sintering aids on the deposition process was also carefully examined.

Su et al. [70] had performed hydrothermal synthesis in combination with colloidal processing to prepare PZT films in aqueous solutions. Here PZT powders were synthesised and electrophoretic deposition was then employed to deposit PZT films directly from the hydrothermal PZT suspensions. The effects of synthesis conditions on the particle size distribution of PZT as well as the stabilisation mechanisms for the hydrothermal slurries were investigated.

Boccaccini et al. [71] reported the electrophoretic deposition of PZT films from colloidal dispersions of PZT powder in acetyl acetone solvent with controlled addition of iodine. PZT films were prepared on different metallic substrates such as stainless steel plates, fibres, fibre mats, nichrome wires etc. Iodine was added to the suspension to give a charge to the PZT particles. PZT particles were found to acquire a positive charge which eventually helped in the electrophoretic process and the concentration of iodine to be added was also optimised during the experiments.

Jan Ma et al. [72, 73] performed the colloidal characterisation, electrophoretic deposition and packing studies of sub-micron PZT ceramics using an ethanol based suspension. Zeta potential and conductivity measurements were carried out to optimise the suspension conditions for deposition. Colloidal stability of the ethanol suspensions

were studied and the electrosteric effect resulting from the addition of PVA polymer to the suspensions was also investigated.

Sakka et al. [74] studied the relevance of the EPD technique as a colloidal processing method in ceramics production. Work was carried out on the stability of PZT – ethanol suspensions, stability studies on TiO_2 – (2 – propanol, 2, 4 – pentanedione) suspensions, pulsed current EPD technique using aqueous suspensions and preparation of laminated textured ceramics by EPD process with the aid of a strong magnetic field. Likewise, Abellard et al. [75] did research on PZT film fabrication EPD for high frequency medical imaging applications. Here the PZT and PbO particles are suspended in the in ethanol solvent and then electrophoretically deposited on porous PZT substrates.

Doungdaw et al. [76] also studied the electrophoretic deposition of PZT powder/films from ethanol suspensions prepared with phosphate ester (PE) as dispersant. It was found that the phosphate ester addition resulted in a good dispersion and surface charging of the PZT particles in the ethanol solvent. The effect of PE concentration on the suspension stability, deposition weight, and relative density of the PZT films were investigated. The electrical properties of the PZT ceramics were also studied.

Danjela Kuscer et al. [77, 78] described the electrophoretic deposition of niobium doped lead zirconate titanate (PZT Nb) films of micrometer thickness using an ethanol based solvent. The PZT Nb particles were stabilised in the ethanol solvent using poly acrylic acid (PAA) and the interactions of the PZT Nb with PAA in ethanol – PVB suspension was studied using Fourier Transform Infrared Spectroscopy (FTIR). The properties of the suspensions, the deposition yield and the morphology of the PZT Nb films were also studied.

Van Tassel et al. [79] reported the work on electrophoretic deposition of PZT films using acetic acid based suspensions. PZT films were formed on alumina substrates and sintered at 900 °C along with Lithium and PbO sintering aids. Electronic properties of the films were studied and pyroelectric coefficients were determined and charge/voltage hysteresis loops were also measured. Wu et al. [80] also carried out EPD studies using acetic acid suspensions for the preparation of PZT films on copper foils. A PbO coating was applied on the top of the PZT films and its effect on the film properties were studied. It was also found that at higher sintering temperatures (> 950 °C), inter-

diffusion of copper and PZT occur and a Cu_xPb alloy is formed which spreads through the film.

1.10 SCOPE AND OBJECTIVES OF THE WORK

There have been many developments in the synthesis and applications of piezoelectric materials since many years. Among the available piezoelectric materials, PZT ceramics are the most preferred and commonly used for underwater transducer applications. A significant limitation of PZT is its hard and brittle nature which restricts its application as conformal sensors on non-planar or curved surfaces and profiles. The main criterion for a material to be used for conformal array applications is high flexibility. Nevertheless, flexible polymeric piezomaterials such as PVDF, copolymers of PVDF and other piezoceramic-polymer composites available currently they lack acceptability due to their inferior piezoelectric properties.

However, realising a flexible/conformal form of PZT could be a phenomenal accomplishment in the existing underwater sensing scenario. Much studies are reported on PZT film fabrication using other techniques such as sputtering, pulsed laser deposition, sol gel method, vapour deposition, etc. which have many limitations such as, depositing thick films through these techniques are very laborious and time consuming. However, the electrodeposition route is not much explored. Electrodeposition is a simple, fast and cost effective process which can provide deposits with effective control on the structural and morphological characteristics, allows in situ deposition on selected areas of the substrate or on complex geometry surfaces and also facilitates low temperature sintering. This work aims at the development of PZT-based flexible piezoelectric material for the fabrication of conformal acoustic sensor arrays for underwater applications. Literature survey has shown that the following aspect was not studied systematically, i.e. dielectric and piezoelectric analysis along with sensor fabrication and characterisation studies from an underwater application point of view has not been reported, although studies were carried out on synthesis of PZT films using electrodeposition techniques. In view of this, it is proposed to deposit PZT on to different flexible substrates such as metal foils (stainless steel, titanium) using electrodeposition techniques which includes both electrolytic deposition (ELD) and electrophoretic deposition (EPD) and study systematically various factors that affect the nature, structure and properties of the PZT.

The objectives of the study are framed as follows:

1. Electrolytic deposition (ELD) of PZT
    i. Study the effect of solvent system: Aqueous and non-aqueous deposition techniques on PZT film deposition.
    ii. Study of reaction mechanism for different solvent systems such as aqueous and non-aqueous (DMSO based) for PZT film depositions.
    iii. Study the effect of ELD process parameters such as current density, time of deposition on PZT film characteristics.
    iv. Study the effect of sintering temperature and time on the PZT film properties.
    v. Physical, morphological and chemical characterisation of the electrolytic PZT films using the techniques such as SEM, TEM, AFM, XRD and Raman spectroscopic techniques.
    vi. Study the dielectric properties (dielectric constant, loss factor) of the electrolytic PZT films.
    vii. Study the piezoelectric properties (d_{33} values, hysteresis) of the electrolytic PZT films.
2. Electrophoretic deposition (EPD) PZT
    i. Study in detail, the mechanism of electrophoretic PZT film deposition.
    ii. Study the effect of EPD process parameters such as suspension concentration, deposition voltage, time, thickness of deposit on PZT film development.
    iii. Physical, morphological and chemical characterisation of the electrophoretic PZT films using the techniques such as SEM, TEM, AFM, XRD and Raman spectroscopic techniques.
    iv. Study the dielectric properties (dielectric constant, loss factor) of the electrophoretic PZT films.
    v. Study the piezoelectric properties (d_{33} values, hysteresis) of the electrophoretic PZT films.

3. Sensor fabrication and testing

    i. Fabrication of underwater acoustic sensor using PZT film.

    ii. Underwater acoustic testing of the fabricated sensor.

Chapter – 2

MATERIALS AND METHODS

2.1 EXPERIMENTAL TECHNIQUES FOR PZT SYNTHESIS AND CHARACTERISATION

In this chapter, the adopted methodology of PZT film synthesis by different techniques such as electrolytic (ELD) and electrophoretic (EPD) deposition methods together with their characterisation techniques viz. Scanning Electron Microscopy (SEM), Atomic Force Microscopy (AFM), X-ray diffraction (XRD) and Raman Spectroscopy are discussed. Dielectric studies (dielectric constant, dielectric losses) and piezoelectric evaluation (poling, hysteresis studies) of the prepared PZT films were also carried out and the detailed procedures are described here. The set up for the underwater acoustic measurements are also discussed in detail.

2.2 SUBSTRATES/ELECTRODES FOR DEPOSITION

Stainless steel (SS) and titanium foils were used as substrates for deposition. The metal foils were grounded using emery papers, cleaned and degreased using toluene to get a mirror finish. The specifications of the different materials used are given in Table 2.1. A two electrode system for deposition was adopted with the substrate being the cathode or working electrode and a platinum mesh electrode taken as the anode or the positive electrode.

Table 2.1 Details of the substrate materials used

Sl No.	Material	Supplier/Make	Grade/Purity
1	Stainless Steel foil (0.25 and 0.127mm thick)	Alfa Aesar	Type 304
2	Titanium foil (0.25 and 0.127mm thick)	Alfa Aesar	99%
3	Emery paper	80, 250, 400, 800, 1500	
5	Platinum electrode	Custom made	
6	Reference electrode	PARSTAT	Ag/AgCl

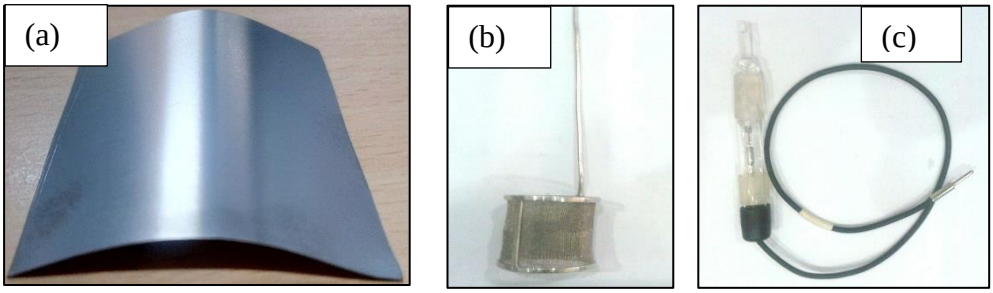

Fig 2.1 (a) Substrate/Cathode, (b) Platinum (Anode), (c) Reference Electrode

2.3 ELECTROLYTIC DEPOSITION (ELD) OF PZT

Electrolytic deposition (ELD) process involves the deposition of a material by passing an electric current between two or more electrodes dipped in an electrolyte solution. The deposition takes place at the electrode/electrolyte interface within the electrical double layer. The success of an electrochemical reaction mainly depends on various parameters such as proper electrode selection, preparation of electrolyte, temperature, pH, mode of electrolysis (potentiostatic/galvanostatic) etc.

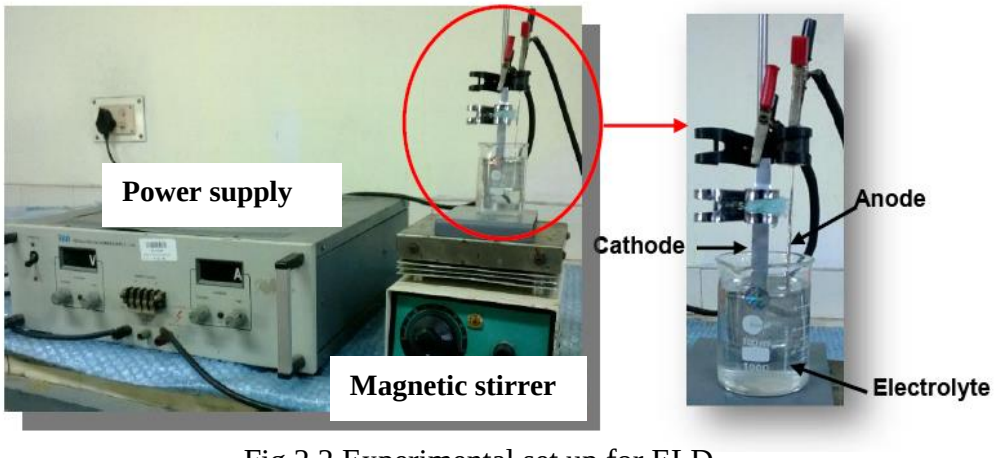

Fig 2.2 Experimental set up for ELD

In the typical cathodic electrolytic deposition set up employed in this work, the deposition takes place on the substrate or working electrode (cathode) with platinum being the counter electrode (anode). The experimental set up is shown in Fig 2.2. The details of the chemicals and instruments used for PZT electrolytic deposition (ELD) are given in Table 2.2.

Two different types of electrolyte systems have been studied in this work for the electrolytic deposition of PZT films. Both water and organic solvents like Dimethyl sulphoxide (DMSO) have been used.

Table 2.2 List of chemicals/instruments for PZT ELD

Sl No.	**Chemicals**	**Supplier**	**Grade/Purity**
1	Lead (II) nitrate ($Pb(NO_3)_2$)	Alfa aesar	AR, 99.99%
2	Zirconium chloride hexa hydrate ($ZrOCl_2.8H_2O$)	Alfa aesar	AR, 99.99%
3	Titanium tetrachloride ($TiCl_4$)	Merck	AR, 99.9%
4	Hydrogen peroxide (H_2O_2)	Acros Organics	30 wt %
5	Dimethyl sulphoxide (DMSO)	Alfa aesar	GR, 99.9%
6	Distilled water	Laboratory grade (prepared in house)	
	Instruments	**Make**	**Model/spec**
1	Digital pH meter	Roy Instruments, Chennai	IR 501
2	Micropipettes	Borosil	20 - 200µl
3	Magnetic stirrer	Rotec Instruments, Kerala	
4	Regulated DC Power Supply	Aplab	L1285
5	Muffle furnace	Rotec Instruments, Kerala	

Various aqueous electrolytes were prepared by dissolving AR grade salts of lead (II) nitrate $Pb(NO_3)_2$, zirconium chloride hexa hydrate $ZrOCl_2.8H_2O$, titanium tetrachloride and H_2O_2 in distilled water in the ratio 1:0.52:0.48:10. The concentration of lead nitrate is taken as 0.03M. A pH of 2-3 and a temperature below 5°C was maintained for aqueous deposition process. Similarly non-aqueous electrolyte was prepared by dissolving the AR grade salts of lead nitrate $Pb(NO_3)_2$, zirconium chloride hexa hydrate $ZrOCl_2.8H_2O$, titanium tetrachloride in DMSO (Dimethyl sulphoxide) in the ratio

1:0.52:0.48). Non aqueous ELD was performed under ambient conditions and magnetic stirring was provided. PZT deposition was performed at constant current density (15 to 40 mA/cm^2) for a specified time interval (1 to 40 minutes). The PZT films obtained by electrolytic deposition were then sintered at 500°C for 1 hour in an electric furnace. The flow chart for PZT ELD is shown in Fig 2.3.

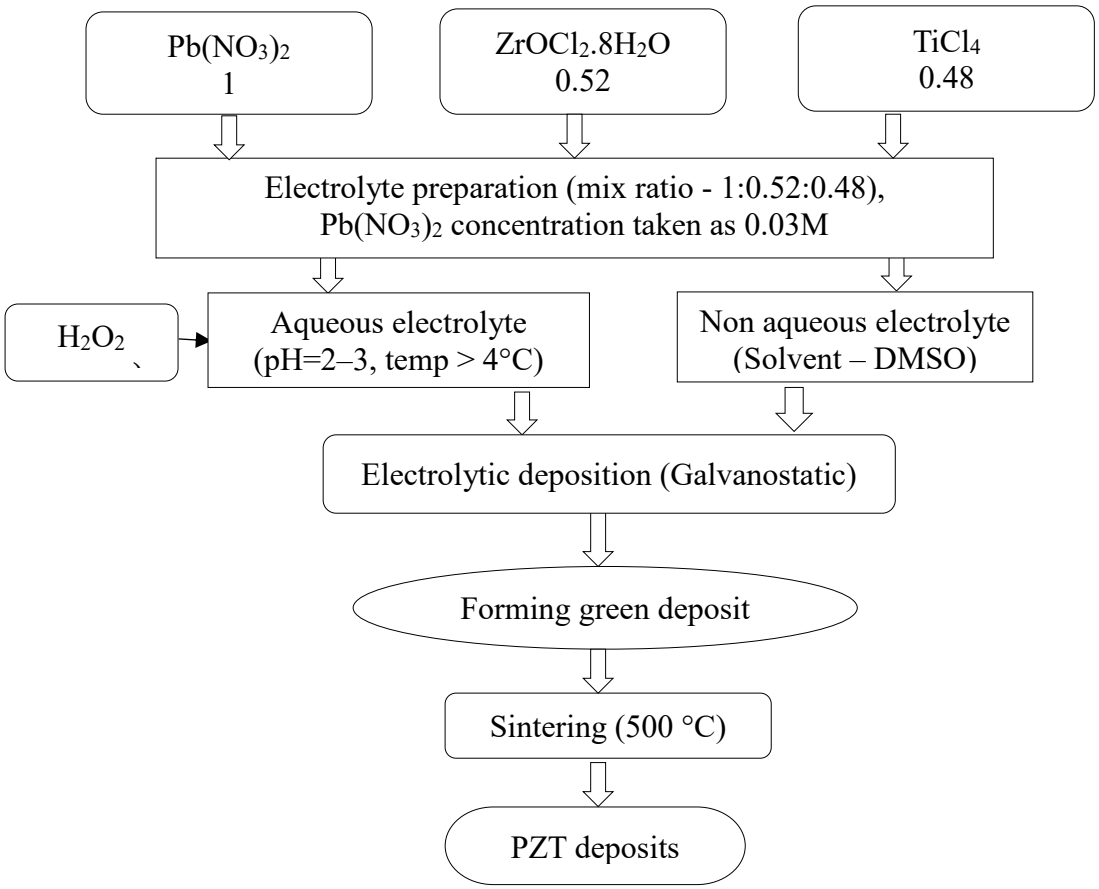

Fig 2.3 Flow diagram for PZT ELD

2.3.1 PZT films using pulsed potentiostatic/galvanostatic techniques

Pulsed electrodeposition or PED is an advanced type of electrolytic deposition (ELD), which utilises a very sophisticated instrumentation such as Electrochemical Workstation (Potentiostat/Galvanostat) to obtain superior quality films/coatings for various applications. Here very short potential or current pulses of equal amplitude, duration, and polarity are applied to an electrolyte to generate high quality films/coatings.

The film composition and other properties can be precisely controlled by regulating the pulse amplitude and width.

Table 2.3 List of chemicals/instruments employed for PZT Pulsed Electrodeposition

Sl.No.	**Chemicals**	**Supplier**	**Grade/purity**
1.	DMSO based Non-aqueous electrolyte	Laboratory synthesised	0.03M
	Instrument	**Make**	**Model Specifications**
1.	Electrochemical workstation	Potentiostat/Galvanostat	PARSTAT 4000
2.	Muffle furnace	Rotec Instruments Kerala	

The electrolyte used in this work for PED was DMSO based non-aqueous electrolyte, and the preparation is same as given in the previous section of this chapter (2.2). In PED, a three electrode set up is utilised where the substrate is taken as the cathode or working electrode (WE), platinum as the anode or counter electrode (CE) and silver/silver chloride as the reference electrode (RE). In this particular work, experiments were performed using pulsed potentiostatic as well as pulsed galvanostatic techniques. The details of the chemicals and instruments used for PZT pulsed deposition are given in Table 2.3.

Fig 2.4 Electrochemical workstation (PARSTAT 4000) employed for PZT thin film deposition

Depositions were carried out at ambient conditions using a 3 electrode system using PARSTAT 4000 Electrochemical workstation (Fig 2.4.). The techniques used were Cyclic Voltammetry (CV) and Regulated Galvanic Pulse (RGP). In Cyclic Voltammetry,

the electrode potential was varied between two limits (- 4 to + 4 V) at a sweep rate of 0.25 V/sec for 6 cycles. In Regulated Galvanic Pulse (RGP) method, a total of 6 current pulses (-0.015A, -0.006A, -0.002A, -0.0006A, 0.0018A) for 5 cycles were applied with a time period of 20 seconds for each pulse. The flow chart for PZT pulsed electrodeposition is depicted in Fig 2.5.

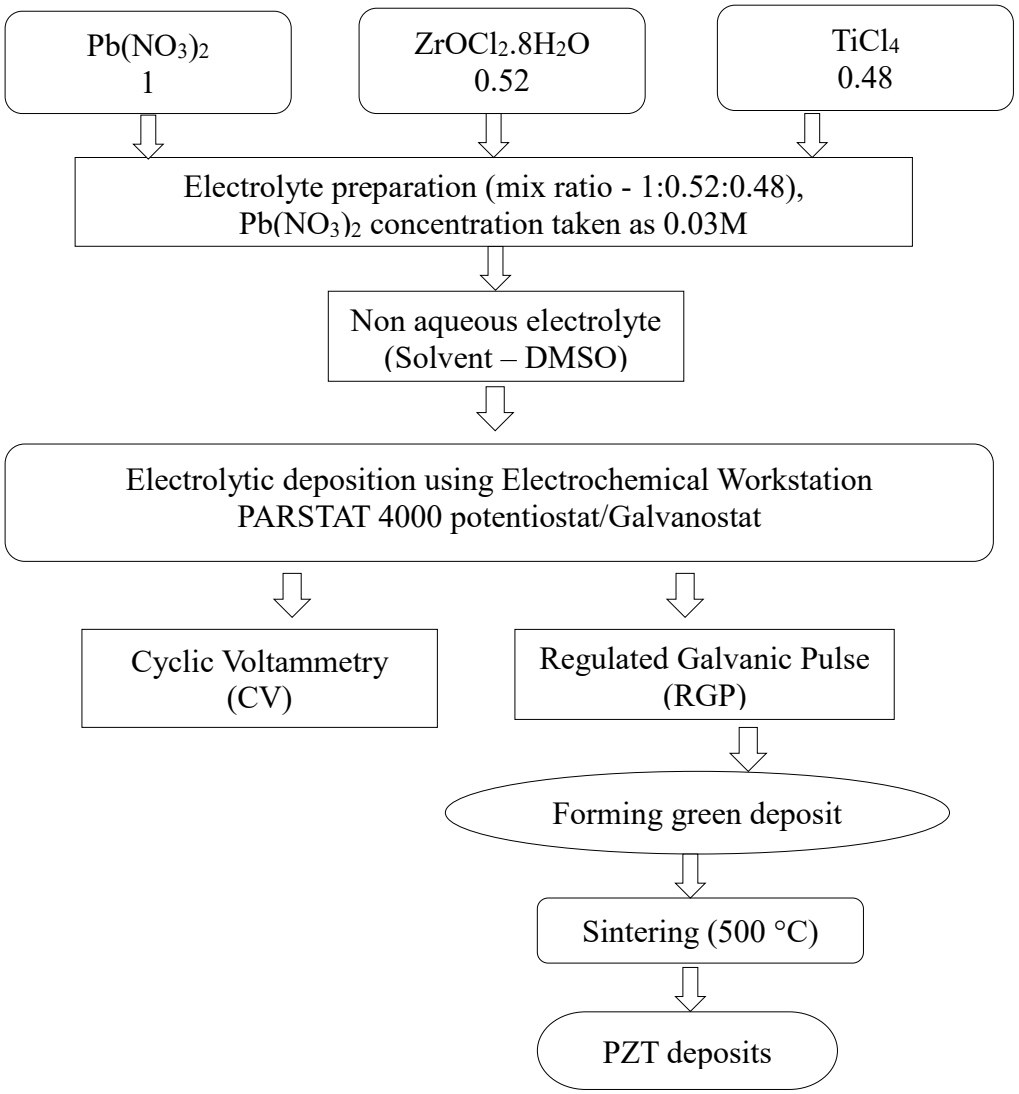

Fig 2.5 Flow diagram for PZT pulsed electrodeposition

2.3 ELECTROPHORETIC DEPOSITION OF PZT

Electrophoretic deposition (EPD) is a particulate forming process. It begins with a dispersed powder material in a solvent and uses an electric field to move the powder particles into a desired arrangement on an electrode surface. There are four defining characteristics of EPD as it is used here: (1) it begins with particles which are well dispersed and able to move independently in solvent suspension, (2) the particles have a surface charge due to electrochemical equilibrium with the solvent, (3) there is electrophoretic motion of the particles in the bulk of the suspension, and (4) a rigid (finite shear strength) deposition of the particles is formed on the deposition electrode.

The experimental set up for EPD is similar to ELD, where deposition occurs on the cathode or working electrode and platinum kept as the anode or counter electrolyte. The details of the material/chemicals/instruments used for PZT EPD are listed in Table 2.4.

Table 2.4 List of material/chemicals/instruments for PZT

Sl.No.	**Chemicals**	**Supplier**	**Grade/purity**
2.	PZT powder (0.6µm particle size)	Sparkler ceramics	PZT 5J
3.	Acetic acid	Merck	GR
	Instrument	**Make**	**Model Specifications**
1.	Ultrasonic Homogeniser	Orchid Scientific	PS 500
2.	High voltage DC power supply	Aplab Limited	H1010
3.	Muffle furnace	Rotec Instruments	
4.	Coating thickness gauge	Phynix Gmbh	

The first step in electrophoretic deposition is the preparation of a stable colloidal suspension. PZT powder (3 wt. %) was ultrasonically mixed in the solvent (acetic acid) for a time of 2 minutes and to obtain a suitable suspension of PZT particles in acetic acid solution. The deposition was done at ambient conditions using a high voltage power

supply. Potentiostatic deposition was adopted here wherein a high voltage in the range 50 to 500V were applied between the electrodes dipped in the colloidal suspension for a suitable time period (10 seconds to 2 minutes) to obtain a PZT deposit which was then sintered in a muffle furnace at a temperature of 600 °C for a time of 30 minutes. The flow chart for PZT EPD is shown in Fig 2.6.

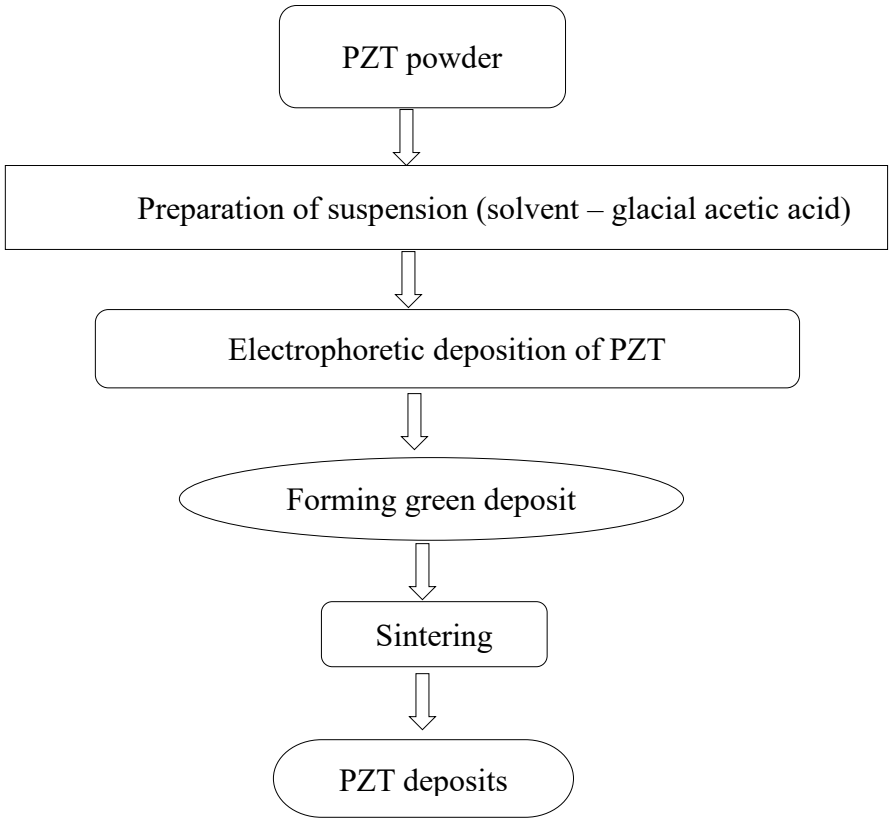

Fig 2.6 Flow diagram for PZT EPD

2.4 PIEZOELECTRIC POLING OF PZT DEPOSITS

Poling [81] is the process of inducing piezoelectricity in a piezoelectric material by the application of a large electric field near the Curie temperature (Tc). During this process, the high electric field forces the domains to reorient in the direction of the applied electric field. Poling is possible only in ferroelectric materials. Before poling, the ferroelectric ceramic does not possess any piezoelectric and pyro electric properties owing to the random orientation of the ferroelectric domains in the ceramics. For effective poling or domain reorientation, field must be applied on the sample and maintained over a period of time. For a given field and poling time, better domain

rearrangement results at high temperature just below Tc. Above Tc, the material loses its piezoelectricity as the crystal symmetry becomes cubic (paraelectric).

Contact poling is the procedure adopted in this work to pole the PZT film samples. In contact poling, samples are placed in vacuum or submerged in an insulating fluid such as silicon oil which can prevent arcing. Sample is poled in thickness direction and so the voltage to be applied is determined according to the thickness of the samples. Top and bottom electrodes, which are either evaporated, sputtered, or painted on the sample surfaces. The details of the materials/instruments used for poling are listed in Table 2.5.

Table 2.5 Materials/Instruments for poling process

Sl. No.	**Chemicals/Instruments**	**Supplier/Make**	**Grade/Purity/Range**
1.	Silicone oil	Fluka Chemicals	DC 200
2.	Silver-epoxy paste	Chomerics	Resistivity: 0.002 Ω-cm
3.	Hot plate	Rotec Instruments	Temperature: 0 to 200 °C
4.	High voltage regulated power supply	Aplab Limited	Voltage: 100 to 1000V

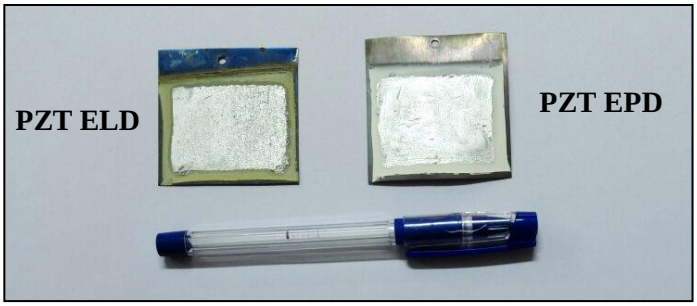

Fig 2.7 EPD and ELD PZT samples after coating with silver epoxy paste

In this particular work, conductive silver- epoxy paste was used as electrode material and is finely coated over the sample surfaces and continuity is checked so that the sample quality is ensured before poling. The EPD and ELD PZT film samples electroded using silver epoxy are shown in Fig 2.7. Images for silver epoxy paste and

Stainless steel – Teflon jig are given in Fig 2.8. During poling, the samples were kept in an in-house designed Stainless steel- Teflon jig and placed in a temperature controlled silicone oil bath connected to the high voltage dc regulated power supply as shown in Fig 2.9.

Fig 2.8 (a) Silver epoxy paste for electroding, (b) In-house designed Stainless steel-Teflon jig for poling

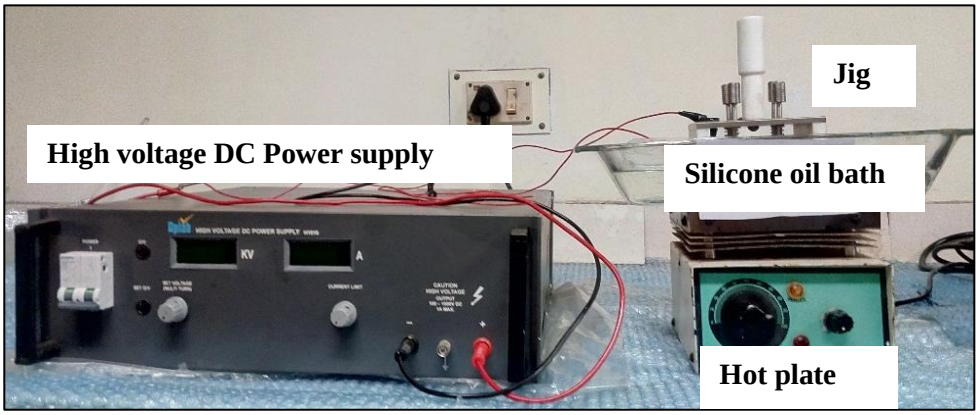

Fig 2.9 Experimental set up for poling

The system was heated up to the poling temperature, voltage was gradually increased up to the required voltage value and was held at that voltage for a particular time. After the required time was reached, temperature of the bath was reduced until room temperature was attained and after that point, voltage was switched off. Voltage applied was in the range of 1-3 kV/mm for PZT samples. The stepwise poling process is explained in Fig 2.10.

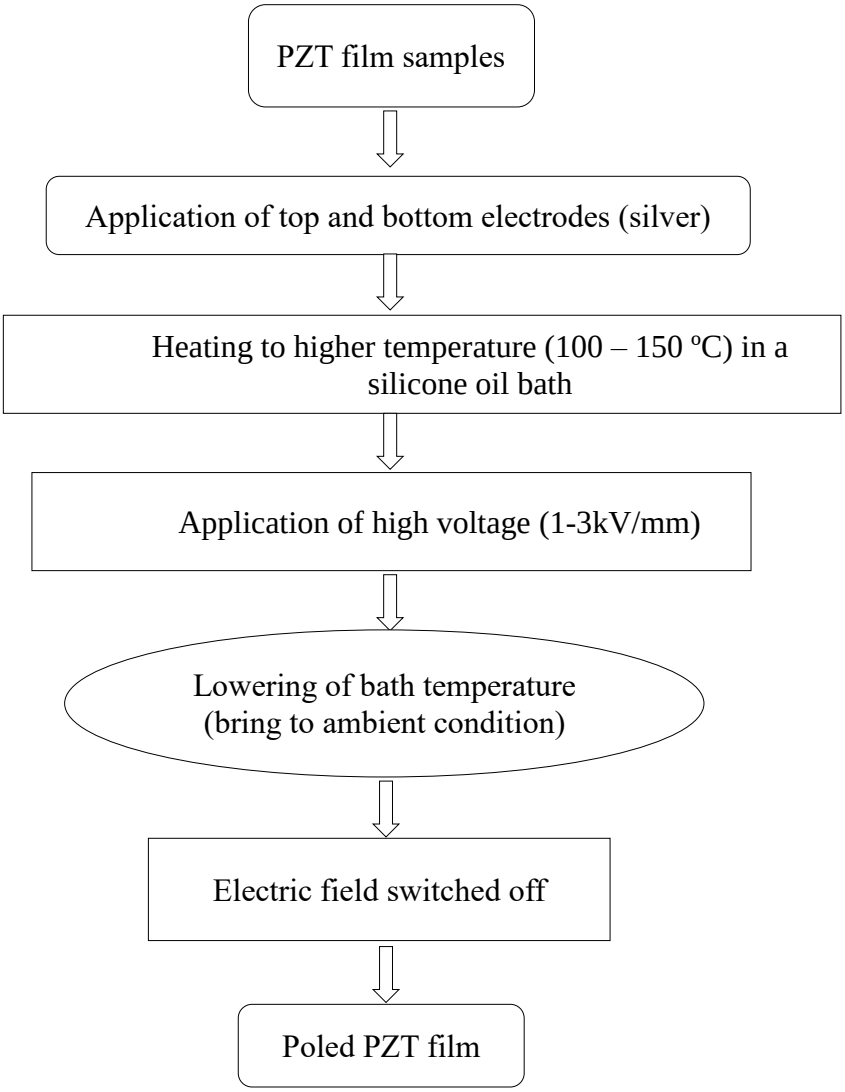

Fig 2.10 Flow diagram for PZT poling

2.5 CHARACTERISATION TECHNIQUES

2.5.1 X-ray diffraction (XRD)

The phase identification, crystal structure, lattice parameters and particle sizes have been determined by the X-ray diffraction (XRD) technique using a Bruker AXS D8 Advance model diffractometer with Ni-filtered Cu Kα (λ = 1.54 Å). A schematic drawing of the instrumental set-up is shown in Fig 2.11.

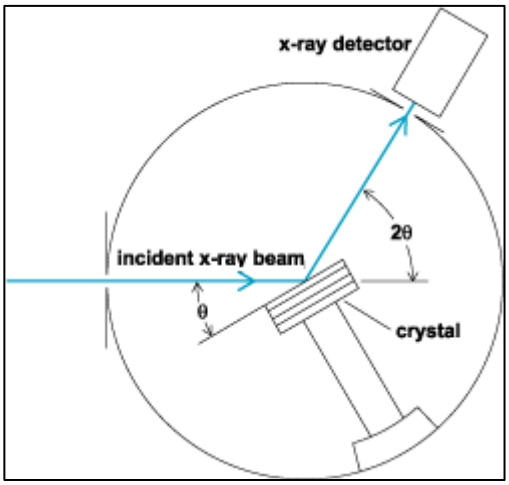

Fig 2.11 Schematic diagram of XRD instrumental set up [74]

A typical powder XRD instrument consists of four main components viz. X-ray source, specimen stage, receiving optics and X-ray detector [82]. The source and the detector with its associated optics lie on the circumference of 'focusing circle' and the sample stage is at the center of the circle. The angle between the plane of the specimen and the X-ray source is θ, known as Bragg angle and the angle between the projection of X-ray and the detector is 2θ. Wide angle X-ray diffraction (WAXRD) is used to characterize the crystal structures of the prepared and annealed films. A continuous scan was performed on the XRD with 2θ angles ranging from 10 to 70 degrees.

For the XRD analysis, fine powder samples are mounted on the sample holder and the powder is assumed to consist of randomly oriented crystallites. When a beam of X-ray is incident on the sample, X-rays are scattered by each atom in the sample. If the scattered beams are in phase, they interfere constructively and we get the intensity maximum in that particular angle. The atomic planes from where the X-rays are scattered are referred to as the "reflecting planes (lattice planes)". The Bragg's Law relates the wavelength (λ) of the X-rays reflected, the spacing between the atomic planes (d) and the angle of diffraction (θ) and is given by

$$2d_{hkl}\sin\theta = n\lambda \tag{2.1}$$

For the first order diffraction, n=1 and knowing θ and λ, the d-value for a particular plane can be calculated. After recording the X-ray diffraction pattern, first step

involves the indexing of XRD peaks which means assigning the correct Miller indices to each peak of the diffraction pattern.

By using X-ray diffractograms, 2θ values of diffraction peaks are obtained. The number and position of peaks or the 2θ values give information about the crystal class, lattice type and cell parameters of a particular material. The interplanar distances and intensity values are also determined.

The powder diffractogram of a compound is called as its fingerprint which can be used to identify different compounds. By experience, it is possible to identify the spaces by analyzing the d spacing and the intensity (I) readings are obtained. Phase determination can be carried out by comparing a set of experimental d & I values with a database of d – I files. To simplify the process, powder diffraction data from known compounds have been compiled into a database by the Joint Committee on Powder Diffraction Standard (JCPDS) where each corresponding compound has a particular JCPDS card number. Different programs are used to compare experimental diffractograms with those of known compounds already included in the database. JCPDS was founded in 1944 and it was later changed to ICDD (International Centre for Diffraction Data) in 1978.

2.5.2 Raman spectroscopy

Raman spectroscopy [83] provides information about molecular vibrations that can be used for sample identification and quantification. The technique involves shining a monochromatic light source (normally laser) on a sample and detecting the scattered light. The majority of the scattered light is of the same frequency as the excitation source and this is known as Rayleigh scattering or elastic scattering. A very small amount of the scattered light is shifted in energy from the laser frequency due to the interactions between the incident electromagnetic waves and the vibrational energy levels of the molecules in the sample. Plotting the intensity of this shifted light versus frequency results in a Raman spectrum of the sample. Raman spectra are often plotted with respect to the laser frequency such that the Rayleigh band lies at 0 cm^{-1}. On this scale, the band positions will lie at frequencies that correspond to the energy levels of different molecular vibrations. The Raman spectrum can thus be interpreted similar to the infrared absorption spectrum.

Instrumentation for the measurement of Raman spectra consists of 4 components: (1) Excitation source, (2) Illumination and light collection optics, (3) Wavelength selector unit, (4) Detector. Schematic diagram of a Raman spectroscopic set up is shown in Fig 2.12. The excitation source plays an important role in the performance of a Raman spectrometer including its sensitivity and stability. Usually lasers are used as excitation source which is directed on to the sample through an optical mirror and lens. The scattered signals (Rayleigh and Raman) from the sample is collected and is given to the wavelength selector. The wavelength selector is the most critical component in a Raman spectrometer, through which the intensity information of individual frequencies can be extracted. The next part is the detector. Due to the low scattering efficiency, detection of Raman signal is very challenging and the detector should be very sensitive. The detectors exploit the photoelectric effect which uses the incoming light energy to generate charge carriers that are separated and can subsequently be measured as a current at the terminals.

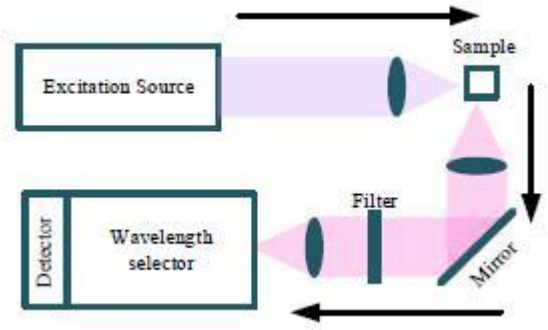

Fig 2.12. Schematic set up of Raman spectroscopy [84]

In this particular work, the crystal structure or phase analysis of PZT depositions were characterised using Raman spectroscopy (Witec Instruments, 532 nm laser source). A typical Raman spectroscopy instrumentation is shown in Fig 2.13.

Fig. 2.13 Instrumental setup for Raman spectroscopy

2.5.3 Particle size distribution by dynamic light scattering

Dynamic light scattering technique was used in this particular work to study the stability of the EPD dispersions with different concentrations with the passage of time. Preparation of dispersion medium wherein each single particle is able to move independently in a suitable solvent system is one of the most important processes in EPD. The particle size distribution of the PZT powder in the dispersion was determined by light scattering technique using a particle size analyser (Zetasizer-Ver-7.02, Malvern Instruments) and the setup is shown in Fig 2.14.

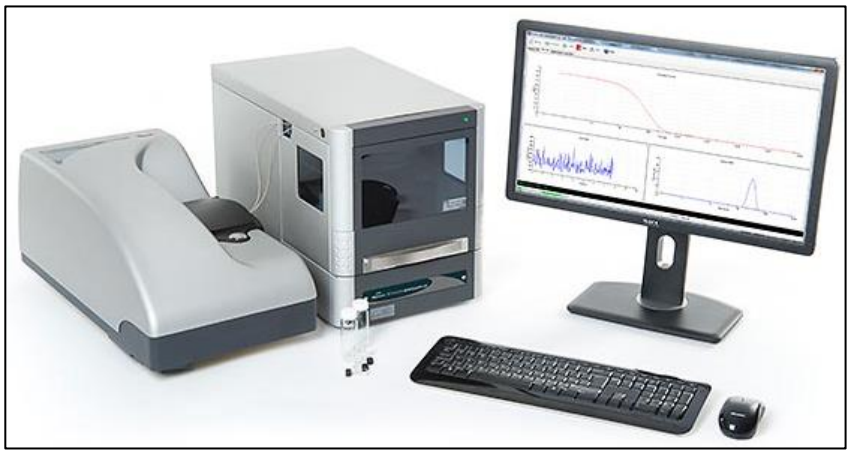

Fig 2.14 Instrumentation for dynamic light scattering technique

Dynamic light scattering [84] is a non-invasive technique used for measuring the size of the particles undergoing Brownian motion in a suspension. By this technique, the speed of particles undergoing Brownian motion is measured. The speed of the particle is determined by its particle size, temperature and sample viscosity. The smaller the particles, larger the speed and vice versa. The velocity of the Brownian motion is defined by the diffusion coefficient (D) which in turn is used to determine the size of the particles using the Stokes – Einstein equation,

$$d_H = \frac{kT}{3\pi\eta D} \tag{2.2}$$

Where d_H is the hydrodynamic diameter, k is the Boltzmann constant, T is the absolute temperature, η is the viscosity, and D is the diffusion coefficient.

2.5.4 CHNS elemental analysis

CHNS elemental analysis is used for the determination of mass percentage of carbon, hydrogen, nitrogen and sulphur in organic compounds or other types of materials. The analysers can be set up in different configurations to determine CHN, CHNS, CNS or N depending upon the application In this particular work, C-H-N analyser Elementar Vario EL III was used which is having operation modes such as CHNS, CHN, CNS, CN, N, S and O.

During CHNS analysis, the sample is subjected to a high temperature combustion process in an oxygen rich environment [85]. The instrument may be static or dynamic. In static type, a predetermined amount of oxygen is introduced to the combustion process. But in dynamic method, a constant flow of oxygen is maintained for a set period of time. During the combustion process, carbon is converted to carbon dioxide, hydrogen to water, nitrogen to nitrogen gas or oxides of nitrogen and sulphur to sulphur dioxide. Additional combustion products are then removed from the system. The detection of gases is carried out by different techniques such as gas chromatography or other methods. Quantification of the elements are carried out by calibration using high purity micro analytical standard compounds. A schematic of the CHNS analysis method is shown in Fig 2.15.

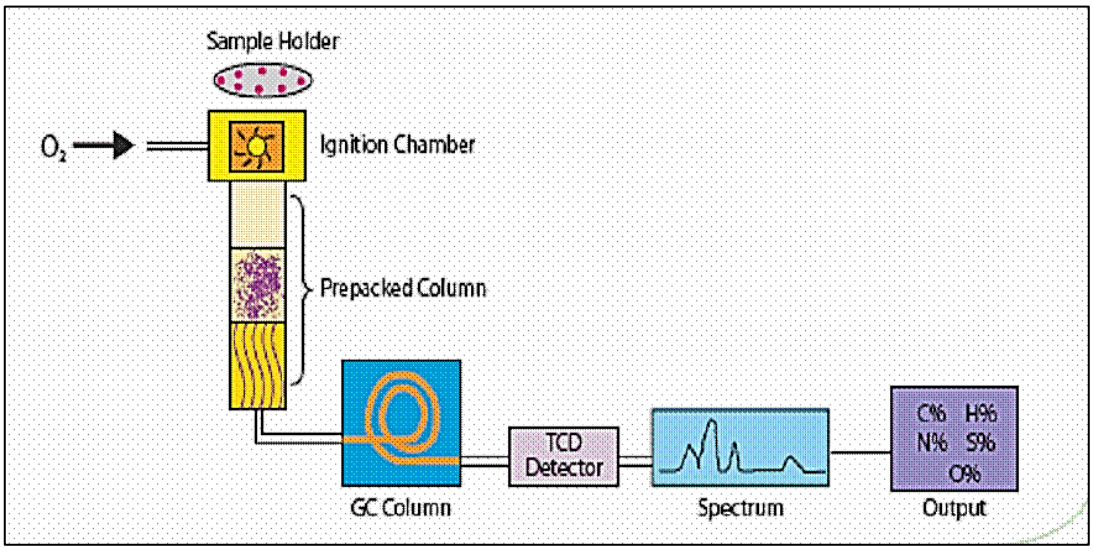

Fig 2.15 Schematic of CHNS elemental analysis method

2.5.5 Scanning electron microscopy (SEM)

Scanning electron microscopy was used to examine the surface morphology of the PZT films. The apparatus used for imaging was a JEOL Model JSM - 6390LV Scanning Electron Microscope. All samples were coated with an approximately 300 Å thick layer of gold in an Edwards S150B sputter coater. Magnifications of 500×, 1500×, 5000× and10000× were used to view the samples. Particle size determination was done qualitatively by taking an average of the particles viewed in the electron microscope. Experimental set up of a scanning electron microscope is shown in Fig 2.16.

Fig 2.16 Experimental set up of SEM

Electron microscopes are highly sophisticated scientific instruments that use a beam of high energy electrons to examine objects on a very fine scale. They were developed to overcome the limitations of normal optical microscopes whose magnification was limited. SEM can be used to obtain characteristic information about the topography, morphology, composition and crystallographic data about a particular specimen [86].

During SEM analysis, a beam of high energy electrons from a source (usually an electron gun) is focussed on a spot of the sample which is schematically shown in Fig 2.17. These high energy electrons, also known as primary electrons dislodge electrons from the samples. The removed or dislodged electrons which are also referred as secondary electrons are then attracted and collected by a positively charged grid or detector and transformed into a signal. In order to obtain a good quality SEM image, the electron beam is swept across the inspection area to produce many different signals. These signals are then amplified, analysed and translated into topography images of the inspected samples. A SEM may be equipped with EDAX (Energy Dispersive Analysis

of X-rays) system which can be used to perform compositional analysis on different samples. EDAX is mainly a qualitative technique which helps to provide an idea about the composition of different materials or any contaminants present on the surface of a particular sample.

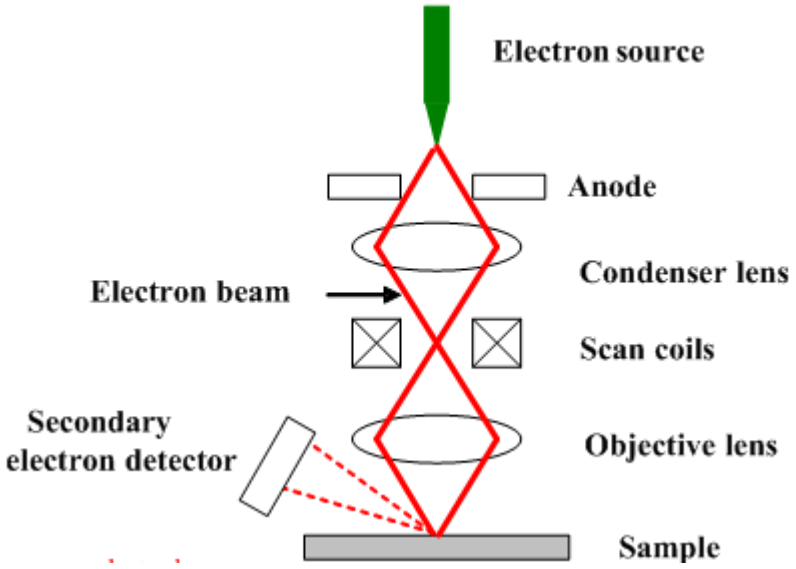

Fig 2.17 Schematic representation of SEM

2.5.6 Transmission electron microscopy (TEM)

In this study, a JEOL/JEM 2100 (200 kV) scanning transmission research electron microscope was used with a magnification 2000× to 1500000× and a resolution of point - 0.23 nm (LaB_6 Source). Experimental set up of a Transmission electron microscope is shown in Fig 2.18.

Fig 2.18 Experimental set up of TEM

Transmission electron microscopy (TEM) [72] is a microscopic technique which involves the transmission of a beam of electrons through a very thin sample to obtain information about the particular specimen. The electron beam interacts with the sample as it passes through and an image is formed which is then magnified and focussed onto an imaging device as shown in Fig 2.19. In a TEM, a monochromatic beam of electrons is accelerated through a potential of 40 to 100 kV and passed through a strong magnetic field that acts as a lens. In a TEM image, a resolution of around 0.2 nm can be obtained which is equal to the separation of two atoms in a solid. Imaging, measuring, modelling and manipulating matter in nanoscale range is achievable using a TEM instrument [87].

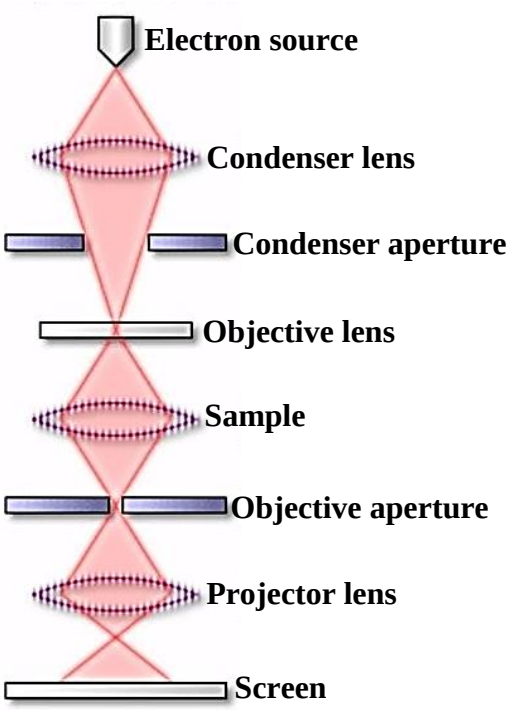

Fig 2.19 Schematic imaging set up of TEM

2.5.7 Atomic force microscopy (AFM)

Scanning probe microscopes (SPMs) are a family of instruments used for studying surface properties of materials from the atomic to the micron level [89]. The AFM is a type of SPM which consists of a microscale cantilever with a sharp tip (probe) at its end that is used to scan the specimen surface. The cantilever is typically silicon or silicon nitride with a tip radius of curvature of the order of nanometers. When the tip is brought into proximity of a sample surface, forces between the tip and the sample lead to a deflection of the cantilever according to Hooke's law [88]. Depending on the situation, forces that are measured in AFM include mechanical contact force, Van der Waals forces, capillary forces, chemical bonding, electrostatic forces, magnetic forces,

Casimir forces, solvation forces etc. The AFM schematic set up is given in Fig 2.20. All atomic force microscopes have five essential components [90]:

i. A sharp tip mounted on a cantilever spring
ii. A way of sensing cantilever's deflection (usually laser beam deflection system)
iii. A feedback system to monitor and control the deflection.
iv. A mechanical scanning system (usually piezoelectric) that moves the sample with respect to the tip in a raster pattern.
v. A display system that converts the measured data into an image.

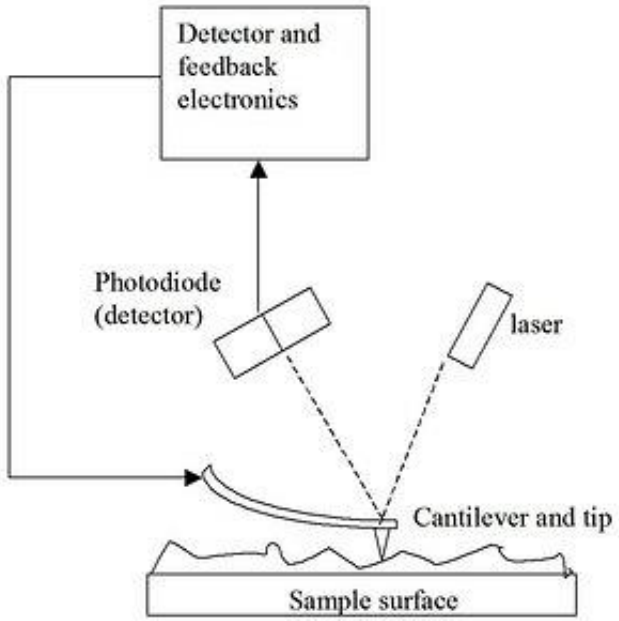

Fig 2.20 Schematic representation of AFM setup

The AFM can be operated in a number of modes, depending on the application. In general, possible imaging modes are divided into static (also called contact) modes and a variety of dynamic (or non-contact) modes where the cantilever is vibrated. For cases where a sample of low moduli may be damaged by the dragging of an AFM tip across its surface, another mode of AFM operation is available: intermittent-contact mode or tapping mode. Intermittent-contact atomic force microscopy (IC-AFM) is similar to NC-AFM, except that for IC-AFM the vibrating cantilever tip is brought closer to the sample so that at the bottom of its travel it just barely hits, or "taps," the sample.In this particular work, the morphology and topography of the PZT films developed using

ELD and EPD techniques were studied using an AFM set up of Bruker Instruments (Fig .2.21) AFM was done in tapping mode utilising line scan profilometry.

Fig 2.21 AFM experimental set up

2.5.8 Thickness measurements using coating thickness gauge

In this particular work, thickness measurements of the prepared PZT films were carried out using a coating thickness gauge (Surfix Easy, PHYNIX Gmbh and Co. KG) with a measurement range of 1 – 1000 µm with a resolution of 1 µm. The instrument is used to determine thickness of coatings/films deposited/applied on metallic substrates. The instrument consists of a precision sensing element and a probe attached to it as shown in Fig 2.22.

Fig 2.22 Coating thickness gauge [91]

This technique is used to determine the thickness of coatings prepared on ferrous as well as on non-ferrous metallic surfaces. The sensor element consists of an exciter coil

wrapped around an iron core through which a current is passed. The coating thickness gauge works on two basic principles mainly:

a. Magnetic induction
b. Eddy current mechanism

The magnetic induction method is used to measure thickness of coatings on ferrous substrates. There are two different coils. Here a low frequency alternating current is circulated through the first coil which then generates a magnetic field in the air space around the poles. When the pole approaches any ferrous substrate, the magnetic field is amplified which in turn generates a voltage in the second coil. The voltage generated is then electronically evaluated and digitally displayed as the coating thickness.

In the eddy current method, only single coil is used and a high frequency alternating current flows through it. This generates an alternating field around the coil and when it approaches a non-ferrous metal an eddy current is induced in the metal which causes a change in the inductance of the coil. This inductance is then electronically evaluated and displayed as coating thickness.

There are combination probes available which can be used on both ferrous as well as on non-ferrous substrates. The measuring procedure is selected according to the base material and thickness is displayed accordingly. In this particular work, a combination probe was used for PZT film thickness measurement.

2.5.9 Dielectric studies

Ferroelectric materials are generally very good dielectric materials. Further, from the application point of view, dielectric constant and dielectric loss (tan δ) are important parameters that provide information about a material which decide its suitability for various purposes [92, 93, 94]. In this work, both these parameters were determined for a frequency range 1 kHz to 1 MHz using Precision impedance analyser (Wayne Kerr 6500 B) instrument shown in Fig 2.23.

(a) (b)

Fig 2.23 Instrumentation for dielectric studies: (a) Impedance analyser (b) Sample holder

(i) Dielectric constant

For any material, the ratio of the capacitance of a capacitor with that particular material as dielectric, to the capacitance of the same capacitor with vacuum for dielectric is known as the dielectric constant of that particular material. It is a measure, therefore, of the amount of electrical charge the material can withstand for a particular electric field strength and is the electrical equivalent of relative magnetic permeability. The dielectric constant is the ratio of the permittivity of a substance to the permittivity of free space. The capacitance, C for a parallel plate capacitor is given by

$$C = \varepsilon_0 \frac{A}{d} \tag{2.3}$$

where ε_0 is the permittivity of free space, 8.85×10^{-12} F/m, A is the area of sample and d is separation between the two electrodes.

When a dielectric (electrical insulator) fills the space between the plates, the capacitance of the capacitor is increased by a factor, ε_r, which is called the dielectric constant of the dielectric material. Therefore, for a parallel plate capacitor with a dielectric in between the capacitance plates, the capacitance, C is given by

$$C = \varepsilon_0 \varepsilon_r \frac{A}{d} \tag{2.4}$$

Thus the energy stored in a capacitor of a given volume at a given voltage is increased by a factor of the dielectric constant when the dielectric material is present. For normal substances, the value of ε_r is low, usually under 5 for organic materials and under 20 for most inorganic materials. Generally, ferroelectric ceramics have much higher ε_r, typically several hundred to several thousands.

(ii) Dielectric loss factor (tan δ)

The dielectric loss factor (dielectric dissipation factor), tan δ, for a ceramic material is the tangent of the dielectric loss angle, tan δ. It is determined by the ratio of effective conductance to effective susceptance in a parallel circuit, measured by using an impedance bridge. Dielectric loss is related to non-instantaneous polarisation due to the inertia of charges and absorption of electrical energy by the dielectric. Polarisation is time dependent as a new charge distribution will take time to establish. The final static charge distribution forms after the instantaneous atomic and ionic polarisations.

2.5.10 Hysteresis studies

A defining, and the most important, characteristic of ferroelectric materials is polarization reversal (or switching) by an electric field [95]. It is found that the natural state of a ferroelectric material is a multi-domain state. Application of an electric field will reduce (in ceramics) or completely remove (in crystals) domain walls. One consequence of the domain-wall switching in ferroelectric materials is the occurrence of the ferroelectric hysteresis loop. An ideal hysteresis loop is symmetrical, so the positive and negative coercive fields and positive and negative remnant polarizations are equal. The coercive field, spontaneous and remnant polarization, and shape of the loop may be affected by many factors including the thickness of the sample, presence of charged defects, mechanical stresses, preparation conditions, and thermal treatment.

In addition to the polarization-electric field (P-E) hysteresis loop, the polarization switching by electric field in ferroelectric materials leads to the strain-electric field (S-E) hysteresis which resembles the shape of a butterfly and is called the butterfly loop. This butterfly loop occurs due to three types of effects. One is the normal converse piezoelectric effect of the lattice, and the other two are due to switching and movement of domain walls. Typical P-E hysteresis loops and butterfly loops are shown in Fig 2.24.

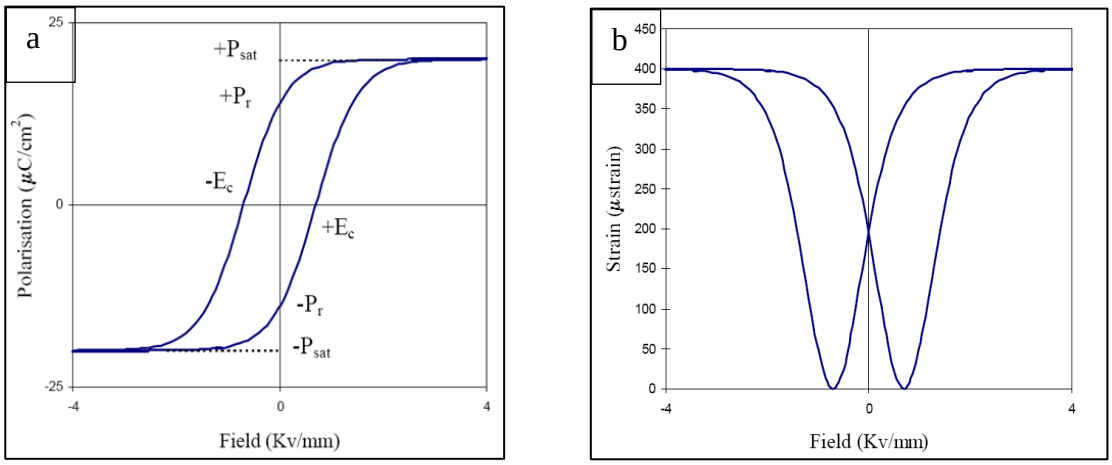

Fig 2.24 (a) P-E hysteresis loop for a ferroelectric material, (b) S-E loop exhibiting a butterfly loop [95]

The measurement methods used have been developed over the years with advances in electronics hardware and software. The most often quoted method of hysteresis loop measurement is based on a paper by Sawyer and Tower [93, 94]. A schematic of the experimental setup is shown in figure 2.25. Here the field applied across the sample is attenuated by a resistive divider, and the current is integrated into charge by virtue of a large capacitor in series with the sample. Both these voltages are then fed into the X and Y axes of an oscilloscope to generate the P-E loop. The applied voltage was usually a sinusoid at mains frequency as this was the simplest method to generate the required voltage and current.

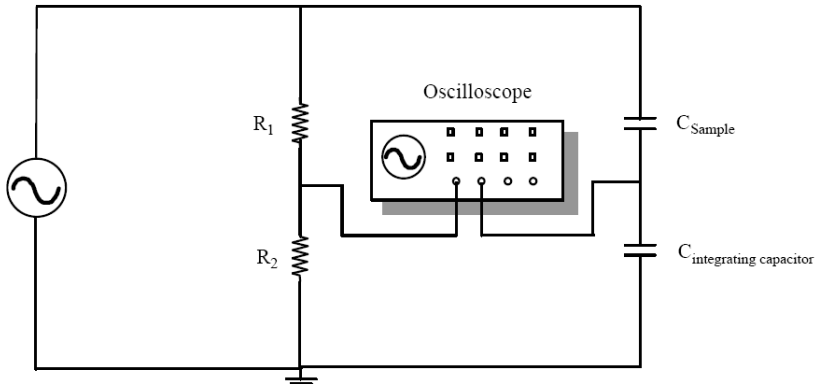

Fig 2.25 Sawyer Tower circuit

Most of the current hysteresis measurement uses a modified Sawyer-Tower circuit where the initial wave shape is formed by the function generator, which is then amplified by the high voltage amplifier, which sends the amplified waveform to the sample. The current passing through the sample is then converted to a voltage, which is captured on a digital storage oscilloscope, along with the monitor output from the high voltage amplifier, and waveforms from any displacement measuring devices connected. The captured waveforms are then sent to the PC for subsequent analysis. In this work hysteresis data was obtained using a standard ferroelectric PE loop tracer (Radiant Technologies, precision 4 kV, HVI).

2.5.11 d_{33} measurement

A piezometer measures the d_{33} value of the piezoelectric sample and gives an idea about the polarisation and hence piezoelectricity induced in the samples. A Piezotech piezometer (Fig 2.26) is used in this study.

Fig 2.26 Piezometer used for measuring piezo properties

The sample is clamped on the holder of the piezometer and subjected to a low frequency force. Processing of the electrical signals from the sample, and comparison with a built-in reference, enables the system to give a direct reading of d_{33} value, which is one of the most important and useful parameters in evaluating the material. This is a material coefficient representing charge developed per unit force in the direction of polarisation.

The method of operation of this type of d_{33} meter is sometimes called the "quasi-static" or "Berlincourt" method. A key principle is that the test frequency is low compared with any likely system or sample resonances, yet high enough that a conclusive measurement can be made in a few seconds.

2.6 PZT FILM SENSOR FABRICATION AND UNDERWATER EVALUATION

PZT film (of thickness 50 µm) deposited using EPD on a stainless substrate (of thickness 250 µm) over an area of 50 × 50 mm was taken as the base material. Silver epoxy paste was applied on the top of the film as the top electrode and the SS substrate was kept as the bottom electrode. The film was poled at an effective voltage of 2 kV/mm at 150°C for a time of 12 hours by a contact poling technique. The PZT film was then connected to the preamplifier (- 44 dB gain) and this whole assembly was encapsulated in a soft epoxy matrix (Araldite AY103 + Aradur 76 BD, Mixing ratio – 1:1.3), and the PZT film sensor fabricated is shown in Fig 2.27.

Fig 2.27 PZT film sensing element

2.6.1 Receiving sensitivity measurements

Underwater acoustic measurements were carried out in a small tank (4×3×3 m) and the schematic of the set-up is shown in Fig 2.28. Acoustic projector was lowered at the centre of tank at a depth of 1.5 m and the PZT sensor and a standard hydrophone were lowered at the same depth but on opposite sides of the projector. Impulse signal generated by the function generator was first amplified by an L-6 power amplifier. This amplified signal was then fed to the projector for acoustic signal generation. The signals received from the standard hydrophone and PZT sensor were then fed to a nexus preamplifier for filtering and signal amplification. Receiving sensitivity (RS) was then calculated by the equation,

$$RS\ of\ sensor = \frac{Voltage\ output\ of\ sensor}{Voltage\ output\ of\ std\ hydrophone} * RS\ of\ std\ hydrophone \qquad (2.5)$$

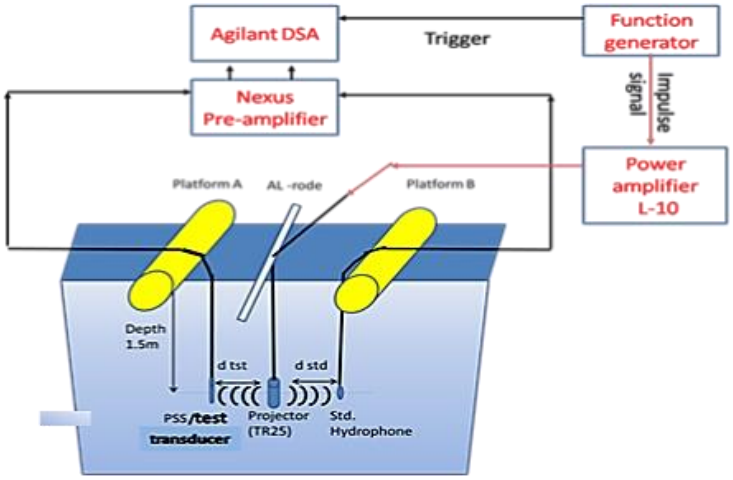

Fig 2.28 Receiving Sensitivity (RS) measurement setup

2.6.2 Directivity measurements

Receiving beam pattern measurement set up is shown in figure 2.29. Tone burst signal (4 kHz) generated by function generator is amplified by L-6 power amplifier and used for driving projector for acoustic transmission. The received signal from the sensor (Hydrophone) was subjected to amplification and signal conditioning using Nexus pre amplifier. The amplified signal was then monitored using a Lab-view controlled oscilloscope and the numerical values were displayed in the Lab view GUI (Graphical User Interface).

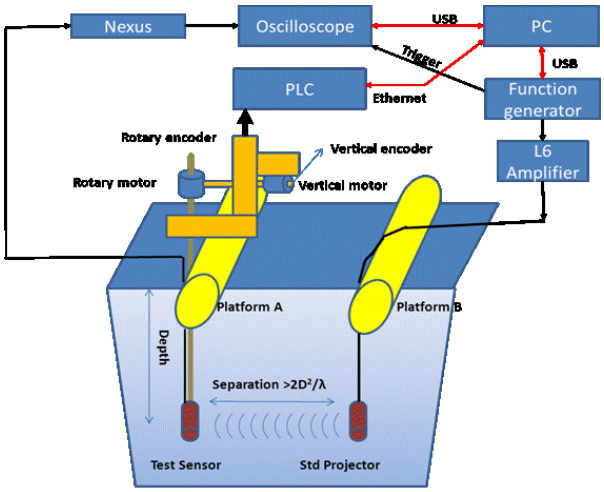

Fig 2.29 Receiving beam pattern measurement setup

This measurement was repeated for different angles using an automated rotary system controlled by lab-view program. Angular resolution and speed of the rotation were set according to the requirement. After completing the rotation, the peak response voltage was measured and the beam pattern plot of the corresponding sensor was displayed. Beam pattern plot is a normalised directional response of a sensor, expressed in dB and normalisation constant is the peak response voltage measured during the rotation. Angular separation between -3 dB points will give beam width of the sensor.

Chapter – 3

ELECTROLYTIC DEPOSITION OF PZT

3.1 INTRODUCTION

Investigations on complex ceramic oxides such as lead zirconate titanate (PZT) thin and thick films has attracted the attention of researchers around the world due to its enormous application in sensors, actuator and micro electro mechanical systems. Much studies are reported on PZT film fabrication using other techniques such as sputtering, pulsed laser deposition, sol gel method, vapour deposition, etc. however, the electrochemical route is not explored much. Electrochemical deposition or Electrolytic deposition (ELD) is a simple, fast and cost effective process which can provide deposits with effective control on the structural and morphological characteristics. This process allows in situ deposition on selected areas of the substrate/complex geometry surfaces and facilitates low temperature sintering. In recent years, many advantages provided by the ELD method in growing thin films has stimulated the research for the development of many complex ceramic oxides via electrolytic deposition route.

ELD of PZT is a bottom up approach wherein it is deposited as a thin or thick film/coating on to a substrate/electrode from the corresponding electrolyte solution when an electric current is passed through the system. Here the synthesis occurs at the electrode surface within the electrical double layer. An electrochemical process is normally a low temperature method involving an oxidation or reduction reaction. The constitution of the electrolyte bath decides the film composition. An electrochemical synthesis depends on the various reaction parameters:

i. Selection of electrode

ii. Selection of electrolyte/solvent

iii. Selection of pH, temperature, electrolyte composition etc.

iv. Mode of control: potentiostatic or galvanostatic.

There are different electrolytic techniques used in inorganic solid state chemistry which are: (1) Electromigration, (2) Electrolysis of fused salts, (3) Electrogeneration of the base by cathodic reduction, (4) Anodic oxidation, and (5) Alternate current synthesis.

Electrogeneration of base is an important technique which has a widespread use in plating industry to render superior quality metal coatings, synthesis of electrode materials for secondary cells etc. The method of base generation (or cathodic electrolytic deposition) was first explained by Switzer in his work utilised for the plating of cerium oxide films [96]. This method has been successfully utilised to deposit metal oxides, metal hydroxides and metal phosphates. Using this method, electric current is passed through a metal salt (usually nitrates or chlorides) solution and resultantly the metal is deposited at the cathode. Various chemical reactions [97] which mark the base generation in the cathodic deposition process includes the reactions that generate OH^- and that consume H^+ which results in a small increase in pH at the electrode surface. Cathodic reactions which produce OH^- are the reduction of water and dissolved oxygen.

$$2H_2O + 2e^- \longleftrightarrow H_2 + 2OH^- \quad (3.1)$$

$$NO_3^- + H_2O + 2e^- \longleftrightarrow NO_2^- + 2OH^- \quad (3.2)$$

$$NO_3^- + 6H_2O + 8e^- \longleftrightarrow NH_3 + 9OH^- \quad (3.3)$$

$$O_2 + 2H_2O + 4e^- \longleftrightarrow 4OH^- \quad (3.4)$$

$$ClO_4^- + H_2O + 2e^- \longrightarrow ClO_3^- + 2OH^- \quad (3.5)$$

$$ClO_4^- + H_2O + 8e^- \longrightarrow Cl^- + 8OH^- \quad (3.6)$$

Reactions which consume H^+ ions near to the electrode includes:

$$H^+ + e^- \longrightarrow H_{ads} \quad (3.7)$$

$$2H^+ + 2e^- \longrightarrow H_2 \quad (3.8)$$

$$NO_3^- + 2H^+ + 2e^- \longrightarrow NO_2^- + H_2O \quad (3.9)$$

$$NO_3^- + 10H^+ + 8e^- \longrightarrow NH_4^+ + 3H_2O \quad (3.10)$$

The method of ELD by base generation has been very much useful in the synthesis of nanoscale powders and good quality films/coatings. The synthesis involves galvanostatic or potentiostatic reduction of the respective mixed metal nitrate/chloride solutions at various current densities. This results in the formation of colloidal particles of the hydrolysed compounds of the respective metals on the cathode which after heat treatment or sintering yield the corresponding oxides. Different compounds have been successfully prepared by this technique over the years which includes ZrO_2, TiO_2, $ZrTiO_4$, Al_2O_3, PZT, CrO_3, CeO_2 etc.

This chapter deals with deposition of PZT ceramics using the base reduction/cathodic electrolytic deposition technique. It is tried to overcome the brittle ceramic nature of PZT slabs by depositing it as a film/coating on flexible metallic foils (stainless steel and titanium) for conformal sensor applications. The effect of different key parameters like electrolyte medium (aqueous and non-aqueous), current density, time of deposition, sintering temperature and heating time are extensively studied and discussed. The morphology and topography examination of the films by scanning electron microscopy (SEM) and Atomic Force Microscopy (AFM), PZT phase formation using X-ray diffraction (XRD) and Raman spectroscopic studies along with the dielectric and piezoelectric characterisation is comprehensively detailed. Moreover, in this chapter, PZT electrochemical deposition using pulsed potential/current techniques have been discussed.

3.2 AQUEOUS ELECTROLYTIC DEPOSITION (ELD) OF PZT

Aqueous ELD is the conventional method for deposition of various materials. Various research papers have reported the synthesis of PZT by electrolytic deposition using aqueous electrolytes [48 – 53]. The method of aqueous electrolytic deposition can be used for the formation of deposits and films of various individual oxides (Al_2O_3, CeO_2, ZrO_2 [42 – 47, 97, 98], CrO_3 etc.) and complex oxide compounds (PZT [48], $BaTiO_3$, $YBa_2Cu_3O_{7-x}$ etc.). Ren et al. [52] and Matsumoto et al. [53] reported a method for synthesis of PZT by electrochemical reduction technique. Zhitomirsky et al. [48 – 50] followed a peroxo precursor route where H_2O_2 was added to the electrolyte solution to co-deposit peroxo complexes of Pb, Zr and Ti which up on sintering rendered PZT films. Although the method of synthesis for PZT aqueous electrolytic deposition has been reported, the detailed chemical and physical characterisation has not been covered elsewhere.

When compared to simple metal oxide ELD, deposition of complex ceramic oxides like PZT is tedious task. PZT being a mixture of different oxides of lead, zirconium and titanium, each component has different rates of deposition which can seriously affect the final stoichiometry of the deposit. Some problems can arise when depositing PZT from an aqueous electrolyte. Titanium salts when dissolved in water precipitate out as titanium hydroxide, also titanium salts are mostly unstable. These issues can be eliminated by the addition of peroxide compound in the electrolyte. Titanium ions can form peroxo complexes on reaction with peroxides which are mostly

stable in aqueous conditions and paves the way for trouble-free ELD of various complex oxides.

In this study cathodic electrodeposition was carried out to obtain PZT films. The aqueous electrolyte solution was prepared by careful mixing of compounds such as lead nitrate, zirconium chloride hexa hydrate, titanium tetra chloride and hydrogen peroxide in de-ionised water in the ratio 1:0.52:0.48:10. The concentration of lead nitrate was taken as 0.005 M and the pH of the electrolyte was found to be in the range 2 – 2.5. The platinum electrode was taken as the anode, connected to the positive terminal of the power supply. The PZT deposit or film was obtained on the cathode (negative electrode) which is the substrate (titanium & stainless steel foils). The details/grade of the chemicals, instruments and the process have been given in the Chapter 2, in the section 2.2. Depositions were done at a temperature of 2 °C at galvanostatic conditions for current densities ranging from 10 to 40 mA/cm^2. Low temperatures were usually preferred for aqueous electrolytes. Aqueous electrolytes due to their increased conductivity, had very high rate of deposition which can lead to poor film quality; so in order to exercise proper control over the deposition process, it was carried out at lower temperatures. After deposition the PZT film obtained (green deposit) was amorphous which was then sintered at 500 °C for 1 hour to obtain perovskite (crystalline PZT). The PZT films prepared by aqueous ELD are shown in Fig 3.1.

Fig 3.1 Aqueous PZT films, (a) Green deposit, (b) Sintered deposit

3.2.1 Reaction mechanism of aqueous deposition

The PZT ELD process started with base generation at the cathode. H^+ ions are simultaneously consumed at the anode. Both these reactions have been given in section 3.1 equations (3.1 – 3.10). Next step was the dissociation of the salts to the corresponding ions in the electrolyte.

$$Pb(NO_3)_2 \longrightarrow Pb^{2+} + 2NO_3^- \qquad (3.11)$$

$$ZrOCl_2.nH_2O \longrightarrow ZrO^{2+} + 2Cl^- + nH_2O \quad (3.12)$$

$$TiCl_4 \longrightarrow Ti^{4+} + 4Cl^- \quad (3.13)$$

The ions formed get combined with the hydrogen peroxide to form a peroxo complex which was then hydrolysed by the base (OH^-) to form a peroxo hydrate deposit on the cathodic substrate.

$$Pb^{2+} + H_2O_2 + (n-2)H_2O \longrightarrow PbO_2(OH)_{n-2}^{(2-n)+} + nH^+ \quad (3.14)$$

$$PbO_2(OH)_{n-2}^{(2-n)+} + mOH^- + kH_2O \longrightarrow PbO_2(H_2O)_y \quad (3.15)$$

$$ZrO^{2+} + H_2O_2 + (n-2)H_2O \longrightarrow [ZrO_3(OH)_{n-2}]^{(2-n)+} + nH^+ \quad (3.16)$$

$$[ZrO_3(OH)_{n-2}]^{(2-n)+} + mOH^- + kH_2O \longrightarrow ZrO_3(H_2O)_y \quad (3.17)$$

$$Ti^{4+} + H_2O_2 + (n-2)H_2O \longrightarrow [TiO_2(OH)_{n-2}]^{(4-n)+} + nH^+ \quad (3.18)$$

$$[TiO_2(OH)_{n-2}]^{(4-n)+} + mOH^- + kH_2O \longrightarrow TiO_3(H_2O)_y \quad (3.19)$$

The peroxo hydrated deposit was the film obtained on the cathode as the green deposit. It was then sintered at 500 °C to obtain crystalline single phase PZT deposit. During sintering or heat treatment, the peroxo hydrated deposit decomposes, water molecules were removed and gets converted into a single lead zirconium titanium oxide ceramic.

$$nPbO_2(H_2O)_y + nZrO_3(H_2O)_y + nTiO_3(H_2O)_y \longrightarrow nPbZrTiO_3 + n(x+y+z)H_2O + 5n/2\ O_2 \quad (3.20)$$

3.2.2 Effect of process parameters on aqueous deposition

An electrochemical reaction is dependent on different process parameters such as cathode/substrate selection, electrolyte composition, current density, duration/time of deposition etc. in order to obtain best results, all these above parameters need to be optimised by performing a large number trials/ experiments keeping in view the product requirements.

In this study, optimisation of process parameters such as (i) current density, (ii) time of deposition for electrolytic deposition of PZT were studied in aqueous electrolytes. The Faradaic Coating Efficiency (E_{ff}) for the ELD process was also determined and its variation for different current densities and time intervals were studied.

Faradaic Coating Efficiency (E_{ff}) which is also known as Current Efficiency [99, 100] can be defined as the ratio of actual weight of material deposited to the theoretical weight calculated by Faraday's laws (expressed in percentage) by the equation,

$$E_{ff} = \frac{W_{act}}{W_{th}} \times 100 \tag{3.21}$$

Where E_{ff} is the Faradaic Coating Efficiency, W_{act} the actual deposit weight and W_{th} is the theoretical weight of the deposit. The theoretical weight (W_{th}) can be calculated using Faraday's laws of electrolysis as,

$$W_{th} = \frac{Q\,M}{nF} \tag{3.22}$$

Where Q is the total electrolytic charge, M is the molecular weight of PZT, n is 2 for reactions (3.21) or (3.22), and F is Faraday's constant (96500 C).

Fig 3.2 shows the variation of PZT deposit weight and faradaic efficiency obtained at various current densities viz. (i) 10 mA/cm^2 (ii) 15 mA/cm^2 (iii) 20 mA/cm^{2,} (iv) 25 mA/cm^2 (v) 30 mA/cm^2 (vi) 40 mA/cm^2 for a constant time period of 5 minutes. The deposit weight as well as the faradaic efficiency of the ELD process showed a similar trend i.e. an initial increase and after reaching an optimum value it decreases. A maximum efficiency of 17 % was obtained at a current density around 15 mA/cm^2. The decrease in efficiency at higher current densities can be attributed to the higher rates of reaction and also due to the hydrogen bubbling phenomenon. As a result, the electrode surface gets blocked by hydrogen evolution which prevents further deposit formation [100].

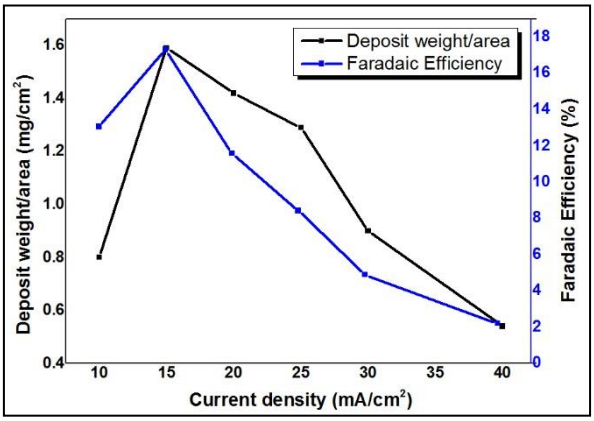

Fig 3.2 Deposit weight and faradaic efficiency vs. current density for aqueous deposition

It can be seen from the figure (Fig 3.2) that maximum deposit weight as well as maximum Faradaic efficiency were obtained at a current density of 15 mA/cm^2. Earlier, Ren et al. [52] obtained an optimum value of 20 – 30 mA/cm^2 for current density for PZT thin film deposition by electrochemical reduction in an electrolyte containing only constituent salts. However, effect of faradaic efficiency was not studied. The shift in optimum current density in this experiment may be probably due to the formation of peroxo complexes as it contains hydrogen peroxide.

The PZT deposition weight and faradaic efficiency have also been studied for different deposition time and the resulting plot is shown in Fig 3.3. It was found that the weight increases with time, reaches a maximum, after that slightly decreases and then remains constant. Maximum efficiency and deposit weight was obtained around 5 minutes. The slight decrease in weight (after 5 minutes) can be due to the relative decrease in adhesion of the deposit to the substrate as the film becomes heavy with the passage of time. As the weight gets saturated and remains more or less constant, consequently the efficiency should decrease (as observed in Fig 3.3.) with increasing time for intervals > 5 minutes.

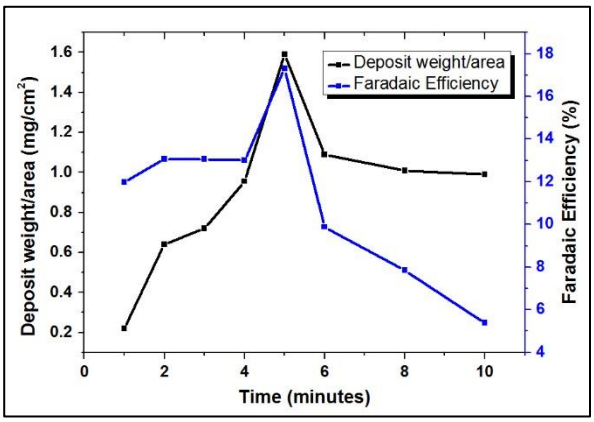

Fig 3.3 Deposit weight and faradaic efficiency vs. time for aqueous deposition

3.2.3 Morphology of the prepared PZT films

The surface morphology, microstructure and topography of the PZT films prepared using aqueous ELD process were characterised using optical microscope, SEM, TEM and AFM studies. The information about the film morphology, particle size, surface anomalies like cracking etc. can be obtained from SEM and TEM images, whereas AFM technique sheds light on the important aspects like surface roughness and topography of the film.

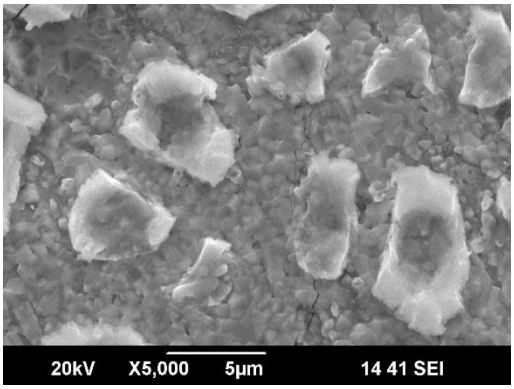

Fig 3.4 SEM of aqueous PZT on titanium surface

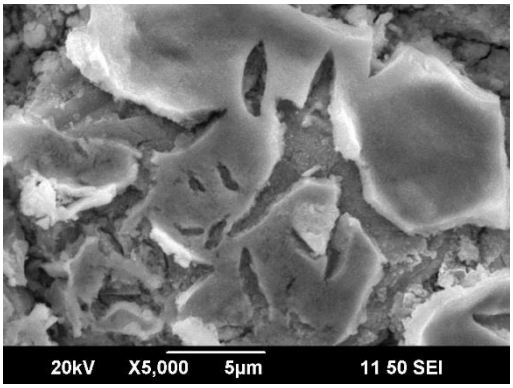

Fig 3.5 SEM of aqueous PZT on SS surface

Fig 3.4 and 3.5 shows the SEM images of PZT deposition obtained on titanium and SS foils respectively. It could be seen from the images that a more continuous or conformal deposition had occurred on titanium foil than that on SS. Crack formation of the PZT was also more prominent for films on SS substrates. Crack formation in the film could have occurred due to the mismatch in the thermal expansion coefficient of PZT and that of the substrate during high temperature sintering. The morphology of the obtained PZT films were similar to the work reported by Zhitomirsky et al. [49] where they deposited PZT on graphite substrates. Also it was found that adhesion of the PZT film on to the substrate was more proper for titanium foils in comparison with SS which could be due to the matching lattice parameters of PZT and titanium. The optical microscope images of the as prepared (green deposit) and sintered PZT films obtained for aqueous electrolytic deposition is given in Fig 3.6 and 3.7 respectively. Sintering at higher temperature (at 500 °C) removed adsorbed water and converted the amorphous material to a crystalline form.

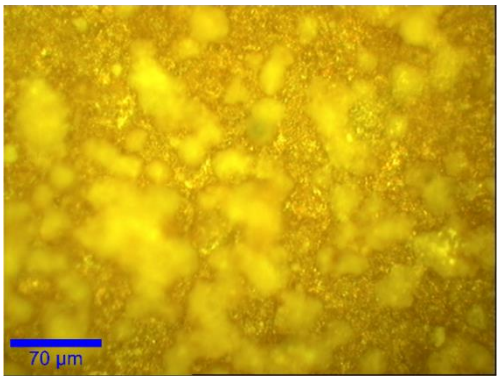

Fig 3.6 Aqueous PZT green deposit

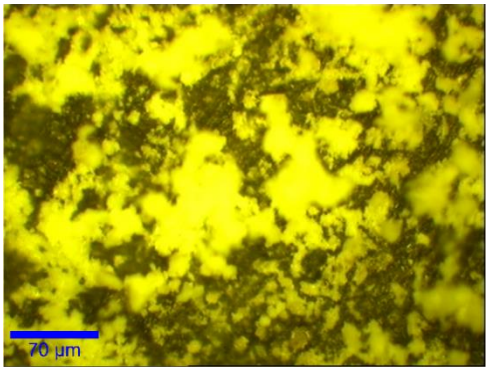

Fig 3.7 Sintered PZT film by aqueous ELD

Fig. 3.8 shows the AFM profile of the sintered PZT film prepared by aqueous ELD route.Tapping mode AFM was used with the area of scan taken as 1x1 μm^2. The surface/topography profile of the PZT film was obtained and it can be seen that the film is not very smooth. The maximum height obtained in the film was 208 nm which indicates that the average roughness is also very high. This may be attributed to the loosely bound PZT film which leaves the substrate making it free of deposit at some place resulting in an enhanced average roughness. Espitia Cabrera et al. [46] have demonstrated the electrolytic deposition of zirconia films with average surface roughness value of around 30 nm with the highest zone being 144 nm but the scanned area in that case was comparatively smaller and oxide deposition is a single oxide ZrO_2.

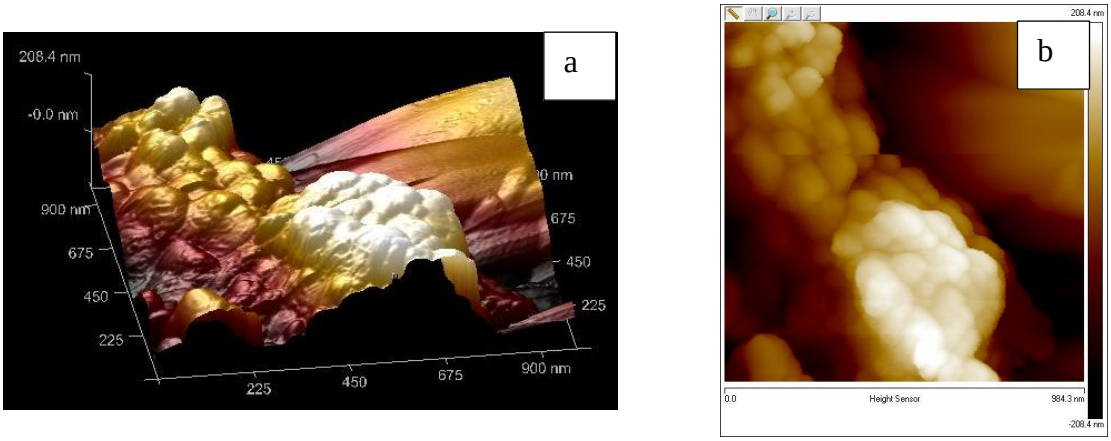

Fig 3.8 AFM of PZT film using aqueous ELD method: (a) 3D image, (b) 2D image

The microstructure of the aqueous deposited PZT particles were also observed by TEM and the corresponding images are shown in Fig 3.9. A transparent or bright field image micrograph was observed. Morphology analysis using these images clearly showed spherical nanostructured PZT particles with grain sizes in the range of 20 – 40 nm. The film was mostly composed of nanoparticle agglomerates of PZT ceramics.

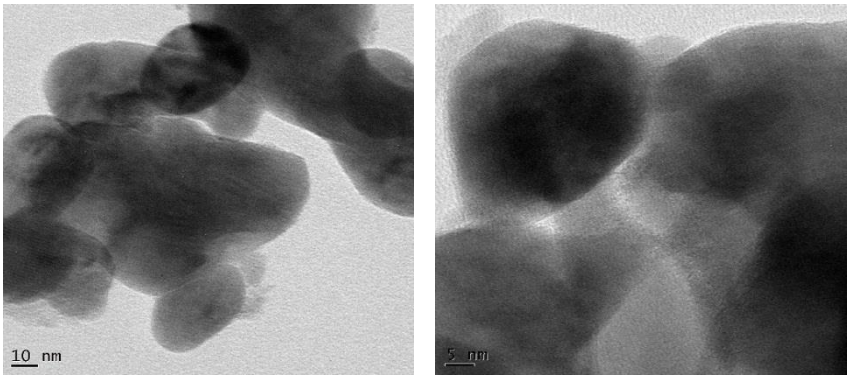

Fig 3.9 TEM images of aqueous PZT film

3.2.4 PZT crystal phase characterisation

The electrolytic deposition process generated PZT green deposit in a complex hydrated form which was in an amorphous state. In order to obtain PZT as a film in its crystalline perovskite form, a heat treatment or sintering method was usually adopted. During sintering, as a result of the thermal decomposition of the complex hydrated precursor, formation of PZT films was observed at 500 °C. Sintering is an indispensable step for ceramics after electrolytic deposition process, as it facilitates the crystalline phase formation of the corresponding film or coating. Sintering also helps in removing the adsorbed water molecules and densification of the green deposit by reducing the porosity and also enhances the grain size of the material. In order to ascertain and analyse the crystal structure and phase formation of the PZT film produced, techniques such as XRD and Raman spectroscopy were utilised in this particular work.

3.2.4.1 XRD studies

In this study sintering of the PZT films was carried out at 500 °C for a time of one hour. In order to study the effect of sintering temperature on the phase formation of PZT, XRD patterns were recorded before and after deposition i.e. for green deposit as well as for sintered films. Fig 3.10 and 3.11 show the X-ray diffraction patterns of green and sintered (at 500 °C) respectively. It can be seen from the diffractograms that the green deposit shows very broad and undefined peaks which was mainly due to its amorphous nature. However sintered deposit was found to give sharp and well-defined peaks at 2θ values; 22.557°, 28.143°, 31.750°, 44.417°, 51.488° and 55.733° which indicates a perovskite crystalline structure of PZT (JCPDS card No. 00 - 033 - 0784). The results were in accordance with earlier works reported for aqueous deposition of PZT [42]. The particle size of the PZT coating was calculated using Scherrer formula (3.23) and was found to be 13 nm.

$$D = \frac{k\lambda}{FWHM\ Cos\theta} \tag{3.23}$$

where k is Scherrer constant, ~ 0.89, FWHM is the full width at half maximum of the reflection peak that has the same maximum intensity in the diffraction pattern, λ is the wavelength of X-rays, and θ is the diffraction angle.

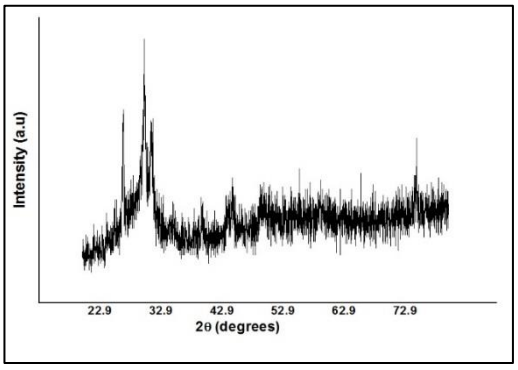

Fig 3.10 XRD of an aqueous PZT green deposit

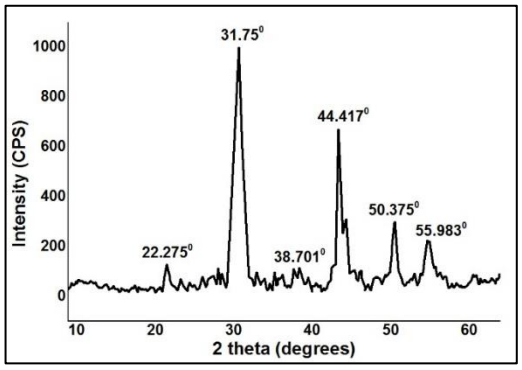

Fig 3.11 XRD of sintered aqueous PZT film

3.2.4.2 Raman spectroscopy studies

PZT being a solid solution of $PbZrO_3$ (rhombohedral, antiferroelectric) and $PbTiO_3$ (tetragonal, ferroelectric), rhombohedral and tetragonal phases coexist at Morphotropic Phase Boundary (MPB) [76] and this phase is very essential for the PZT formed for practical applications. Raman spectroscopy helps in studying the phase formation of the PZT films [101,102, 103]. Frantti et al. [104] reported that PZT can be represented by the 12 optical modes at the centre of the Brillouin zone. These modes are simplified as $3T_1u+T_2u$ in the cubic paraelectric phase and can be a doubly degenerate TO (transverse) mode or a single LO (longitudinal) mode. T_2u mode transforms into $E+B_1$ in the tetragonal system and A_2+E in the rhombohedral system which are non-active for infrared (IR). The T_1u modes translates into A+E which is both IR and Raman active.

Fig 3.12 and 3.13 show the room temperature Raman spectrum of the PZT green deposit and that of sintered film respectively. It can be seen from the figures that the two spectra showed a different pattern with respect to various peaks. Green deposit peaks were mostly broad which indicates the lack of particular symmetry or crystal structure. But it was clear from the spectra of the sintered PZT film that tetragonal as well as rhombohedral peaks were present. Major rhombohedral peaks found were 150 cm^{-1} A_1(TO), 204 cm^{-1} A_1(LO) & E(TO) and 324 cm^{-1} A_1(TO). Tetragonal peaks obtained were 604 cm^{-1} $A_1(TO)_T$ and 694 cm^{-1} $E(LO)_T$. Liang Ting et al. [105] have reported that $E+B_1$ (silent mode) at 285 cm^{-1} usually represents a rhombohedral – tetragonal coexistence phase and this is the most significant peak of PZT, in Raman spectra. It is evident that this rhombohedral – tetragonal coexistent peak was present in both the

spectra obtained i.e. for green and also sintered PZT aqueous films. The results from Raman spectra also corroborated the results obtained from X-ray diffraction.

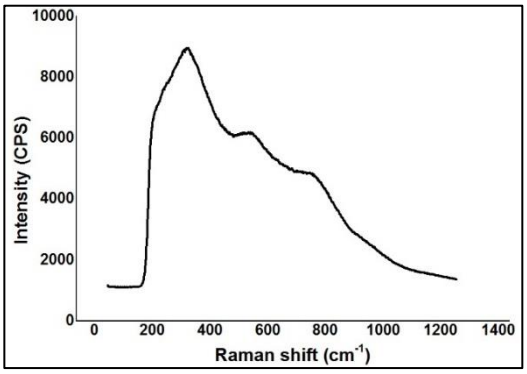

Fig 3.12 Raman spectra of green aqueous PZT film

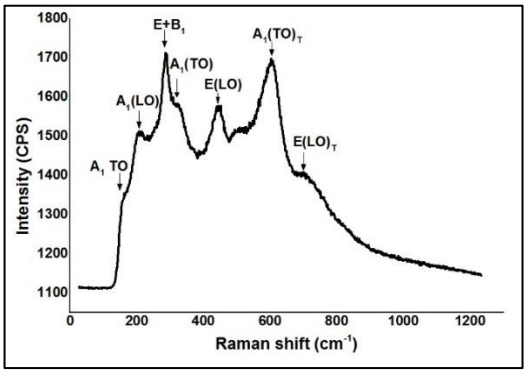

Fig 3.13 Raman spectra of sintered aqueous PZT film

3.3 NON-AQUEOUS ELECTROLYTIC DEPOSITION (ELD) OF PZT

Most of the electrochemical studies on PZT, other ceramics or any individual oxides reported till now have utilised the aqueous electrolyte method. Electrolyte solutions based on water have been considered ideal for electrochemical applications due to the high polarity and dielectric constant. Water thus dissolves a large variety of salts giving highly conducting solutions of low resistivity. Even though aqueous electrochemical deposition is the widely accepted or conventional technique used, it is found to have certain limitations/disadvantages. It was found that water as an electrochemical medium can result in adsorbed water in deposits which cause problems like porosity, non-uniformities or cracks in the film after sintering. Moreover, the electrochemical window of water is too narrow which limits its use for depositing materials which are oxidised at higher potentials. As a result, there is an emerging interest shown by researchers all over the world for an alternate electrolyte system which can be used to overcome the above limitations. Non aqueous electrolyte systems can be mainly divided into five sub-groups:

i. Liquid solutions based on organic and inorganic solvents
ii. Liquid systems based on molten salts (ambient and high temperature)
iii. Ionically and electronically conducting polymers
iv. Solutions based on liquefied gases
v. Conducting solids (doped oxides and glass)

In this work, non-aqueous electrolyte systems based on inorganic solvent such as Dimethyl sulphoxide (DMSO) was selected for deposition of PZT films, due to the following reasons.

i. Potential electrolyte for electrochemical deposition.
ii. Not much studies were reported with this medium.

Non-aqueous [106] electrolyte systems can be used in order to reduce cracking or porosity and can result in superior quality electrochemical deposits or films. Earlier Gheorgies [55] studied the electrodeposition of $ZrTiO_3$ coatings from a methanol-water electrolyte system. Also, pure dimethyl formamide (DMF) and mixed DMF-water systems [54] have been used for the deposition of ZrO_2, TiO_2, Y_2O_3 and $PbZrO_3$ films. Bhattacharya et.al [56, 57] had demonstrated the feasibility of PZT deposition using DMSO based non-aqueous system however, optimisation of process parameters, detailed material characterisation, dielectric and piezoelectric studies were not reported. Furthermore, a detailed study with respect to topography, dielectric and hysteresis studies of PZT were not reported in literature for aqueous as well as non-aqueous medium to the best of our knowledge.

DMSO is a polar aprotic solvent having a dielectric constant value of 46.6. In these type of solvents, conductivity is achieved by the dissolution of the salts and the appropriate charge separation of the dissolved species, allowing free migration under electric field. The deposition process starts with the preparation of electrolyte solution. The detailed description of the grade of the chemicals, instruments and the process is given in Chapter 2 (section 2.2). The substrates were titanium and SS foils which were used as the cathode/working electrode and platinum was used as the anode/counter electrode. The electrolyte solution was prepared by careful mixing of compounds such as lead nitrate, zirconium chloride hexa hydrate, titanium tetra chloride DMSO in the ratio 1:0.52:0.48. The concentration of lead nitrate was taken as 0.03 M. The non-aqueous deposition was carried out at ambient temperature at galvanostatic conditions for current densities ranging from 10 to 35 mA/cm^2. The reaction was exothermic and non-aqueous deposition process occurred at a higher voltage range when compared to aqueous due to the low conductivity of the DMSO solvent. Similar to aqueous ELD, the PZT green deposit obtained by non-aqueous ELD was also amorphous which should be sintered at higher temperatures (here taken as 500 °C) for converting to a crystalline film. The images for PZT films prepared by non-aqueous ELD is shown in Fig 3.14.

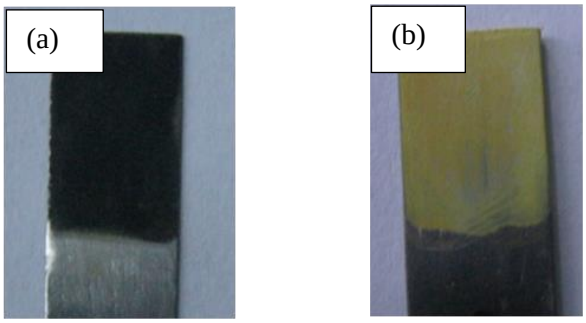

Fig 3.14 Images of non-aqueous PZT films, (a) Green deposit, (b) Sintered deposit

3.3.1 Reaction mechanism of non-aqueous deposition

The non-aqueous deposition similar to aqueous deposition is initiated with a base generation. Base generation requires water for the reactions to take place. For non-aqueous ELD water of crystallisation present in the salts were utilised for this purpose. The reactions up to base generation, at cathode, anodic reactions and dissociation of salts (3.1 – 3.13) were similar for both aqueous and non-aqueous ELD of PZT.

In non-aqueous deposition using DMSO electrolyte, titanium salts were stable and hence hydrogen peroxide is not required for the deposition process. Here, all the metal ions such as Pb^{2+}, Zr^{4+} and Ti^{4+} were deposited at the electrode as their respective hydroxides which were then converted to oxides during sintering. The non-aqueous deposition mechanism is shown below;

$$Pb^{2+} + 2OH^- \longrightarrow Pb(OH)_2 \quad (3.24)$$

$$ZrO^{2+} + H_2O \longrightarrow Zr(OH)_2^{2+} \quad (3.25)$$

$$Zr(OH)_2^{2+} + 2OH^- \longrightarrow Zr(OH)_4 \quad (3.26)$$

$$Ti^{4+} + 4OH^- \longrightarrow Ti(OH)_4 \quad (3.27)$$

Dehydration and formation of a complex oxide,

$$Pb(OH)_2 + Zr(OH)_4 + Ti(OH)_4 \longrightarrow PbZrTiO_3 + 5H_2O + O_2 \quad (3.28)$$

In DMSO the base generation is limited and occured only from the water of hydration present in constituent salts. In addition, insoluble reduction products of trace H_2O, O_2 and CO_2 precipitated on the electrode. Therefore, the mechanism of formation of peroxo complex was not present in the case of non-aqueous electrodeposition. The reaction mechanism of non-aqueous ELD is not given in detail in literature and the above mechanism was proposed based on the analysis of the results obtained in this work.

Moreover, the role of DMSO in electrochemical process was not understood and there was no mention of it in the literature. Hence, elemental analysis of the electrolyte solution was carried out before and after the deposition of PZT, mainly for the elements such as sulphur and carbon which were present in the solvent DMSO. Elemental analysis was carried out using CHNS analysis and the results are given in Table 3.1. From the results, it is clear that the amount of carbon and sulphur remained unchanged before and after the electrochemical deposition process. Thus, it can be assumed that DMSO was not involved in the electrochemical reaction process but only acted as a medium for ion transport and deposition.

Table 3.1 CHNS Element analysis results of non-aqueous electrolyte

Sample No	Sample Name	N%	C%	S%	H%	Sample Weight, mg
1	Electrolyte (Before deposition)	1.06	29.29	38.23	7.50	3.77
2	Electrolyte (After deposition)	0.63	29.74	38.39	7.49	6.54

3.3.2 Effect of process parameters on non-aqueous deposition

Although non-aqueous ELD of PZT was already reported, much research work were not carried out for the optimisation process parameters, characterisation, evaluation of piezo properties etc. Non-aqueous ELD is a promising research area for electrodeposition due to its many advantages over other mainstream methods. Optimisation of process parameters such as current density, duration/time of deposition etc. was essential to obtain good PZT deposit.

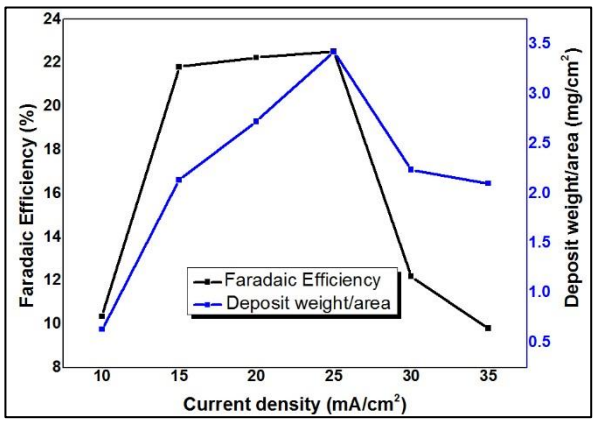

Fig 3.15 Deposit weight and faradaic efficiency vs. current density for non-aqueous deposition

Fig.3.15 shows the effect of current density on the weight as well as the faradaic efficiency of the PZT deposition obtained on stainless steel substrates. Deposition at various current densities viz. 10 mA/cm^2 (ii) 15 mA/cm^2 (iii) 20 mA/cm^2, (iv) 25 mA/cm^2 (v) 30 mA/cm^2, (vi) 35 mA/cm^2 were carried out keeping the deposition time constant as 5 minutes. It can be seen from the figure that deposit weight as well as efficiency increased with current density and a maximum value was obtained at 25 mA/cm^2. Ren et al. [52] reported that the optimum current density obtained in aqueous medium was 20 – 30 mA/cm^2. In the case of non-aqueous medium also a similar trend as in the case of aqueous deposition was observed for both deposit weight and faradaic efficiency. However, the maximum deposit was obtained at 25 mA/cm^2. This may be due to the fact that basic mechanism of deposition followed in aqueous and non-aqueous media were more or less similar.

Fig.3.16 shows the PZT coating obtained on SS at a current density of 25 mA/cm^2 for different duration viz. (i) 1min, (ii) 5 min, (iii) 10 min, (iv) 20 min, (v) 30 min and (vi) 40 min. The highest value for deposition weight and faradaic efficiency were obtained for a time period of 5 minutes. Efficiency of non-aqueous PZT deposition thereafter decreased for higher time intervals above 5 minutes.

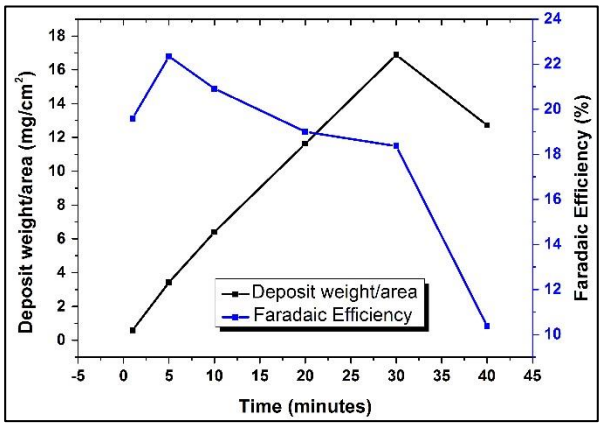

Fig 3.16 Deposit weight and faradaic efficiency vs. time for non-aqueous deposition

Although the weight increased linearly with time up to 30 minutes, the nature of the coating became non-homogenous and powdery and as a result, the inter-particle adhesion was found to be less causing some kind of ‘exfoliation’ which was easily detached during testing and measurements. However, the coating obtained for the time 5

minutes and lesser showed good adhesion. The trend is similar to aqueous electrodeposition of PZT films as reported by Zhitomirsky et al. [49] where a linear relation of weight and time is obtained up to a time period of 5 minutes after which the weight remains more or less constant.

3.3.3 Morphology of the prepared PZT films

The surface morphology, microstructure and topography of the PZT films prepared using DMSO based non-aqueous electrolyte (deposited at 25 mA/cm^2, 5 minutes) were characterised using SEM and AFM studies. Fig 3.17 and 3.18 show the SEM images of PZT deposit obtained on SS and titanium foils respectively. It was found that the morphology of the PZT coating is distinctly different from the films prepared using aqueous [48, 49] electrolytes. Aqueous electrolytes generate films with a flaky nature of particles with cracks. In contrast, the films produced using DMSO solutions were found to have a continuous and uniform surface morphology with minimal porosity.

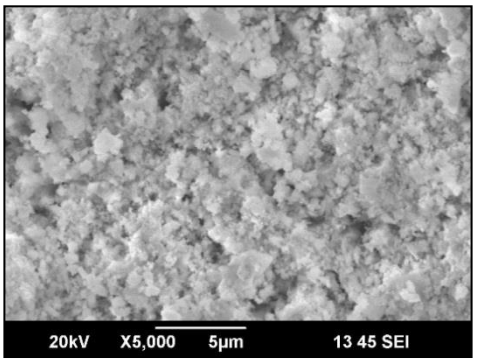

Fig 3.17 SEM image of PZT on SS foil

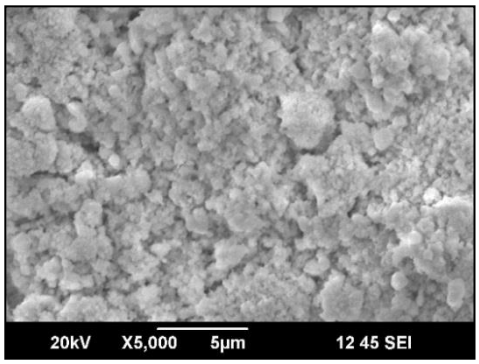

Fig 3.18 SEM image of PZT on titanium foil

It can be seen from the figures that the morphology of the films on both SS and titanium are more or less the same but like in aqueous ELD, adhesion to the substrate was found to be better for titanium substrates. It was found that PZT films had a thickness of around 100 – 140 µm were and the thickness measurements were carried out using SEM studies (Fig 3.19), profilometer and also using a coating thickness gauge.

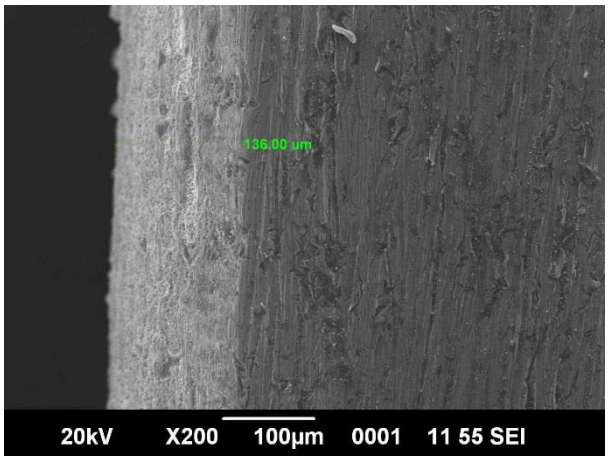

Fig 3.19 Thickness measurement of PZT films using SEM

Figure 3.20 and 3.21 respectively give the optical microscope images of non-aqueous PZT films before and after sintering. It can be seen that sintering helped in densification of the films and reduction of porosity.

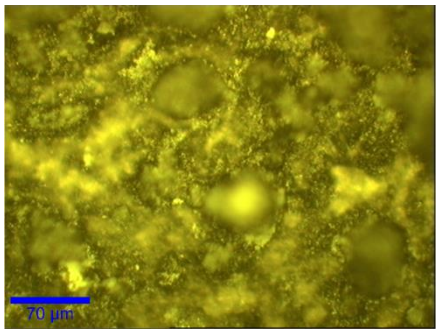

Fig 3.20 Optical image of non-aqueous PZT green deposit

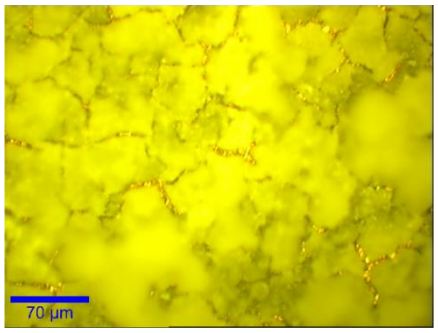

Fig 3.21 Optical image of non-aqueous PZT sintered deposit

Fig 3.22 shows the topography of the PZT film obtained using AFM, keeping the scanned area as 1×1 μm^2. It was clear from the AFM micrograph that a more or less uniform coating with an average roughness of 2 nm is obtained. The roughness value obtained using electrodeposition technique is comparable to sol gel [107, 108] method and pulsed laser deposition [109] which are among the conventional techniques widely used for obtaining PZT films. Hence it was felt that electrochemical deposition in DMSO based non-aqueous media can be used as a cheap, cost effective alternative to pulsed vapour deposition technique and sol-gel technique. Moreover, it can also be used for deposition on substrates of complex geometry.

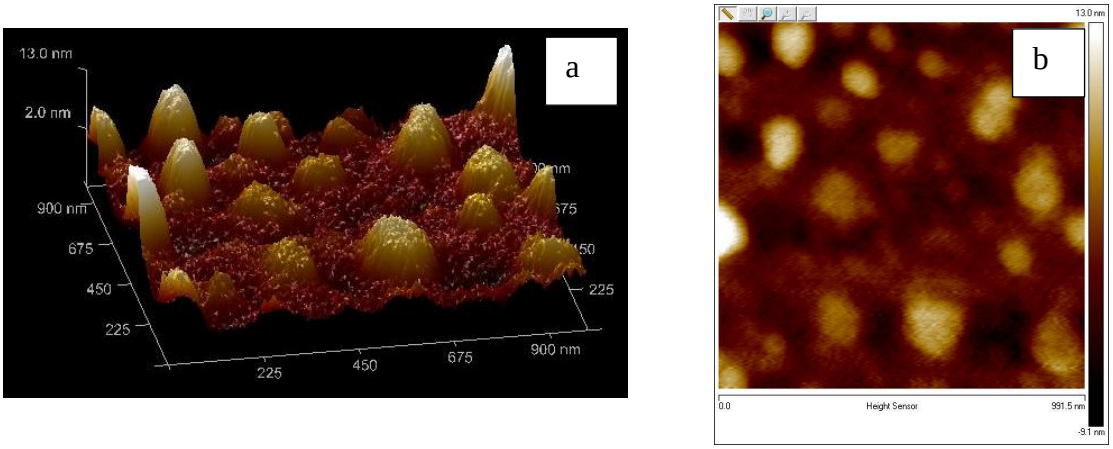

Fig 3.22 AFM image of non-aqueous PZT film (a) 3D image, (b) 2D image

TEM images of the non-aqueous PZT deposit obtained is given in the Fig 3.23. Similar to aqueous PZT, a transparent field image was found with spherical nanoparticle agglomerated particles with grain sizes also in the range of 20 – 50 nm. It was observed that agglomeration was more prominent in the case of non-aqueous than that in aqueous PZT deposit.

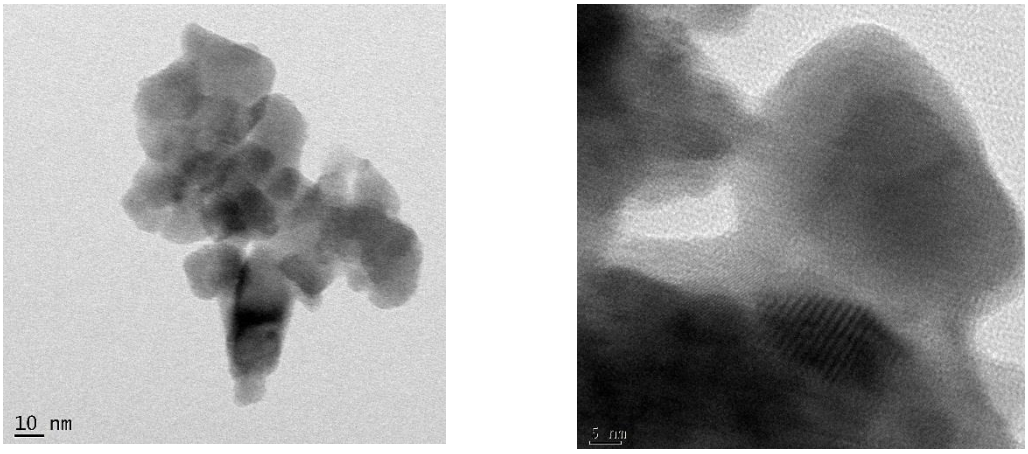

Fig 3.23 TEM images of non-aqueous PZT film

3.3.3.1 Effect of sintering time on the morphology of PZT films

From the study on aqueous deposition of PZT, it was found that the electrochemical deposition yields amorphous PZT films which needed to be subjected to heat treatment/sintering at higher temperatures to obtain a crystalline film. It was observed that the same was the case with DMSO based non-aqueous ELD of PZT. The role of sintering time on morphology of the PZT film was also studied by keeping the

temperature at 500 °C (same as that of aqueous ELD) and the time for sintering was varied from 0 to 1 hour.

Fig 3.24 gives the SEM images of PZT non-aqueous films subjected to sintering for different time intervals such as: (a) 0 time (green deposit), (b) 15 minutes, (c) 30 minutes, (d) 45 minutes and (e) 1 hour at a temperature of 500 °C. By close inspection of the SEM micrographs it can be noticed that porosity decreases as the time of sintering is increased. It can be understood that a 15 minute sintering rendered a highly porous PZT film which was not desirable, as porosity can degrade the piezoelectric performance of the PZT film for its use as piezoelectric sensors. When the time is increased from 30 minutes to 45 minutes to 1 hour, the porosity observed in the film was much less compared to that observed for 15 minutes.

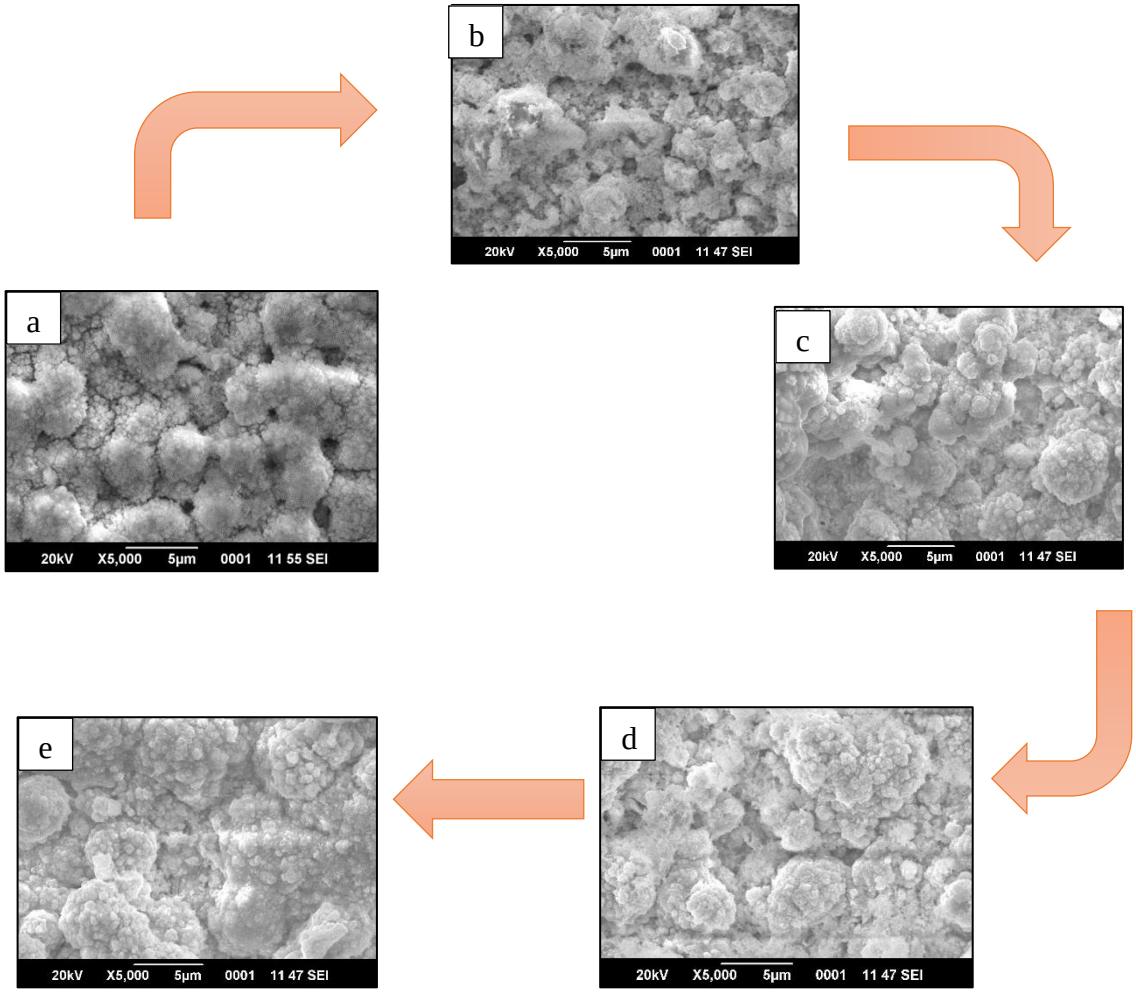

Fig 3.24 SEM images of PZT films sintered for different time durations: (a) green deposit, (b) 15 minutes, (c) 30 minutes, (d) 45 minutes, (e) 1 hour

3.3.4 PZT crystal phase characterisation

Crystalline perovskite phase formation is one of the detrimental steps in any PZT film formation technique. The efficiency of sintering of DMSO based non-aqueous ELD PZT films were extensively studied to confirm the required crystalline phase formation in these films. Structural characterisation of the synthesised PZT films was carried out using techniques such as XRD and Raman spectroscopy.

3.3.4.1 XRD studies

The XRD pattern for the DMSO based non-aqueous PZT is shown in Fig 3.25. Diffraction peaks at 2θ values viz. 21.288°, 30.409°, 37.566°, 43.662°, 49.248° and 54.285° indicates a perovskite crystalline structure as that of PZT (JCPDS card No. 00 - 033 - 0784). PZT being a solid solution of $PbZrO_3$ (rhombohedral, antiferroelectric) and $PbTiO_3$ (tetragonal, ferroelectric), rhombohedral and tetragonal phases coexist at Morphotropic Phase Boundary (MPB) [76] and this phase was very essential for the PZT formed for practical applications. The tetragonal, rhombohedral and tetragonal-rhombohedral phases were identified by the analysis of the peaks in the 2θ range of 42 – 45°. For the PZT coating, the peaks corresponding to (002) tetragonal, (200) tetragonal and (200) rhombohedral coexisted at the 2θ value 43.665°.

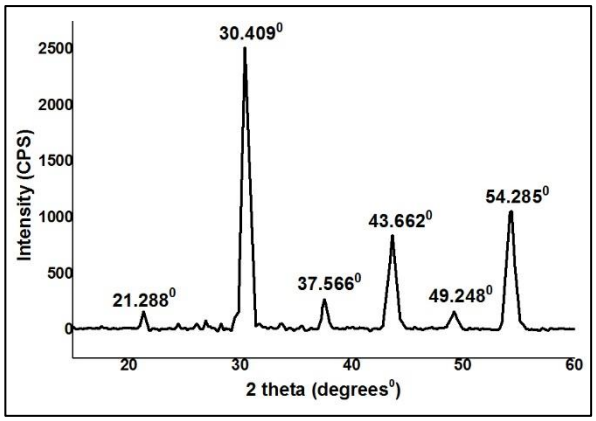

Fig 3.25 XRD of PZT film using non aqueous ELD

From earlier studies [40] done on aqueous deposition it was determined that the crystallisation of the electrodeposited PZT occurs at temperatures of 500 °C indicating the formation of the perovskite PZT phase. From these results it can be substantiated that the minimum temperature required for electrodeposited PZT film crystallisation for non-

aqueous method was similar to aqueous and was found to be 500 °C. The sintering temperature for obtaining PZT crystalline phase for electrochemical method (both aqueous and non-aqueous) was found to be very low when compared to other techniques. This feature can give ELD an edge over other conventional techniques where low temperature formation is important for integration of films in different electronic circuits. The particle size of the PZT coating was calculated using Scherrer formula (Eq. 3.22) and was found to be 20 nm.

3.3.4.1.1 Effect of sintering temperature and time on phase formation in the PZT films

To study the effect of sintering temperature and time on the perovskite phase formation in PZT non-aqueous films, XRD diffractograms were recorded for PZT films sintered at different temperatures viz. 300 °C, 400 °C, 500 °C and also for different durations viz. 15 minutes, 30 minutes, 45 minutes and 1 hour.

In order to optimise the sintering temperature, for PZT phase formation, films were sintered at various temperatures: (a) 0 °C (green deposit), (b) 300 °C, (c) 450 °C, (d) 500 °C for a fixed time interval of 1 hour as given in Fig 3.26. Green deposit was found to be amorphous, showing only undefined peaks or peaks corresponding to substrate. It was found that similar aqueous deposits, as explained by Zhitomirsky et al. [48, 49] peaks were found to get sharper with increase in sintering temperature and a complete and single perovskite phase formation was obtained at a sintering temperature of 500 °C.

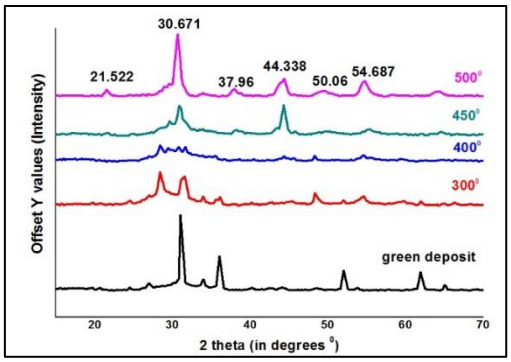

Fig 3.26 Sintering done at different temperatures for a constant time of 1 hour

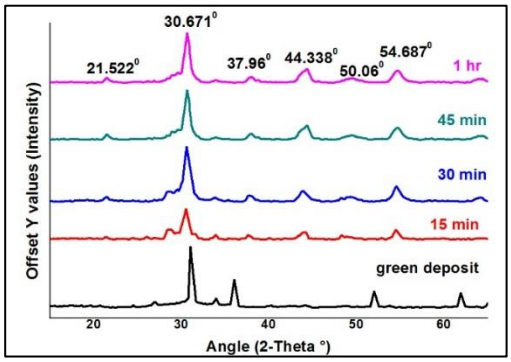

Fig 3.27 Sintering at 500°C for different time intervals

Further in order to optimise the heating duration experiments were performed for different durations viz. (i) 15 minutes (ii) 30 minutes (iii) 45 minutes (iv) 1 hour (Fig

3.27). It was found that a minimum time heating time of 45 minutes at 500°C resulted in good perovskite structure for the deposit. Further increase in sintering time does not have any significant effect on the structure of the PZT deposit.

3.3.4.2 Raman spectroscopy studies

Raman spectroscopy was also used to confirm the phase formation of the non-aqueous PZT films. Figure 3.28 and 3.29 respectively give the Raman spectra of PZT green and sintered films prepared by non-aqueous ELD. By close examination of both the spectra, it can be found that both green and sintered films showed a different spectral pattern. Green films were characterised by vague broad peaks whereas sintered films displayed more sharp and defined peaks. The sintered PZT films of non-aqueous ELD method were also found to have both tetragonal and rhombohedral peaks. Major rhombohedral peaks found were 150 cm^{-1} A_1(TO), 210 cm^{-1} A_1(LO) & E(TO) and 331 cm^{-1} A_1(TO). Tetragonal peaks obtained were 600 cm^{-1} $A_1(TO)_T$ and 731 cm^{-1} $E(LO)_T$. The peak corresponding to $E+B_1$ (silent mode) at 285 cm^{-1} which represent a rhombohedral – tetragonal coexistence phase was also obtained.

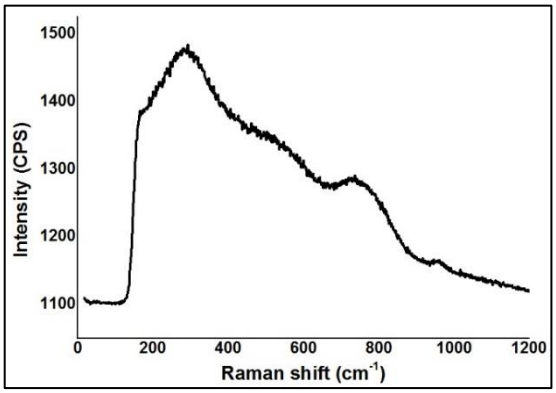

Fig 3.28 Raman spectra of green non-aqueous PZT film

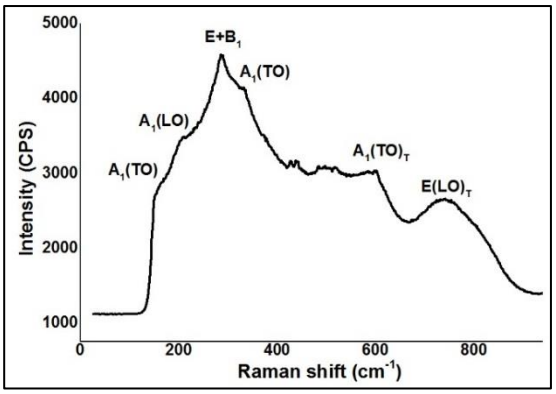

Fig 3.29 Raman spectra of sintered non-aqueous PZT film

3.3.5 Dielectric and piezoelectric studies

Dielectric and piezoelectric characterisation is very important for a ferroelectric material because they provide information about parameters/properties which decides its suitability for sensor applications. The dielectric constant is a measure of the amount of electrical charge the material can withstand for a particular electric field strength. The dielectric loss in a material is known as its dissipation factor or tan δ. A piezoelectric material needs to possess high dielectric constants and low tan δ for effective use in

sensor applications. Moreover, ferroelectric material should exhibit polarisation reversal (or switching) by the application of electric field resulting in a hysteresis loop. Hysteresis measurements also give an idea about the leakage current of the material which should be low for optimum sensor performance.

Fig 3.30 shows the dielectric plot (frequency vs. dielectric constant) for the PZT film (thickness 100 µm) on SS substrate obtained from non-aqueous electrochemical deposition measured for a frequency range 1 kHz to 1 MHz. The dielectric constant and tan δ at 1 kHz were obtained as 452.9 and 0.046 respectively. Capacitance and tan δ values for the given frequency range were directly obtained from the impedance analyser. Dielectric constant was then calculated from the capacitance values by rearranging the parallel plate capacitor equation as,

$$\varepsilon_r = C\frac{d}{(\varepsilon_0 A)} \tag{3.29}$$

where is ε_r is the relative permittivity or dielectric constant, C is the capacitance of the coating, ε_0 is the permittivity of free space, 8.85×10^{-12} F/m, A is the area of sample and d is the thickness of the coating.

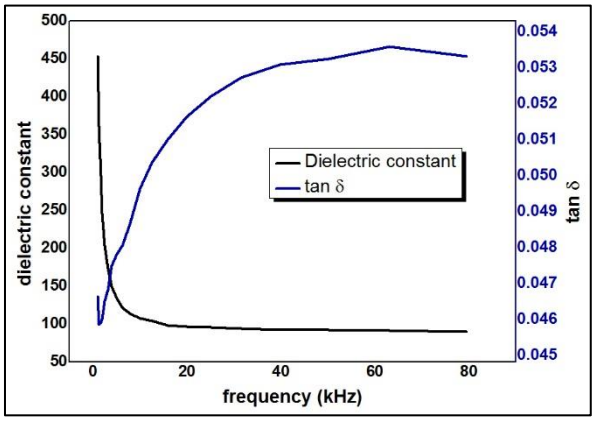

Fig 3.30 Dielectric studies of non-aqueous PZT film

It was found that with increase in frequency, the dielectric constant decreased for all frequencies. Jang et al. [108] had obtained a dielectric constant value of 160 at 1 kHz for sol gel deposited PZT thin films on SS substrates however, no dielectric studies were found in literature on electrochemically deposited PZT films. In contrast to sol gel method, non-aqueous electrodeposition was found to render PZT films with better dielectric properties. This may be due to the superior properties of the films prepared by non-aqueous electrolytic deposition such as better uniformity (low surface roughness), crack free deposit without porosity. Moreover, the film thickness of sol gel deposited

films are generally lower (>10µm). The charge accumulation associated with the material electric dipole is proportional to the film thickness which in turn can affect actuation strength and sensing performance.

Fig 3.31 shows the Polarisation vs. Electric field (P-E) hysteresis loop for a PZT film of thickness 100 µm deposited on SS. Hysteresis measurements were done for 100 V, 500 V, 1000 V and 1500 V and the resultant saturation polarisation (P_S), remnant polarisation (P_R) and coercive field (E_C) are given in Table 3.2. It was observed that, with increase in the applied voltage, the resultant saturation polarisation (P_S), remnant polarisation (P_R) and coercive field (E_C) increases. The obtained polarisation values are lower when compared with the reported results of bulk PZT [110, 111] which could be due to the lower density of PZT thin films.

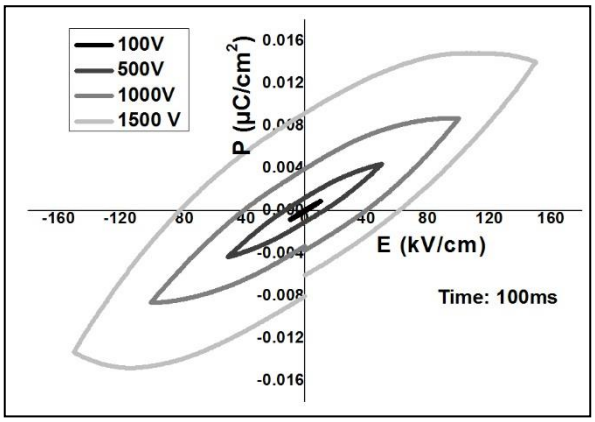

Fig 3.31 Polarisation vs. electric field of PZT film

Table 3.2 Saturation (P_S), remnant (P_R) polarisation and coercive field (E_C) determined for the ELD PZT deposit

Applied Voltage (V)	Saturation Polarization (P_S) (µC/cm^2)	Remnant Polarization (P_R) (µC/cm^2)	Coercive field (E_C) (kV/cm)
100 V	0.000865	0.0000324	0.3814
500 V	0.00437	0.00121	13.9618
1000 V	0.00865	0.00389	39.75
1500 V	0.014	0.0092	87.44

The leakage current characteristics (I – V plots) were also measured for the prepared PZT films. Fig 3.32 shows leakage current density of non-aqueous electrodeposited PZT films as a function of voltage in the range – 500 V to + 500 V with a delay time of 100 milliseconds. Leakage current is an undesirable phenomenon which may occur due to several mechanisms including Schottky emissions, Frenkel Poole emission and space charge limiting current in materials. The leakage current density obtained was maximum (1.91×10^{-7} A/cm^2) for positive bias conditions and minimum (1.16×10^{-7} A/cm^2) for reverse bias conditions. The variations in I – V characteristics was mainly due to the change in conductivity of the electrodes. The results were in agreement with the previous studies [112, 113].

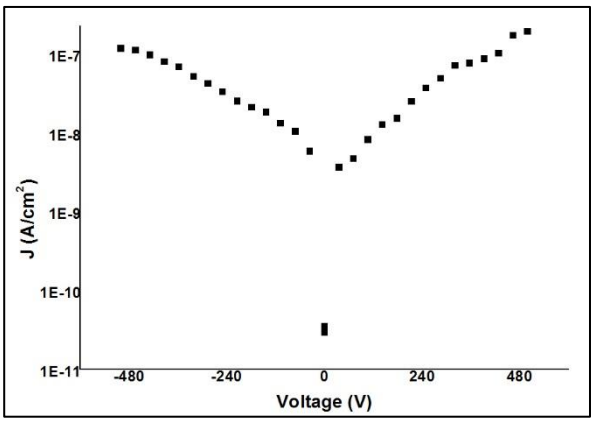

Fig 3.32 I – V Plot for the electrodeposited PZT film

3.3.6 Poling of ELD PZT films

The non-aqueous PZT films were subjected to a poling process to align the dipoles in the poling direction and induce piezoelectricity in the prepared films. Contact poling was the technique used and the details of poling procedure have been given in Chapter 2, section 2.4. During poling the PZT films were kept in a temperature controlled silicone oil bath (at 100 ºC) and high electric fields (1 – 3 kV/mm) were applied to it for specific time periods. The poling measurements for electrodeposited PZT films is not reported till date and no previous literature is available in this field. In this work, the poling results were reported for the first time for non-aqueous electrochemical PZT films.

d_{33} measurements were performed for the PZT films to assess the extent or efficiency of poling that has occurred in the material. d_{33} is the ratio of short circuit charge per unit area flowing between connected electrodes perpendicular to the 3rd direction (3rd

axis) to the stress applied in the direction 3. Once a force F is applied to the transducer, in the 3 direction, it generates the stress which results in the electric charge flowing through the short circuit. d_{33} value (pC/N) is measured using a conventional piezometer.

In this work, non-aqueous PZT films (area 2.5 × 2.5 cm^2) 100 µm thickness, prepared on SS substrates were poled at 100 ºC using an electric field of 1.5 kV/mm for different time periods (up to 10 hours) and the measured d_{33} values are shown in Fig 3.33. The electric field and temperature were constant during the poling process and the time period was varied. d_{33} values were found to increase from 0.3 to 1.3 pC/N as the time of poling was increased from 0 to 10 hours. It is seen that the values obtained here were less when compared to the values obtained for bulk PZT materials. However, considering the fact that the PZT films is only 100 µm thick, substrate/electrode effect will affect d_{33} value. Moreover, poling results of electrochemical PZT films were reported for the first time.

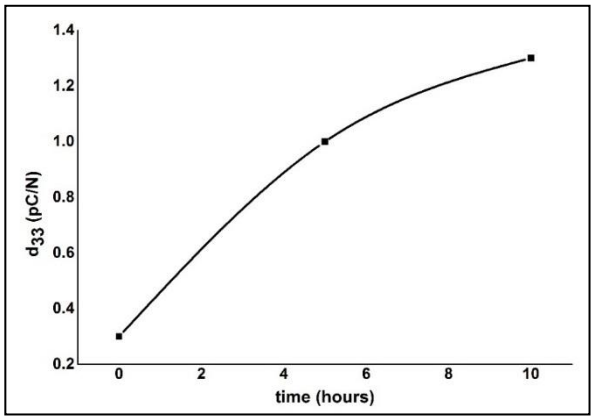

Fig 3.33 d_{33} vs. poling time for non-aqueous ELD PZT films

3.4 DEPOSITION OF PZT THIN FILMS USING PULSED POTENTIOSTAT/GALVANOSTAT ELECTRODEPOSITION TECHNIQUES

Pulsed electrolytic deposition (PED) is also a type of cathodic electrolytic deposition wherein the current or potential are applied to the electrolyte as pulses of very short time duration using very sophisticated and precise instrumentation like an electrochemical workstation. Here, the potential or current is alternated swiftly between two different values which result in a series of pulses of equal amplitude, duration and polarity, separated by zero current as shown in Fig. 3.34.

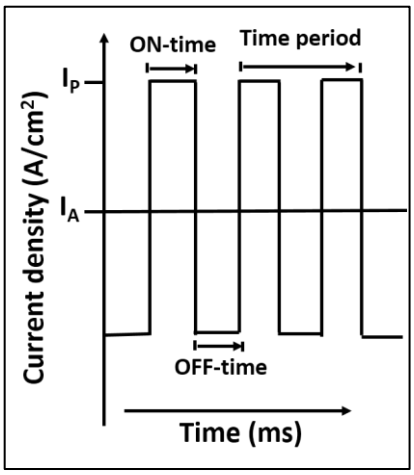

Fig. 3.34 Typical pulse-current waveform.

Each pulse consists of an ON-time (T_{ON}) during which potential and/current is applied, and an OFF-time (T_{OFF}) during which zero current is applied. It is possible to control the deposited film composition and thickness in an atomic order by regulating the pulse amplitude and width. They favour the initiation of grain nuclei resulting in finer grained thin film deposit with controlled thickness and better properties than conventionally plated coatings.

In the regular method of electrochemical deposition, a negatively charged layer is formed around the cathode as the process continues. In the electrodeposition using, conventional DC regulated power supply, this layer charges to a defined thickness and obstructs the ions from reaching the cathode. In PED, the output is periodically turned off to cause this layer to discharge. This allows easier passage of the ions through the layer and onto the cathode. Various metal oxides such as ZrO_2 [115, 116], CeO_2 thin films, Y_2O_3 nanoparticles, WO_3 – TiO_2 [117] etc. have been prepared using this technique.

In this work, electrochemical deposition of nanoscale PZT using non-aqueous pulsed deposition technique (PED) was effectively used and studied. Much studies on deposition of PZT using PED is not reported in literature. In this work, the technique of galvanostatic and potentiostatic pulsed deposition was utilised for the development of PZT thin films on flexible stainless steel and titanium foil substrates.

3.4.1 PZT films using Potentiostat/Galvanostat

An electrochemical workstation with a potentiostat/galvanostat is a very accurate and complex sophisticated instrument. It can be used to perform electrochemical

experiments at very low voltage and current values which is helpful in precisely controlling the final deposit properties by controlling the electrochemical parameters. DMSO based non-aqueous electrolyte (same as non-aqueous ELD) was used.

The instrumentation set up as well as the experimental details have been explained in Chapter 2, Section 2.3. A three electrode set up was used for deposition and a schematic representation is given in Fig 3.35. The substrates (metal foils) were taken as the cathode (also called working electrode or WE), a circular platinum mesh electrode as the anode (also called counter electrode or CE) and a reference electrode or RE (Ag/AgCl) were utilised. Here all the experiments were done at room temperature.

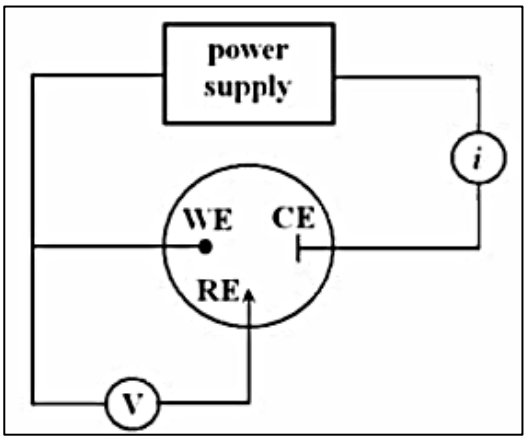

Fig 3.35 A typical three electrode Electrochemical cell

It was found that this technique resulted in PZT thin film with thickness below 10 µm having very good adhesion to the metal substrates. The major methods used for PZT PED were Cyclic Voltammetry (CV) and Regulated Galvanic Pulse (RGP). Cyclic Voltammetry was carried out mainly to get information about the reduction potentials of the different elements used in the electrolyte. Fig 3.36 (a) shows the Cyclic Voltammetry curve of the electrolyte used for electrodeposition of PZT. It was clear from the figure that three reduction potential values viz. – 0.12 V, – 1.53 V and – 1.63 V were obtained for Pb, Zr and Ti respectively. In Regulated Galvanic Pulse (RGP) technique, a total of 6 current pulses for 5 cycles with a time period of 20 seconds were applied as shown in Fig 3.36 (b) for obtaining the deposits.

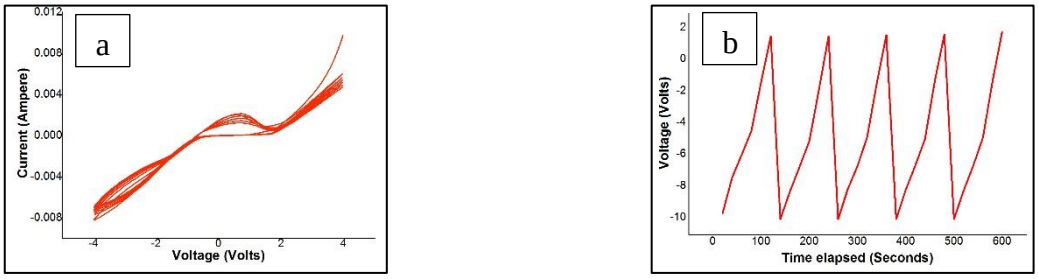

Fig. 3.36 Deposition curves: (a) CV, (b) RGP

3.4.2 Morphology studies of PED PZT deposits

The surface morphology, microstructure and topography of the PZT films prepared were characterised using SEM and AFM studies. Figure 3.37 shows the SEM images of PZT films prepared by RGP. When compared to PZT films prepared by non-aqueous deposition using conventional regulated power supply (RPS), the PZT films produced using RGP were very thin. From the micrographs it can be seen that the RGP films were continuous and covers the whole substrate surface. Films deposited by RGP also showed some cracks in the deposit which may be due to its lower thickness values (> 10 µm). However the cracks observed were few nanometre wide and seems to be only at the surface and hence not significant.

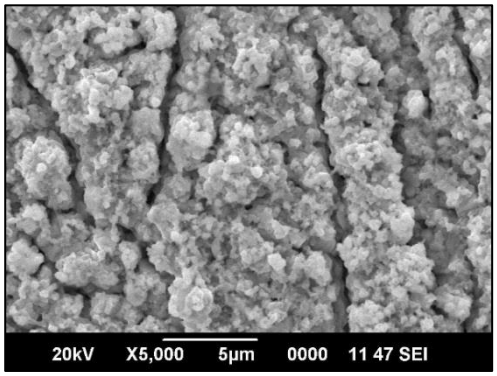

Fig 3.37 PZT electrodeposition using RGP.

Fig. 3.38 shows the topography studies of the PZT films deposited by RGP using AFM technique. The films deposited by pulsed deposition were found to be very thin when compared to films prepared by continuous deposition using RPS. It is clear from the images that the PZT films prepared using RGP are having more or less uniform surfaces with surface roughness values > 10 nm.

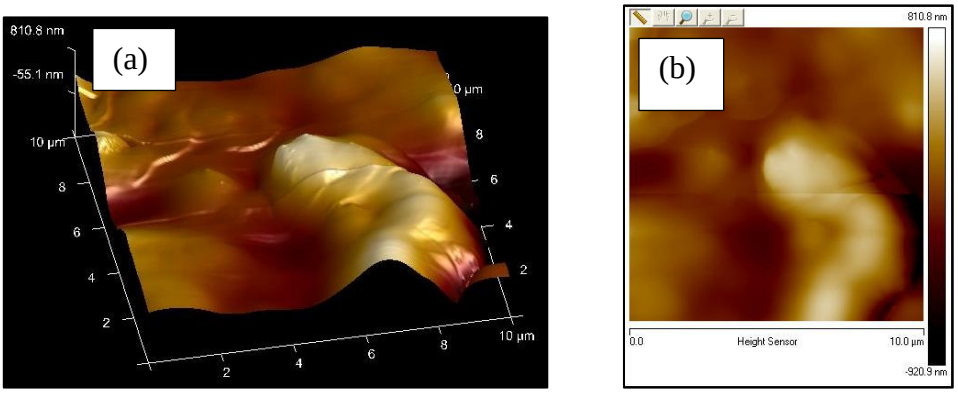

Fig. 3.38 AFM of PZT by RGP (a) 3D image, (b) 2D image.

3.4.3. Crystal phase characterisation of PED PZT deposits

In order to ascertain crystal structure and phase formation of the PZT films produced, techniques such as XRD and Raman Spectroscopy were utilised. Figures 3.39 gives the XRD plots of the PZT deposits prepared by using RGP technique. It was found that RGP deposits showed a perovskite crystalline structure verified using JCPDS card No. 00 - 033 - 0784.

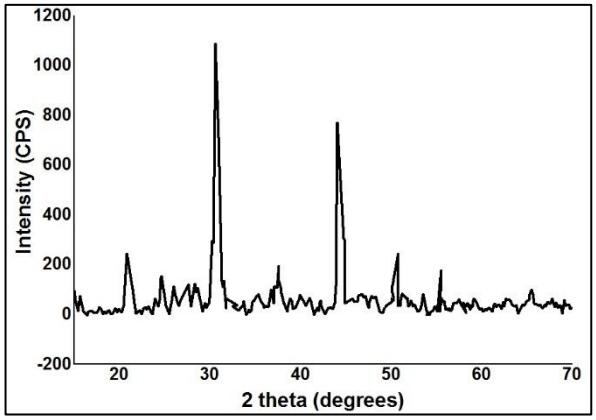

Fig. 3.39 XRD of PZT films prepared by RGP

The perovskite structure of the PZT films prepared using RGP technique was also confirmed using Raman spectroscopy studies. Fig 3.40 gives the Raman spectra obtained for RGP PZT deposit. The perovskite crystalline phase formation was clearly seen and the tetragonal peaks mainly $A_1(TO)$ and E(LO), rhombohedral phase shown by $A(TO)_T$ and $E(LO)_T$, as well as the tetragonal-rhombohedral coexistent phase (E + B_1) were clearly observed.

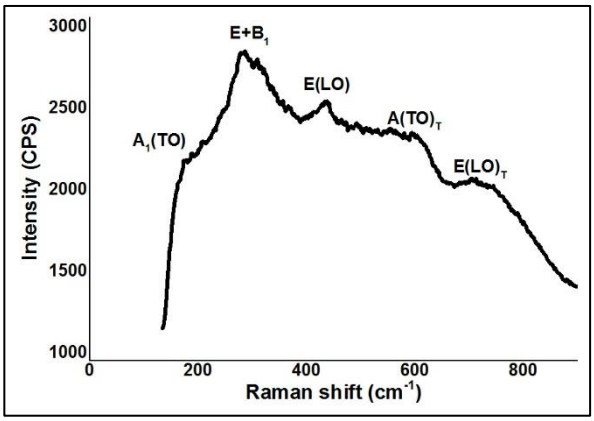

Fig. 3.40 Raman spectra of PZT film by RGP.

3.5 CONCLUSIONS

On the electrochemical technique for deposition, although an excellent method much studies have not been carried out. In this chapter, deposition of PZT films using electrolytic techniques has been studied in detail. The two methods of electrolytic deposition (ELD) i.e. aqueous ELD and non-aqueous ELD have been extensively studied and discussed. The process parameters such as current density, time of deposition were optimised for both aqueous and non-aqueous ELD of PZT. For aqueous ELD, maximum yield for the PZT deposits were obtained at a current density 15 mA/cm^2 for a time of 5 minutes. However, for non-aqueous PZT deposition, current density and time were optimized as 25 mA/cm^2 for a time of 5 minutes. Faradaic efficiency was also calculated and was observed as 17 % for PZT films prepared by aqueous ELD and 22% for non-aqueous method. The sintering temperature and time for the PZT films were optimised as 500 ºC and 1 hour respectively. More continuous and uniform deposition with good adhesion were obtained for titanium substrates for both aqueous and non-aqueous methods. Morphology and topography evaluation of the prepared films were carried out using SEM, TEM, and AFM techniques. It was observed that the DMSO based non-aqueous ELD gave better results for PZT film deposition, with respect to film uniformity and other properties. The crystallographic phase characterisation using XRD showed perovskite phase formation for both aqueous and non-aqueous PZT films and was further corroborated using Raman spectroscopy. Dielectric constant of 452.9 and tan δ of 0.0429 were obtained at 1 kHz for the non-aqueous electrodeposited PZT coating. Ferroelectric hysteresis behavior of the PZT films (P-E) was studied for 100 V, 500 V, 1000 V and 1500 V and it showed a maximum value of 0.014 μC/cm^2 for saturation polarisation.

Leakage current measurements (I – V) in the range 0 to ± 500 V revealed a leakage current density of 1.91×10^{-7} A/cm^2 for positive bias conditions and 1.16×10^{-7} A/cm^2 for reverse bias conditions. It was found that the non-aqueous electrodeposition method can be utilised to prepare PZT films with high dielectric properties.

Chapter – 4

ELECTROPHORETIC DEPOSITION OF PZT

4.1 INTRODUCTION

Electrophoretic deposition (EPD) is a technique used exhaustively over the years in the ceramic processing industry. The significance of EPD process lies in its versatility, as it can be used to produce thin/thick films, thickness ranging from nanometre (zero, one, two or three dimensional structures) to several centimetres. The advantages include simple and fast methodology, technology suited for mass production and flexibility in substrate shapes. EPD can be used in various advanced and functional areas of ceramic processing which includes ceramic coatings, porous composite materials, functionally graded ceramics, thin/thick film fabrication etc. The common ceramic materials synthesised using EPD technique includes alumina, zirconia, hydroxyapatite, barium titanate, titania films etc. With increasing use of PZT thin/thick films for various piezoelectric applications such as sensors, actuators, energy harvesting devices etc., the researchers worldwide have focussed on different thin film processing techniques for PZT. Even though some studies have also discussed the electrophoretic deposition (EPD) of PZT, but no exhaustive research on an application level have been reported. EPD of PZT can have an edge over other traditional and existing PZT thin and thick film forming techniques due its many attributes such as:

a. The versatility/flexibility of the multifarious EPD technique enables the formation of thin or thick depositions or coatings with equal ease according to the requirement. This method can be applied to any solid material which is available as a powder (>30 μm) or as a colloidal suspension.
b. When considering the thin film PZT deposition techniques like chemical vapour deposition (CVD), sputtering, molecular beam epitaxy (MBE) and sol-gel etc. the efficient control of stoichiometry is one of the persisting problems. EPD on the other hand, being a particulate forming method, the control of stoichiometry of the film can be ensured during the powder preparation stage wherein complex oxides such as PZT can be prepared with precisely verified dopant addition.

c. Also unlike sputtering and vapour deposition techniques, deposition using EPD can occur even on the back side of electrodes and so uniform films can be easily fabricated on curved or uneven surfaces by three dimensionally controlled polarity and spatial position of the electrodes and electric field potential.
d. The traditional particulate processing techniques for ceramics such as tape casting, screen printing etc. have very high shrinkage rates during drying (20 – 40 %) to attain the optimum densification. As a result those techniques can only be used for preparing films above a critical thickness and preparation of thin films is not possible. Whereas in the case of EPD, as the particles are accumulated on the electrode using an electric field, the densification occurs more properly and shrinkage during drying is also minimum. So EPD can be used to develop thin films even with 2 -3 particle diameter thickness having a continuous and uniform morphology.
e. Another significant attribute is the reduced cost of production of EPD process. The superior thin film techniques are very expensive with high vacuum processing equipment and also they are relatively very slow processes. EPD technique being very simple and inexpensive, deposition can be completed in a few seconds which is an added advantage.

Electrophoretic deposition of materials is accomplished by the motion of charged particles dispersed in a suitable solvent towards an electrode/substrate under the action of an electric field. Hence EPD consists of 3 basic steps [64]:

1. Preparation of stable suspension of particles

   This is one of the most important process in EPD. Here a stable suspension is prepared wherein each single particle is able to move independently in a suitable solvent system. Preparation of a stable suspension is cumbersome due to the Van der Waals attraction force existing between the particles. For obtaining good quality EPD films, there must be stabilising force or entity in the system which prevents the settling or flocculation of particles. Even though deposition is possible with unstable settling suspensions, the resulting deposit shall possess low density with cracks appearing after drying. Suspensions can be stabilised by electrostatic stabilisation or by the addition of a polymer. Polymer additives can form a coating over the particles which prevents their floccing. In the electrostatic method, a charge is developed on

the particle surface which creates a net charge separation between the particle and the solvent molecules. So a high pressure area of solvent is formed around the particles which in turn keeps them stabilised.

2. Electrophoretic motion of particles to the working electrode/substrate

   In this step, a DC electric field is applied to the suspension and as a result the particles starts moving towards the oppositely charged electrode/substrate. It seems to be a simple process but practically, a very complicated and complex process. Here in addition to the phenomenon of electrophoresis, many other processes also can occur such as Brownian diffusion, sedimentation, and convective transport etc. which adds more complexity to the deposition process.

3. Deposition of particles to obtain a film

   In this particular step, the particles accumulated at the electrode by electrophoresis needs to be deposited as a single entity or film by overcoming the stabilising force present in the suspension. All the particles are brought closer so that the van der Waals forces act and the particles come together to form a single deposition (or film) with a reasonable density and packing of the film. Different mechanisms can be used for deposition such as:

   a) Densification
   b) Direct Electrostatic
   c) Electro sedimentary
   d) Ion Depletion Enhanced Electrostatic
   e) Salting Out
   f) Charge Reduction Or Neutralisation
   g) Squeezing Out
   h) Bridging Flocculation
   i) Desorption Of Neutral/Charged Polymer

4.2 ELECTROPHORETIC DEPOSITION OF PZT FILMS

Earlier Sweeny et al. [69] have reported the electrophoretic deposition of PZT films from acetone with the addition of nitric acid and nitrocellulose. Later, Ma et al. [72, 73] utilised an ethanol based solvent system with different additives for the deposition of PZT and carried out studies on the preparation and stabilisation of suspensions,

deposition and packing of PZT films and its chemical characterisation. Alcohol based suspension medium [75, 76, 118] along with different additives and stabilisers are the commonly used solvent systems in use currently for EPD of PZT films. Another significant study by Boccaccini, [71] on the deposition of PZT films using an acetyl acetone based solvent system has also been reported. Kim et al. [119] had utilised EPD for preparing PZT coated SiC fibers.

Most of the published works on EPD of PZT have used solvent systems which require the aid of various additives or suspension stabilisers for effective deposition. This particular work, highlights the use of glacial acetic acid-based suspension medium for depositing PZT film without any type of additives/stabilising agents. Van Tassel et al. [79] had demonstrated EPD of PZT using glacial acetic acid solvent, however the optimisation of process parameters, detailed material characterisation, dielectric and piezoelectric studies were not reported. Moreover, this work focuses on low temperature sintering (600 °C) of EPD films whereas, most of the literature reports were on higher temperatures (900 –1200°C). This work highlights EPD of PZT films on titanium and stainless steel foils using a glacial acetic acid based suspension medium, optimisation of process parameters, and characterisation using techniques like Scanning Electron Microscopy (SEM), Atomic Force Microscopy (AFM), Raman Spectroscopy and X-ray diffraction (XRD). In addition dielectric properties, ferroelectric hysteresis plots and I-V characteristics of the PZT films were studied in detail. Furthermore, underwater acoustic characterisation of PZT films prepared using EPD has been reported for the first time. The receiving sensitivity and the directivity measurements were carried out.

4.2.1 Deposition mechanism of PZT by EPD

In this particular study a stable suspension of PZT was prepared by dispersing 3 wt. % of PZT powder in glacial acetic acid and homogenised using an ultrasonic homogeniser. The electrophoretic deposition was then carried out in the prepared PZT dispersions using a high voltage DC power supply. PZT films were obtained on titanium and stainless steel substrates using the aforementioned technique. The films after deposition were also subjected to sintering procedure at a temperature 600 °C for 30 minutes duration. The details of the deposition is given the Section 2.3. Chapter 2. The PZT films prepared by EPD technique are shown in Fig 4.1.

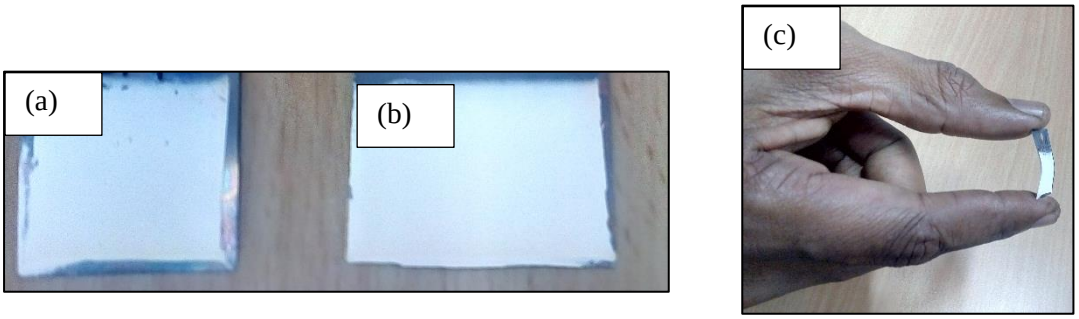

Fig 4.1 Images of EPD PZT films, (a) Green film, (b) Sintered PZT film, (c) flexibility of PZT film

The reaction mechanism involved in the EPD of PZT using acetic acid is mainly particle charging as the suspension medium is able to support particle charge [120]. When PZT powder was introduced into glacial acetic acid solution, the lead oxide present on the surface of the particles readily react with the acetate ions in solution and lead acetate ions were produced in the suspension.

$$2CH_3COOH \longrightarrow 2(CH_3COO)^- + 2H^+ \quad (4.1)$$

$$PbO + 2(CH_3COO)^- \longrightarrow Pb(CH_3COO)_2 \quad (4.2)$$

Zirconium and titanium acetates were also produced but their concentrations were found to be comparatively less than lead acetate. The lead acetate produced then gets very slightly ionised in suspension and forms a positive lead acetate ion and a negative single acetate ion.

$$Pb(CH_3COO)_2 \longrightarrow Pb(CH_3COO)^+ + (CH_3COO)^- \quad (4.3)$$

The resulting positively charged lead acetate ions then get preferentially adsorbed on the zirconate – titanate rich PZT particle surfaces and the negative acetate ions remained in the solution. On the application of a voltage to this system, the particles with the adsorbed ions migrated towards the substrate/cathode where the lead and titanium acetates gets reduced. In the next step, the accumulated particles at the cathode were deposited as a single entity or film with a reasonable packing density. In the current PZT – acetic acid system, the deposition was believed to take place due to the direct electrostatic force. The high voltage applied was sufficient to overcome the interparticle repulsion keeping the particles apart.

4.2.2 Effect of suspension concentration on electrophoretic deposition of PZT

Preparation of stable suspension is one of the important process in EPD. Preparation of a stable suspension is cumbersome due to the Van der Waals attraction force existing between the particles.

Fig 4.2 PZT – acetic acid suspension

The PZT – acetic acid dispersion prepared after ultrasonic mixing is shown in Fig 4.2. The particle size distribution graphs (obtained from dynamic light scattering or DLS experiments) for the PZT – glacial acetic acid suspensions for various concentrations are shown in Fig 4.3. As the PZT powder used had a particle size of around 0.8 µm, a stable suspension should give a peak around that particular value. It can be observed that, for a PZT concentration of about 3 wt. %, the measurement showed good results with a particle size value around 1 µm which give an indication that the suspension was stable with very little or no aggregate formation. In addition, it was found that for both low (1%) and high (5%) concentrations of PZT, aggregate formation or settling had occurred indicated by the shifting of the particle size towards higher values. The variation in suspension stability for different concentrations can be explained by the particle charging mechanism in the system. For any electrophoretic suspension, there exists a critical/optimum composition of solute and solvent for effective charging of the particles. This charging process can occur in the form of selective dissolution of ions from the particles, selective adsorption of ions from the solvent and also dissociative adsorption of molecules from the solvent followed by preferential desorption of one of the dissociated ions. The obtained optimum concentration of 3 wt. % is in agreement with the results reported by Van Tassel et al. [79] for a PZT—acetic acid solvent system, however, they utilised the Zeta potential measurements for optimisation.

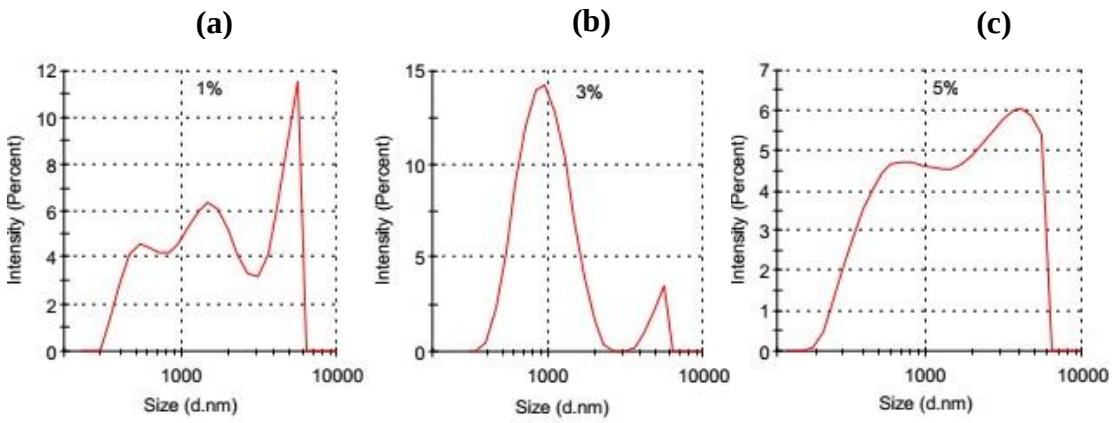

Fig 4.3 Particle size distribution for PZT – glacial acetic acid suspensions for various concentrations: (a) 1 %, (b) 3 %, (c) 5 %

The effect of suspension concentration on PZT film properties such as thickness and weight of deposit were also studied. Fig 4.4 shows the weight and thickness of the EPD films with increasing weight percentage of PZT in the solvent medium. The voltage and time was kept constant at 200 V/cm and 1 minute respectively. It was found that the weight of the deposit and film thickness increases with increase in concentration up to 3 wt. % PZT and after that it drops slightly and remains almost constant irrespective of increase in concentration. Moreover, it was also observed from the particle size distribution studies, that 3 wt. % concentration was the most suitable for PZT electrophoretic process.

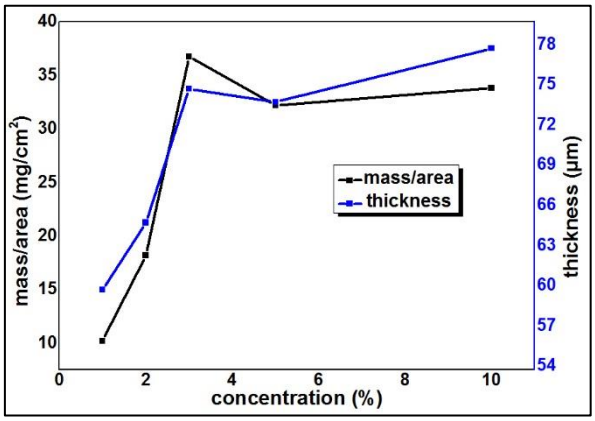

Fig 4.4 Deposit weight as a function of suspension concentration

4.2.3 Effect of process parameters on EPD

Good quality and highly reproducible PZT films were obtained by electrophoretic deposition on both SS and titanium substrates. In order to study the effect of the process parameters (i.e. voltage and time of deposition) on the EPD process, any one of the parameters was varied, keeping all the other conditions fixed and the experiments were carried out using an SS substrate. The resulting PZT mass per unit area obtained for a 3 wt. % suspension for a time of 1 minute was recorded and the results were studied.

Fig 4.5 shows the variation in weight of the PZT film as a function of applied voltage. It was observed that below a threshold voltage of 50 V, no deposition was obtained. At a voltage value of 100 V and higher, superior quality PZT films with increased uniformity and adhesion to the substrate were obtained. Similar to the earlier reported work by Boccaccini et al. [71], the weight of the PZT showed an increasing trend with increase in voltage, although the values differ as the solvent system used was different (acetyl acetone solvent with iodine). Moreover, it was found that at higher voltages (> 500 V), the deposition becomes irregular and non-uniform. This can be due to the electro convection effects generated due to the applied higher voltages resulting in patchy or non-uniform deposits with low density. In addition, at very high voltage values, there is no levelling effects acting on the particles leading to inferior quality EPD films [71]. A voltage range of 200 – 300 V/cm was found to render the best quality PZT films with respect to continuity of the deposit and uniform thickness.

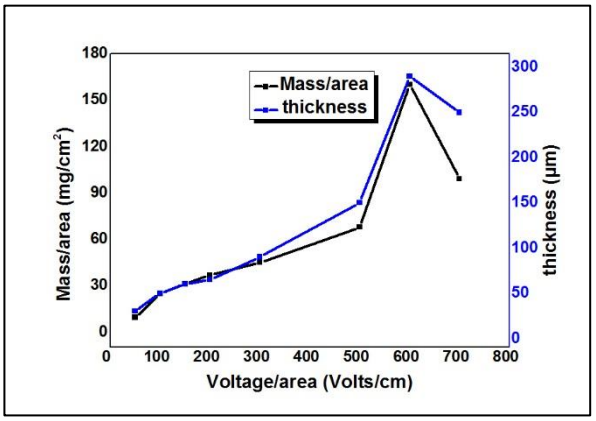

Fig 4.5 Deposit weight as a function of applied voltage

Fig 4.6 depicts the variation of weight of the PZT and film thickness as a function of increasing time of deposition ranging from 10 seconds to 10 minutes keeping the

voltage constant at 200 V/cm. The weight of the PZT and its thickness was found to increase with time. Boccaccini et al. [71] have studied the variation of deposit weight with the passage of time and have obtained an initial increasing trend, attaining saturation after a period of 7 minutes for PZT – acetyl acetone suspensions. Likewise in this particular work, the saturation was found to take place after 5 minutes. The thickness variation of the electrophoretic PZT films have not been systematically studied in the previous reported works. However, here it is observed that the film thickness similar to the weight, increases with time with a minimum obtained as15 µm and maximum 150 to 160 µm above a period of 5 minutes. Therefore, it was obtained that the thickness and weight can be controlled by adjusting the EPD time for a constant voltage and concentration. Besides it was found that thickness uniformity for the films was more for thin films obtained at lesser time periods (1 minute) than for thicker films for larger periods of deposition.

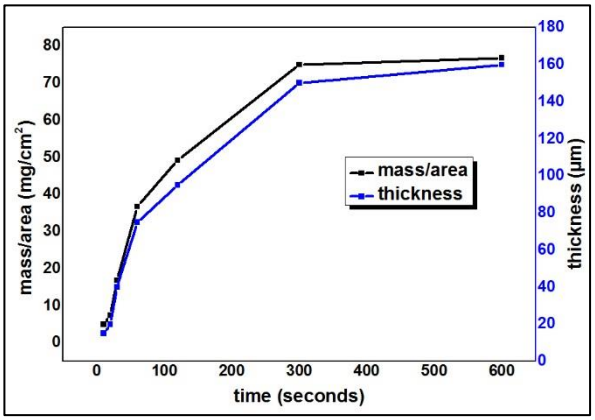

Fig 4.6 PZT film weight and thickness as a function of time of deposition

From the experimental data obtained such as the thickness, weight and deposited area, the density of the electrophoretic PZT films were calculated and was expressed as a percentage value with respect to bulk PZT density or the theoretical density (8 g/cm^3). Table 4.1 show the % of bulk density of electrophoretic PZT films for different deposition time. The density was found to increase up to a time of 2 minutes and further increase in time does not cause any prominent changes in the density of the PZT films. It was possible to achieve 67 % of the bulk PZT density by electrophoretic deposition in this work. The results obtained are also in agreement with the literature [120] which reports 60 % as an average density value achieved after the deposition from PZT – acetic acid suspensions.

Table 4.1 Percentage of bulk density of EPD PZT films for different deposition time

Time of deposition (in seconds)	Density (% of bulk PZT density)
10	43.29
20	48.05
30	54.54
60	63.63
120	67.25
300	64.93
600	62.37

4.2.4 Morphology of the prepared EPD PZT films

The surface morphology, microstructure and topography of the PZT films prepared using electrophoretic deposition were characterised using SEM and AFM studies. Fig 4.7 shows the SEM images for different magnifications obtained for an EPD PZT film on titanium surface.

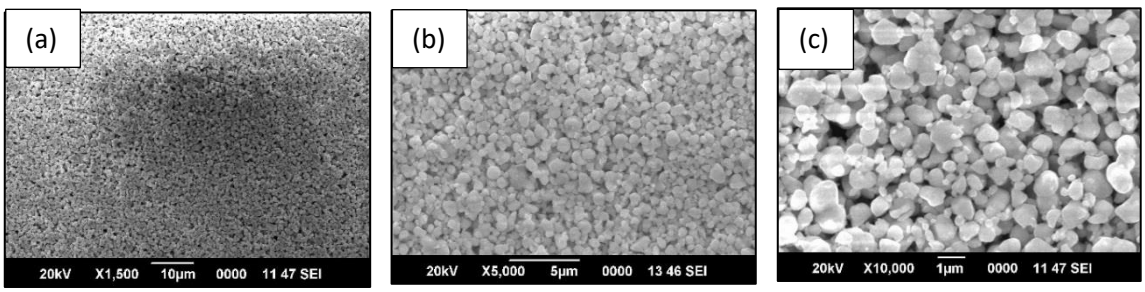

Fig 4.7 SEM image of EPD PZT film (a) magnification ×1,500 (b) magnification ×5,000 (c) magnification ×10,000

It was found that the PZT films prepared using EPD possess uniform microstructure and close packing of particles without cracks. Moreover, there was no agglomeration of PZT particles found in the EPD PZT films. It was also observed that the SEM images for PZT films obtained on SS and titanium had similar microstructure but other properties like adhesion and thickness were different. Qualitative observations revealed that adhesion property of the PZT films and the substrate was the best for titanium foils in comparison to SS. The enhanced adhesion for titanium substrate can be due to the similarity in lattice structure of PZT and titanium. The thickness measurements using portable Coating Thickness Gauge revealed increased film thickness for PZT films obtained on SS substrates than on titanium. A difference of 15 ± 5 μm was apparent between the PZT films on SS and titanium substrates (both prepared under similar conditions). Titanium metal surfaces always have a characteristic oxide layer on its surface which is very difficult to remove. Even after vigorous surface etching and cleaning a small layer of titanium oxide still persist on the metal surface which in turn affected the PZT film thickness during EPD process.

Fig 4.8 shows the surface topography of the EPD PZT film deposited on a titanium surface characterised by the AFM method. The scanned area was taken as 10x10 μm^2. The surface roughness value was found to be 25 nm. For a particulate processing technique such as EPD, the relatively low surface roughness value indicates a very smooth and uniform PZT film which is comparable to other conventional film forming techniques such as sol gel [107, 108], PLD [109] etc.

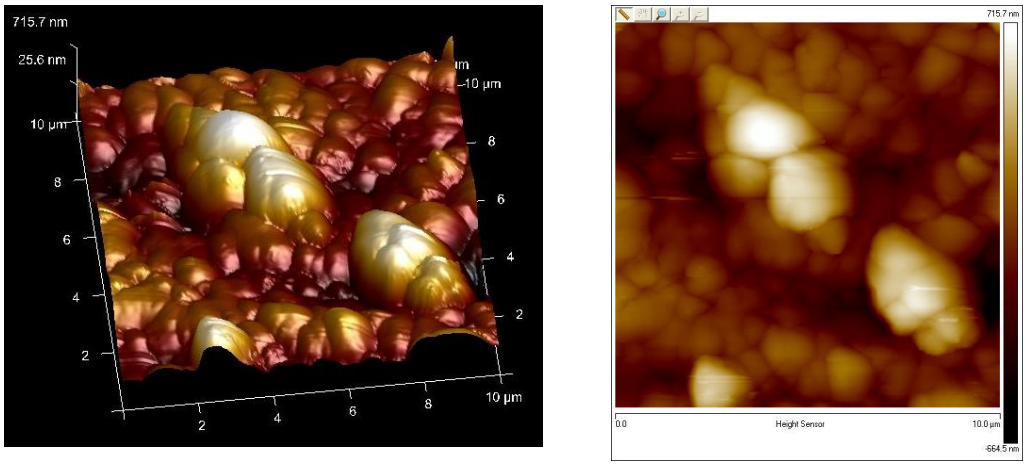

Fig 4.8 AFM image of EPD PZT film (a) 3D image, (b) 2D image

The PZT obtained by EPD which was then removed from the respective substrate was also subjected to TEM studies and the corresponding images have been given in Fig

4.9. The PZT powder used for the EPD studies had a particle size of 800 nm and hence it can be observed from the TEM images that the deposited PZT were also larger particles with particle sizes > 500 nm.

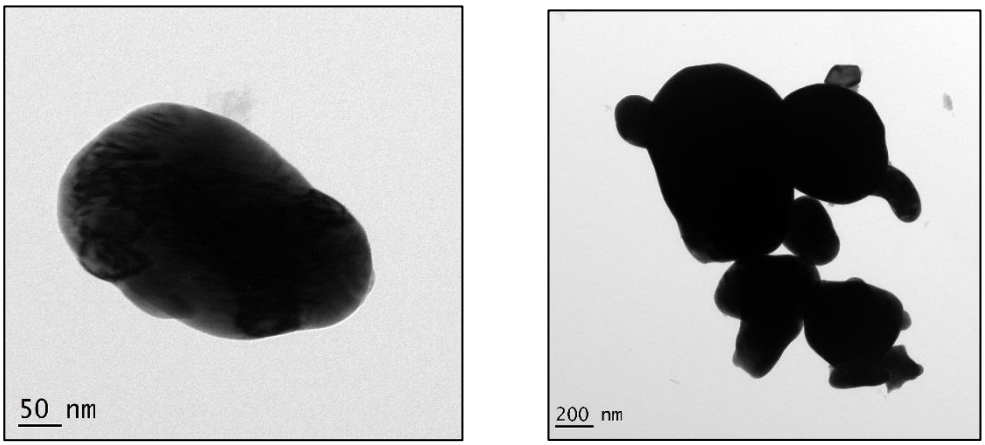

Fig 4.9 TEM images of EPD PZT deposit

4.2.5 Characterisation of crystalline phase of EPD PZT films

The PZT film obtained by electrophoretic deposition were crystallised and compacted by sintering at 600 °C for 30 minutes. The phase formation of the electrophoretic PZT films were studied using XRD and Raman spectroscopy. The normal sintering temperatures utilised for electrophoretic technique are quite high (> 1000 °C) and most of the literature available on PZT electrophoretic deposition have reported higher temperatures of sintering with or without the use of sintering aids. But it is always preferable to use lower temperatures for sintering in order to avoid problems associated with the mismatch of thermal expansion properties of the deposit and the metallic substrates. Therefore in this work, sintering temperatures up to 600°C were utilised.

Fig 4.10 gives the XRD profiles of electrophoretic PZT films (deposited at 200 V/cm, 1 minute on titanium foil) sintered at different temperatures. PZT films were sintered at 300 °C, 500 °C and 600 °C. The XRD pattern of the green PZT film (before sintering) was also studied. It was found that the film showed diffraction peaks corresponding to a standard PZT phase (JCPDS card No. 00-033-0784). Peaks were found at 2θ values 22.497° (001), 31.74° (101), 38.98° (111), 45.237° (200, 002), 50.487° (102), 55.876° (112).

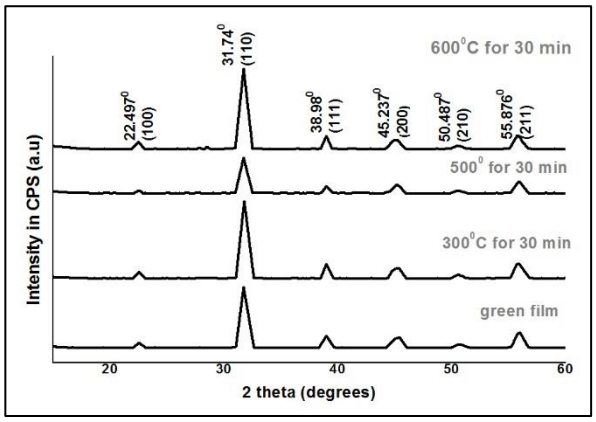

Fig 4.10 XRD of EPD PZT films sintered at various temperatures

In this particular work, Raman spectroscopy was utilised extensively in determining the perovskite crystalline phase formation of the electrophoretic PZT films. Many different studies are available in literature where Raman spectroscopy is used to study the phase transitions of PZT ceramics in the Morphotropic Phase Boundary (MPB) region. Frantti and Lanto [104] use the Raman scattering technique to study the phase transitions of Nd – modified PZT ceramics between 11 and 680 K at MPB. Deluca et al. [102] report the effect of low as well as high temperature on the phase diagram of un-doped PZT in the MPB region using Raman spectroscopy. In all these reported works, PZT samples at MPB concentration were prepared using the mixed-oxide route. Raman analysis of sol-gel prepared films also are reported [121, 105]. But Raman spectroscopy was very rarely used to study the phase formation of electrophoretic PZT films.

The results of Raman spectroscopic analysis of electrophoretic PZT films are shown in Fig 4.11. Similar to XRD, Raman analysis was carried out for electrophoretic PZT films (deposited at 200 V/cm, 1 minute on titanium foil) sintered at different temperatures such as 300 °C, 500 °C and 600 °C and green PZT film (before sintering) was also analysed. From the careful analysis of the Raman data, perovskite phase formation was confirmed for all the four EPD PZT films. Peaks corresponding to tetragonal, rhombohedral and tetragonal-rhombohedral coexistent phases were identified. The optical modes of vibration corresponding to rhombohedral and tetragonal phases are expressed as (A_1 + E) and (E + A_2) and (A_1 + E) & (E + B_1) respectively. From the obtained graphs, major rhombohedral peaks identified were 150 cm^{-1} A_1(TO), 210 cm^{-1} A_1(LO) and E(TO). Tetragonal peaks obtained were 560 cm^{-1} $A_1(TO)_T$ and 731 cm^{-1} $E(LO)_T$. The most important peak corresponding to the

tetragonal-rhombohedral coexistent phase at 285 cm^{-1} was also obtained. The obtained results are in agreement with the existing literature reported on Raman spectroscopic analysis of PZT ceramics. The literature also says that the most prominent PZT perovskite peaks would occur in the Raman shift region within 340 cm^{-1}.

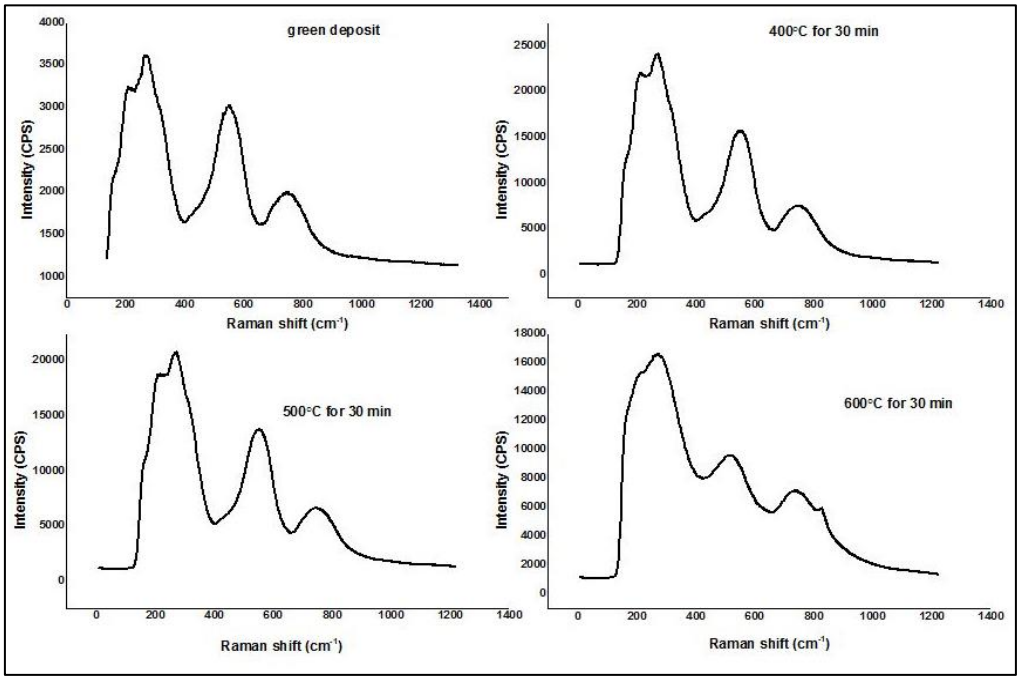

Fig 4.11 Raman spectra of EPD PZT sintered at various temperatures

4.2.6 Dielectric and piezoelectric studies of EPD PZT films

Ferroelectric materials such as PZT are generally very good dielectric materials. From the application point of view, dielectric constant and dielectric loss (tan δ) are important parameters which provide information about a material and decide its suitability for various purposes. A piezoelectric material needs to possess high dielectric constants and low tan δ for effective use in sensor applications. Moreover, ferroelectric material should exhibit polarisation reversal (or switching) by the application of electric field resulting in a hysteresis loop. Hysteresis measurements also give an idea about the leakage current of the material which should be low for optimum sensor performance.

Figure 4.12 shows the dielectric constant and dielectric loss (tan δ) for the PZT film (thickness 50 μm) on titanium foil measured over a frequency range 1 kHz to 1 MHz. At 1 kHz, the dielectric constant and tan δ were obtained as 189 and 0.0686 respectively. It is known that bulk PZT materials with optimum density and greater thickness have higher dielectric constants in the range 2000 – 3000. The lower dielectric

coefficients obtained for PZT films prepared by electrophoretic deposition can be attributed to their lower density and thickness. Literature also report that higher dielectric constants are obtained for PZT films sintered at very high temperatures of the order of > 1000 °C. Van Tassel et al. [79] report a dielectric constant of 750 and tan δ of 0.034 for EPD PZT films. Zhang et al. [122] also obtained values of 1050 and 0.05 for dielectric constant and tan δ respectively. Similarly Wu et al. [123] claim a dielectric constant of 1330 and tan δ 0.06 for PZT films prepared by EPD technique. It was found that all these works used higher temperatures for PZT film sintering. But in this particular work, the focus was mainly on the low temperature sintering on EPD films of PZT. So only sintering temperatures up to 600 °C were utilised. The problems associated with the use of higher temperatures have been explained in the earlier sections of the thesis.

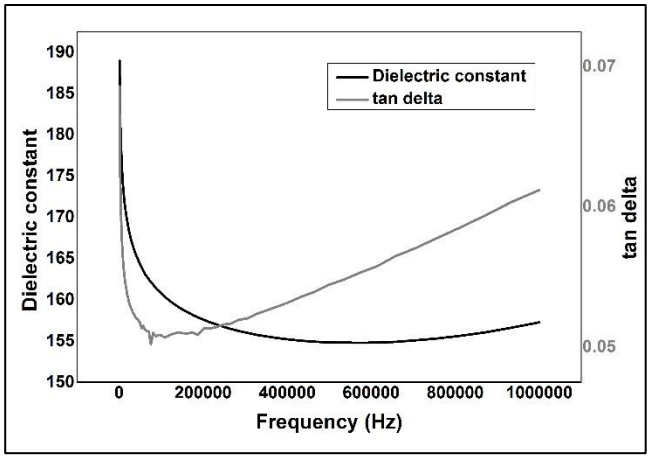

Fig 4.12 Dielectric constant and tan δ vs. frequency (1 kHz to 1 MHz)

From the Fig 4.12, both the dielectric constant and dielectric loss (tan δ) showed a decreasing trend initially followed by a small increase as it approached the resonance frequency. For any piezoelectric material, dielectric constant and tan δ values reach a maximum at a particular frequency called as the Resonance frequency (F_s). The peak in dielectric constant and tan δ at resonance frequency for an EPD PZT film is shown in Fig 4.13. The resonance frequency obtained here is 2.8 MHz.

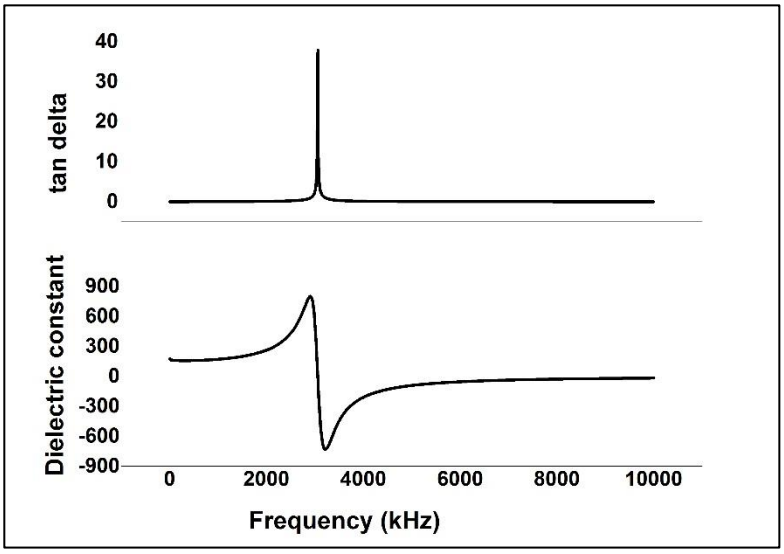

Fig 4.13 Dielectric constant and tan δ at resonance frequency for EPD PZT film

Figure 4.14 gives the hysteresis plots (Polarisation vs. Electric field) obtained for the EPD PZT films deposited on titanium. For a voltage of 800 V, the maximum field applied was 198 kV/cm, with a saturation polarisation of 5.1 C/cm^2 with an average coercive field of 96.3 kV/cm. The remnant polarisation obtained was 3.34 C/cm^2. Hysteresis measurements were done for 400 V, 600 V and 800 V and the resultant saturation polarisation (P_S), remnant polarisation (P_R) and coercive field (E_C) are given in Table 4.2. The polarisation values were low compared to that of bulk PZT ceramics [93] which may be mainly due to the lower density of the obtained films.

Table 4.2 Saturation (P_S), remnant (P_R) polarisation and coercive field (E_C) determined for the ELD PZT deposit

Applied Voltage (V)	Saturation Polarization (P_S) (μC/cm^2)	Remnant Polarization (P_R) (μC/cm^2)	Coercive field (E_C) (kV/cm)
400 V	1.82	0.92	36.27
600 V	3.38	2.10	67.38
800 V	5.10	3.34	96.30

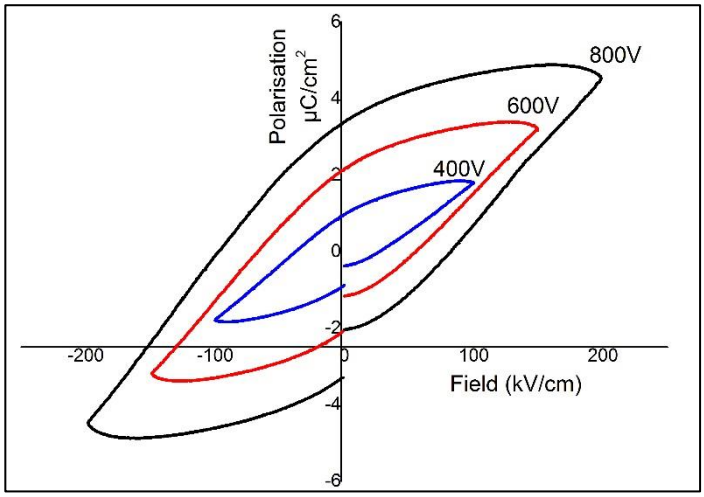

Fig 4.14 Polarisation (*P*) versus electric field (*E*) obtained for PZT film by EPD.

The leakage current characteristics (I–V plots) were also measured for the prepared PZT films. Fig 4.15 shows leakage current density of EPD PZT films for an applied voltage of 50 V and a response time of 100 milliseconds. The leakage current measured was preferably less ($\pm$ 2.85 $\times$ 10^{-7} A/cm^2) and in accordance with the previous studies [112, 113].

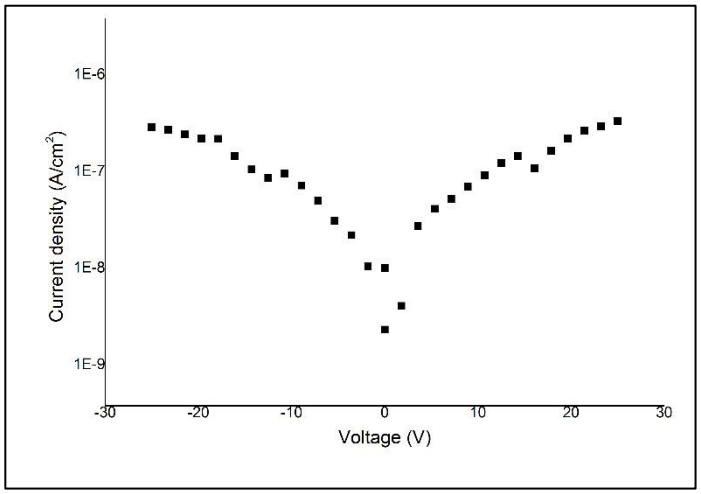

Fig 4.15 Leakage current plot for EPD PZT

4.2.7 Poling of EPD PZT films

Ferroelectric polycrystalline films are known to be composed of multiple domain structure, each of the domains having different directions of polarisation and randomly distributed. The net polarisation value of the material is zero, as the

piezoelectric effects of the domains cancel each other. The process by which polycrystalline ferroelectric materials are converted to a polar state is known as poling. During the poling process, a suitable electric field is applied to the material, whereby reorienting the domains in the direction of the applied field, thus making the material piezoelectric. Poling can be done by different methods such as contact poling technique, corona poling etc. Contact poling is the technique used for bulk piezoelectric materials [123 – 128]. Corona poling is normally used for the poling of piezoelectric polymeric materials such as poly vinylidene fluoride, where larger electric fields (20 – 100 kV/mm) are required [129 - 133]. Most of the earlier reported works are based on contact poling process for PZT materials. Poling results for electrophoretic PZT films have not been widely studied and only very few works are available [120,133].

One of the important parameter that shows the piezoelectric nature of any sample is its d_{33} value, which is defined as the electric polarization generated in a material per unit mechanical stress applied to it. Alternatively, it is the mechanical strain experienced by the material per unit electric field applied to it. The first subscript refers to the direction of polarization generated in the material (at E = 0) or to the applied field strength, the second refers respectively to the direction of the applied stress or to the direction of the induced strain.

In this work, polarisation measurements were carried out for the electrophoretic PZT films using contact poling method. In this method the electroded (using silver paste) PZT film samples, kept in a temperature controlled bath were subjected to high electric fields (1 – 3 kV/mm) for suitable time intervals. The temperature of the silicone oil bath was kept constant at 150 °C. The detailed procedure and equipment set up has been given in Chapter 2, section 2.4. Electrophoretic PZT films (area: 2.5 × 2.5 cm^2) 50 µm thickness were taken and poling studies were carried out at different electric field strengths for various time intervals and substrate materials. The poled samples are then subjected to d_{33} measurements to determine the efficiency of poling. A conventional piezometer (used for bulk samples) were used for the d_{33} measurements of the PZT films.

Fig. 4.16 shows the d_{33} measurements of electrophoretic PZT films for different poling time periods keeping the poling field constant at 2 kV/mm. Poling studies were separately done and d_{33} values measured for PZT films prepared on titanium and stainless steel substrates. From the plot, it was obtained that polarisation increases with poling time. Initially the increase was fast but after a particular period, polarisation reached

saturation, and further increase in poling time did not cause a significant increase in d_{33}. It was also found that d_{33} values obtained were comparatively greater for PZT films on titanium substrates than for SS substrates. This effect may be due to the matching lattice parameters of titanium and PZT ceramics.

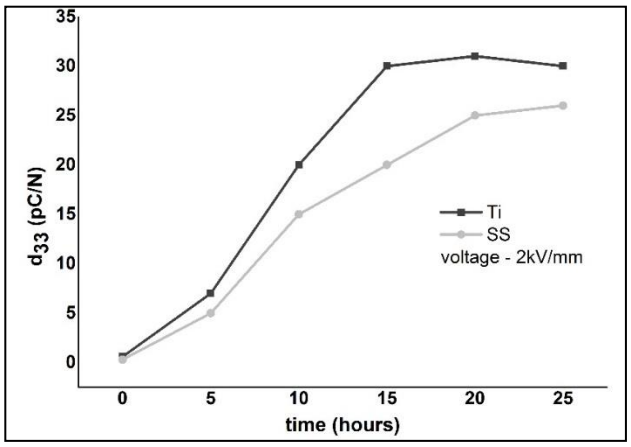

Fig 4.16 d_{33} vs. poling time for EPD PZT films

The d_{33} values obtained here are very low when compared to that of reported PZT bulk materials d_{33} (> 200). It can be accounted to the substrate clamping effect occurring in the prepared PZT films. It was found that strong clamping of the film to the substrate can prevent domain re – orientation during poling. Van Tassel et al. [120] had also reported the reduction in d_{33} values of EPD PZT films due to substrate clamping effects. They had reported d_{33} values for EPD PZT films as 128 pC/N for platinum substrates and 140 pC/N for silver/palladium substrates. However they had carried out the d_{33} measurements using a custom made set up (pressure cell) rather than using the conventional piezometer.

The effect of poling voltage on d_{33} for the electrophoretic PZT films were also studied. Here the poling time was kept constant as 15 hours and the d_{33} values were measured for PZT films deposited on titanium and SS substrates as given in Fig 4.17. It was observed that polarisation increases with increase in poling voltage with a higher d_{33} values obtained for samples prepared on titanium substrates. Poling voltages were increased up to 2 kV/mm and further studies with increase in poling voltage could not be done as the PZT film samples were found to fail and get damaged at higher electric fields.

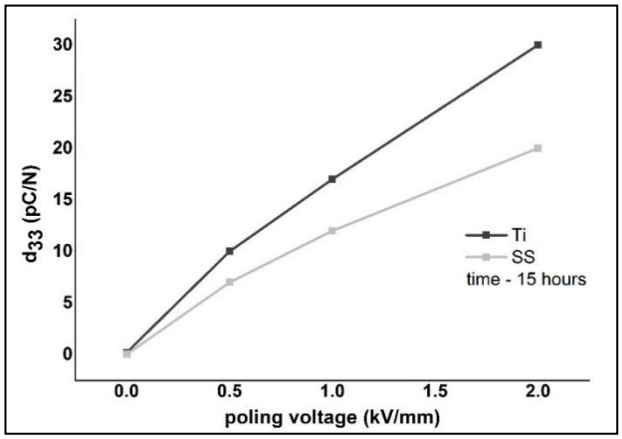

Fig 4.17 d_{33} vs. poling voltage for EPD PZT films

A large area (5 × 5 cm^2) EPD PZT sample of thickness 50 µm was also prepared and poled for carrying out the underwater acoustic measurements which is being explained in the next section (4.2.8.). The poling process for the large area PZT sample were carried at 2 kV/mm at a temperature of 150 °C. The sample was subjected to repeated poling processes at the same poling conditions for a total time period of 25 hours. The d_{33} value obtained for this particular large area EPD PZT film is 71 pC/N. This is the highest d_{33} value obtained for the prepared PZT films in this particular work.

4.2.8 Underwater acoustic measurements of sensor fabricated using EPD PZT film

Literature is available on detailed underwater characterisation of PZT (based on bulk and also films prepared by other conventional methods) [134 – 137]. Piezoelectric materials such as PZT are known as reciprocal elements i.e. they can be used for both receiving and transmitting acoustic signals. Here in this work, mostly the receiving sensitivity or the reception characteristics of the EPD PZT films were mainly focussed as the material for hydrophone (receiver) applications. Receiving sensitivity and directivity patterns were mainly studied in this work. As the material is intended for underwater sensor applications, the acoustic measurements were performed in an acoustic water tank equipped with suitable instrumentation. The base material for the sensor fabrication was the EPD PZT film which was electroded using silver paste and effectively poled. It was then connected to a preamplifier and encapsulated using epoxy resin. The details of the experimental sensor fabrication and the set up for underwater measurements are given in Chapter 2, Section 2.6.

Underwater evaluation of the PZT film sensor was carried out by measuring its receiving sensitivity for various frequency ranges. The receiving sensitivity of the PZT film sensor was determined and is given in Figure 4.18.

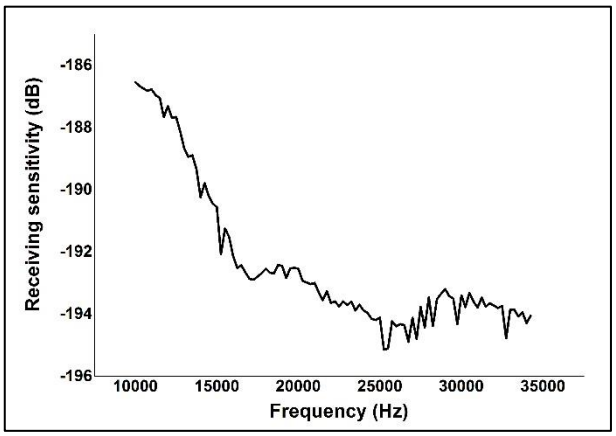

Fig 4.18 Receiving sensitivity plot of EPD PZT film.

It is clear from the figure that the receiving sensitivity is relatively flat from −194 to −193 (dB re 1V/µPa) between 20 and 30 kHz. Hence it can be said that the PZT film sensor fabricated is suitable for high frequency (>20 kHz) underwater applications. Directivity studies of the PZT sensor was also done and the receiving beam patterns obtained at a frequency of 10 kHz are shown in the Figure 4.19. Directivity patterns indicate eminent sensitivity in all directions with maximum values obtained at angles of 90° and 270°.

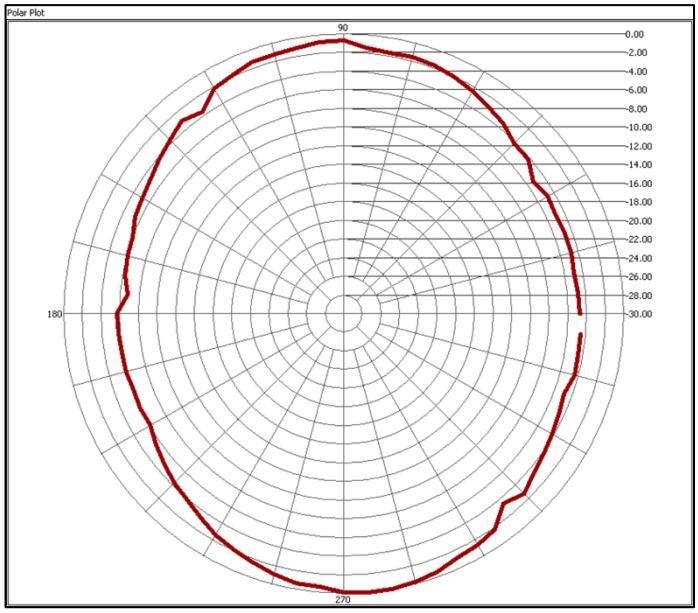

Fig 4.19 Directivity pattern of EPD PZT film.

4.3 CONCLUSIONS

Electrophoretic deposition technique has been successfully utilised to develop conformable/flexible PZT films on titanium and stainless steel foils using PZT – acetic acid based suspensions. The stability of suspension was found to be optimum at a concentration of 3 wt. %. The effect of important process parameters such as voltage, time and deposit thickness etc. as a function of deposit weight was studied in detail. The optimum voltage range and time was obtained as 200 – 300 V/cm and 1 minute respectively. The morphology and microstructure characterisation of PZT films by SEM and AFM reveals a continuous and uniform deposition with a very low surface roughness of approximately 25 nm. The presence of a pure perovskite phase, was confirmed by XRD and Raman spectroscopy. Dielectric and hysteresis studies were also done which decide, the suitability of a particular material for piezoelectric sensing applications. Dielectric constant and tan δ values at 1 kHz was obtained as 189 and 0.0686 respectively. Hysteresis plots gives a saturation polarisation of 5.1 C/cm^2 and the leakage current density was measured as $\pm 2.85 \times 10^{-7}$ A/cm^2. Underwater receiving sensitivity and directivity measurements for the PZT film sensors were done which gave a maximum receiving sensitivity value of – 194 to – 193 (dB re 1V/µPa) and a relatively flat response in the frequency range 20 – 35 kHz, suggesting suitability of the sensor for high frequency underwater applications. The directivity patterns for the PZT films indicated good sensitivity in all directions and maximum values were obtained at angles of 90° and 270°.

Chapter – 5

CONCLUSIONS AND SUGGESTIONS FOR FUTURE WORK

5.1 CONCLUSIONS

In this thesis, electrodeposition techniques have been employed for the development of PZT films for underwater sensing applications. The PZT films (both ELD and EPD) were deposited on thin, flexible metal foils so that flexibility is imparted to the PZT material which otherwise had a hard and brittle nature. Important conclusions that can be drawn from the present work are as follows:

1. **Electrolytic deposition (ELD) of PZT films**.

   Both aqueous and non-aqueous medium were effectively used for the electrolytic deposition of PZT films. Depositions were obtained on titanium foil and SS foil substrates.

   a) ELD of PZT in presence of aqueous medium

   i. The effect of different process parameters on aqueous ELD of PZT were studied.

      Parameters such as (i) current density, (ii) time of deposition, (iii) sintering temperature, and (iv) sintering time were optimised. For aqueous ELD, maximum yield for the PZT deposits were obtained at a current density 15 mA/cm^2 for a time of 5 minutes. Faradaic efficiency was also calculated and was observed as 17 % for PZT films prepared by aqueous ELD. The sintering temperature and time for the PZT films were optimised as 500 ºC and 1 hour respectively.

   ii. It was observed that for aqueous deposition, more continuous and uniform deposition was obtained for titanium substrate, probably due to similar crystallographic structure of titanium and PZT deposition.

   iii. The PZT films prepared by aqueous ELD method were also subjected to extensive material characterisation and the properties were effectively studied. XRD and Raman spectroscopy confirmed the formation of perovskite crystalline phase in the prepared PZT films by ELD. The morphology, microstructure and topography

information about the prepared PZT films were obtained by SEM, TEM and AFM studies. AFM studies indicated that the average roughness of the PZT filme were very high.

b) ELD of PZT in presence of non-aqueous medium

i. The effect of different process parameters on such as (i) current density, (ii) time of deposition, (iii) sintering temperature, and (iv) sintering time on non-aqueous ELD of PZT were studied to obtain optimum yield and film properties. For non-aqueous PZT films, optimum yield and film properties were obtained at a current density of 25 mA/cm^2 for a deposition time of 5 minutes. Faradaic efficiency was found to be 22 % for PZT films prepared by non-aqueous ELD. The sintering temperature and time for ELD PZT films were optimised as 500 ºC and 1 hour respectively.

ii. In the case of non-aqueous deposition, morphology of the ELD PZT films deposited on both SS and titanium substrates were similar but the adhesion to the substrate was better for titanium substrates.

iii. The PZT films prepared by non-aqueous ELD were characterised using techniques such as SEM, TEM, AFM, XRD and Raman spectroscopy. The perovskite crystalline phase formation for the prepared PZT films were confirmed by XRD and Raman spectroscopy. It was seen that the PZT films prepared by non-aqueous ELD had a continuous and uniform surface morphology with minimum porosity. From AFM studies, the non-aqueous PZT films were found to have uniform surface morphology with a very low surface roughness value of 2 nm.

iv. The dielectric and piezoelectric characterisation and hysteresis studies were also performed for the non-aqueous PZT films developed by ELD. For ELD PZT films, the dielectric constant and tan δ values at 1 kHz were obtained as 452 and 0.0429 respectively. Ferroelectric hysteresis behaviour of the PZT films (P-E) were studied.

c) Thin film PZT deposition (non-aqueous) using Potentiostatic/Galvanostatic techniques

i. PZT thin films were prepared by Pulsed Electrodeposition (PED) technique such as Regulated Galvanic Pulse (RGP).

ii. Morphology studies of the films using SEM revealed PZT thin films having continuous microstructure. The topography studies using AFM showed uniform surface with a low surface roughness value of >10 nm. The PZT perovskite structure was confirmed using XRD and Raman spectroscopy.

In the case of ELD method for deposition of PZT films, the DMSO based non-aqueous ELD gave better results with respect to film uniformity and properties. The non-aqueous process gave superior quality PZT films with respect to deposit yield, adhesion, surface topography and microstructure when compared to aqueous method.

2. Electrophoretic deposition (EPD) of PZT films

a) Electrophoretic deposition was effectively utilised for the deposition of PZT films on metallic substrates such as titanium foils and SS foils. The effect of different process parameters on EPD of PZT were studied. It was found that PZT-acetic acid medium containing 3 wt. % PZT, electrodeposited at a voltage range of 200 – 300 V/cm and for a time of 1 minute resulted in good quality PZT films.

b) PZT films of thickness ranging from 15 – 160 µm were deposited using EPD technique. Moreover, PZT films of bulk density up to 67 % were prepared by EPD in this research work.

c) The PZT films formed by EPD techniques were subjected to extensive material characterisation. The morphology, microstructure and topography information about the prepared PZT films were obtained by SEM, TEM and AFM studies. From the microstructure analysis, it was found that the PZT films prepared using EPD had uniform microstructure and close packing of particles without cracks. The perovskite crystalline structure of the PZT films were confirmed by XRD and Raman studies.

d) The dielectric and piezoelectric characterisation and poling studies were also performed for the PZT films. Dielectric constant and tan δ values at 1 kHz were obtained as 189 and 0.0686 respectively. Hysteresis studies were also performed.

It was found that both ELD and EPD could be effectively used for the deposition of PZT films. However, EPD being a particulate method, is simpler and easier to perform technique. The deposition conditions are not very stringent and the film properties like thickness uniformity could be easily ensured by the EPD technique. The chemical composition of PZT film is not a problem during deposition for EPD, as it can be ensured in the PZT powder preparation stage itself. Moreover, the poling process was easier and gave superior hysteresis properties for EPD PZT films.

3. **Fabrication of acoustic sensor using PZT films and underwater acoustic evaluation.**

   An underwater acoustic sensor was fabricated using the PZT films prepared by EPD technique and its underwater acoustic characterisation was carried out. Underwater acoustic sensitivity and directivity studies were performed on the above sensor. The sensor has maximum sensitivity in the high frequency range (20 – 35 kHz) which indicates its suitability for high frequency underwater applications. In this research work, the fabrication of an underwater acoustic sensor based on PZT EPD film and its characterisation has been reported for the first time to the best of our knowledge.

5.2 SUGGESTIONS FOR FUTURE WORK

Few suggestions are also given for future studies.

1. Electroding by sputtering technique need to be explored. Sputtering can give electrode films of high uniformity, precise thickness, and superior surface finish, enhanced conductivity and good contact with the PZT film and can increase the effectiveness of poling and sensing characteristics of the film.
2. Use of sensor for low frequency underwater applications. The currently fabricated sensor using PZT films is suited for high frequency underwater applications due to its high sensitivity at higher frequency ranges such as 20 – 35 kHz. The use of the sensor can be further extended towards a wider range of underwater applications if its sensitivity can be also adjusted for the suitable low frequencies.
3. To maximise sensor performance, pre-stressing of PZT sensor film can to be done and detailed pre-stress mechanism and sensor fabrication need to be studied.

REFERENCES

1. D. Stansfield, *Underwater electroacoustic transducers; a handbook for users and designers*, (Bath University Press and Institute of Acoustics, Great Britain, 1990).
2. Gokhan O. Ozgen, *Introduction to Smart Structures and Materials*, (Spring METU, Ankara, 2011).
3. A. Safari, Development of piezoelectric composites for transducers, *J. Physics III*, 4 (1994) pp. 1129 – 1149 .
4. Jaffe B, Cook W.R, Jaffe H, *Piezoelectric ceramics*, (Academic Press, London, 1971).
5. W. G. Cady, *Piezoelectricity*, (McGraw-Hill New York, 1946).
6. H. Jaffe, D. A. Berlincourt, Piezoelectric transducer materials, *Proc of the IEEE*, 53 (1965) pp.1372 – 1386.
7. A. L. Kholkin, N. A. Pertsev, and A.V. Goltsev, *Piezoelectric and Acoustic Materials for Transducer Applications*, by A. Safari, E. K. Akdogan, (Springer Science, LLC 2008).
8. R. S. Dahiya, M. Valle, *Robotic Tactile Sensing*, (Springer Science, Dordrecht 2013).
9. A. J. Moulson, J. M .Herbert, *Electroceramics*, 2nd Edition, (John Wiley & Sons, England 2003).
10. C. S. Brown, R. C. Kell, R. Taylor, L. A. Thomas, Piezoelectric Materials; A review of progress, *Proc IEE*, 109B (1962) pp. 99 – 114.
11. J. Valasek, Piezoelectric and Allied Phenomena in Rochelle salt, *Phys. Rev*, 17 (1921) pp. 475 – 81.
12. Kawai H, The Piezoelectricity of PVDF. *Jap. J. Appl. Phys*, 8 (1969) pp. 975 – 978.
13. Park S. E, Shrout T. R, Ultra high strain and piezoelectric behaviour in relaxor based ferroelectric single crystals. *J Appl Phys*, 82 (1997) pp. 1804 –1811.
14. Wei Hu, Experimental search for high Curie temperature piezoelectric ceramic with combinatorial approaches, *Ph.D. thesis*, Iowa University, Ames, Iowa, 2011.
15. S. Cochran, *Ultrasonic transducers*, edited by K. Nakamura (Wood head Publishing Limited, Cambridge, UK, 2012).
16. K. Lefki, G. J. M. Dormans, Measurement of piezoelectric coefficients of ferroelectric thin films, *J Appl Physics,* 76 (1994) pp. 1764 – 1767.

17. N. Izyumskaya, Y. I. Alivov, S. J. Cho, H. Morkoc, Processing, Structure and Applications of PZT thin films, *Critical Reviews in Solid State and Material Sciences*, 32 (2007) pp. 111 – 202.
18. Eiichi Fukada, History and recent progress in piezoelectric polymers, *IEEE Transactions on Ultrasonics, Ferroelectrics & Frequency Control,* 47 (2000) pp. 1277 – 1290.
19. Mitchell. L. Thompson, The material properties and constitutive equations of piezoelectric PVDF, *Ph.D thesis*, Drexel University, 2002.
20. R. E. Newnham, L. J. Bowen, K. A. Klicker, L. E. Cross, Composite piezoelectric transducers, *Materials in Engineering*, 2 (1980) pp. 93 – 106.
21. S. K. Pradhan, Amit Kumar, A. N. Sinha, Rabichandra Pandey, Pawan Kumar, Manoranjan Kar, Study of ferroelectric properties on PVDF-PZT nanocomposite, *Ferroelectrics,* 516 (2017) pp. 18 – 27.
22. S. Banerjee, K. A. Cook-Chennault, W. Du, V. Sundar, H. Halim, A. Tang, Piezoelectricity and dielectric characterisation of corona & contact poled PZT – epoxy MWCNT bulk composites, *Smart Mat. Struct.,* 25 (2016) pp. 115018_1 – 115018_11.
23. J. Tolvanen, J. Hanny, Mikko Nelo, J. Juuti, H. Jantunen, Dielectric properties of novel polyurethane – PZT – graphite foam composites, *Smart Mat. Struct.,* 25 (2016), pp. 095039_1 – 095039_12.
24. W. Lee, O. Khahya, C. T. Toh, B. Ozyilmaz, J. H. Ahn, Flexible graphene – PZT ferroelectric non-volatile memory, *Nanotechnology,* 24 (2013), pp. 475202_1 – 475202_6.
25. Robert Y. Ting, A review on the development of piezoelectric composites for underwater acoustic transducer applications, *IEEE transactions on Instrumentation and Measurements*, 41 (1992), pp. 64 – 67.
26. J. Conde, P. Muralt, Dielectric and acoustical high frequency characterisation of PZT thin films, *IOP Conference Series: Mat Sci and Engineering*, 8 (2010) pp. 012009_1 – 012009_4.
27. Z. Zuo, B. Chen, Q. Zhan, Y. Liu, H. Yang, Z. Li, G. Xu, R. W. Li, Preparation and ferroelectric properties of freestanding $Pb(Zr,Ti)O_3$ thin membranes, *J. Phys D*: *Appl. Phys*, 45 (2012) pp. 185302_1 – 185302_5.
28. Shoji Okamoto, P. S. Shankara Rama Krishnan, Satoshi Okamoto, Shintaro Yokoyama, Kensuke Akiyama, Hiroshi Fumakubo, In-plane orientation and

compositional dependencies of crystal structure and electrical properties of {100}-oriented $Pb(Zr,Ti)O_3$ films grown on (100) silicon substrates by metal organic vapour deposition, *Jap. J. Appl. Phys*, 56 (2017) pp. 10PF12_1 – 10PF12_5.

29. H. Hida, T. Hamamura, T. Nishi, G. Tan, T. Umegaki, I. Kanno, Piezoelectric characterisation of $Pb(Zr,Ti)O_3$ thin films deposited on metal foil substrates by dip coating, *Jap. J. Appl. Phys*, 56 (2017) pp. 10PF08_1 – 10PF08_5.
30. Walter Heywang , Karl Lubitz, Wolfram Wersing, *Piezoelectricity*, (Springer, Berlin Heidelberg, 2008).
31. K. Shimomura, T. Tsurumi, Y. Ohba, M. Daimon, Preparation of lead zirconate titanate thin film by hydrothermal method, *Jpn. J.Appl. Phys*. 30 (1991) pp. 2174 – 2177.
32. W. Haessler, R. Thielsch, N. Mattern, Structure and electrical properties of PZT thick films produced by plasma spraying, *Materials Letters*, 24 (1995) pp. 387–391.
33. E. Nieto, J. F. Fernandez, C. Moure, P. Duran, Multilayer piezoelectric devices based on PZT, *Journal of Materials Science: Materials in Electronics*, 7 (1996) pp. 55 – 60.
34. Hongxue Zhang, Antti Uusimäki, Seppo Leppävuori and Pentti Karjalainen, Phase transition revealed by Raman spectroscopy in screen-printed lead zirconate titanate thick films , *J. Appl. Phys*. 76 (1994) pp. 4294 – 4300.
35. Hideko Adachi, Yoshimi Kuroda, Takuya Imahashi and Kazuhisa Yanagisawa, Preparation of Piezoelectric Thick Films using a Jet Printing System, *Jap. J. Appl. Phys*, 36 (1997) pp. 1159 – 1163.
36. Seffner L, Gesemann H. J, Preparation and application of PZT thick film, *Electroceramics IV Proceedings. Vol.1*, Aachen: Augustinus, 1994.
37. James Colliera, Iván A. Cornejoa & Michael J. Hauna, Ferroelectric thick-films for piezoelectric applications, *Ferroelectrics*, 54 (1994) pp. 47 – 52 .
38. I. Zhitomirsky, Cathodic electrodeposition of ceramic and organoceramic materials: fundamental aspects, *Advances in Colloid & Interface Science,* 97, 2002, pp. 279 – 317.
39. I. Zhitomirsky, L. Gal-Or, *Intermetallic & Ceramic coatings*, edited by Narendra B. Dalhotre & T. S. Sudarshan (Marcel Dekkar, New York, 1999).

40. L. Gal–Or and I. Zhitomirsky, Characterisation of zirconium, lanthanum and lead oxide deposits prepared by cathodic electrosynthesis, *J. Mat Sc*, 33 (1998) pp. 699 – 705.
41. I. Zhitomirsky and L. Gal-Or, Cathodic electrosynthesis of ceramic deposits, *J of Eur Cer Soc*, 1 (1996) pp. 819 – 824.
42. M. Aghazadeh, A. M. Barmi, and M. Hosseinifard, Nanoparticulates of $Zr(OH)_4$ and ZrO_2 prepared by low temperature cathodic electrodeposition, *Material Letters*, 73 (2012) pp. 28 – 31.
43. M. Aghazadeh and M. Hosseinifard, Electrochemical preparation of ZrO_2 nano powders; Impact of the pulse current on the crystal structure, composition and morphology, *Ceramics International*, 39 (2013) pp. 4427 – 4435.
44. M. Aghazadeh, Cathodic electrodeposition of ZrO2, Impact of current density on crystal structure, composition and morphology, *J of Electrochem Soc*, 59, (2012) pp. E53 – E58.
45. S. K. Yen, Mechanism of electrolytic ZrO_2 coatings on commercially pure titanium, *Mat Chem & Phys*, 63 (2000) pp. 256 – 262.
46. Espitia Cabrera, H. Oroco Hernandez, R. Torres Sanchez, M. E. Contreras Garcia, P. Bartolo Perez and L. Martinez, Synthesis of nanostructured zirconia electrodeposited films on AISI 316L stainless steel and its behaviour in corrosion resistance assessment, *Material Letters*, 58 (2003) pp. 191 – 195.
47. X. Pang, I. Zhitomirsky, M. Niewczas, Cathodic electrolytic deposition of zirconia films, *Surface & Coatings Tech*, 195 (2005) pp. 138 – 146.
48. I. Zhitomirsky, L. Gal-Or, A. Kohn, Cathodic electrosynthesis of PZT films, *Material Letters*, 25 (1995) pp. 223 – 227.
49. I. Zhitomirsky, L. Gal-Or, A. Kohn, Electrolytic PZT films, *J of Mat Sc*, 32 (1997) pp. 803-807.
50. I. Zhitomirsky, Electrolytic deposition of oxide films in the presence of hydrogen peroxide, *J of Eur Cer Soc*, 19 (1999) pp. 2581 – 2587.
51. Y. Lin, J. W. Shaffer, H. A. Sodano, Electrolytic deposition of PZT on carbon fibers for fabricating multifunctional composites, *Smart Materials & Structures*, 19 (2010), pp. 124004_1 – 124004_8.
52. P. F. Ren, J. L. Zhu, X. P. Zou, J. Cheng, F. Li, H. D. Zhang, M. F. Wang and Y. Su, Preparation of PZT ferroelectric thin films by electrochemical reduction,

Proceedings of 2nd IEEE International Nanoelectronics Conference, Nantes 2008.

53. Yasumichi Matsumoto, Hideki Adachi, Jukichi Hombo, New preparation method for PZT films using electrochemical reduction, *J of Am Cer Soc*, 76 (1993) pp. 769 – 772.
54. H. W. Hennicke, I. Zhitomirsky, L. Gal- or, A. Kohn, Electrodeposition of ceramic films from non aqueous and mixed solutions, *J of Mat Sc*, 30 (1995) pp. 5307 – 5312.
55. C. Gheorgies, The electrolytic preparation and physical characterisation of $ZrTiO_4$ films, *Journal of Crystal Growth*, 213 (2000) pp. 112 – 115.
56. Raghu N. Bhattacharya and David S. Ginley, Preparation of Lead Zirconium Titanium film and powder by Electrodeposition, *J of Electrochem Soc*, 143, (1996) pp. 97 – 99.
57. Raghu N. Bhattacharya and David S. Ginley, *US patent* .5462647 (Midwest Research Institute, Kansas, 1995).
58. I. Zhitomirsky, Electrophoretic and electrolytic deposition of ceramic coatings on carbon fibers, *J of Eur Cer Soc*, 18, (1998) pp. 849 – 856.
59. I. Zhitomirsky, A. Petric, M. Niewczas, Nanostructured ceramic and hybrid materials via electrodeposition, *JOM*, 54 (2002) pp. 31 – 34.
60. Herald Natter, Rolf Hempelmann, Tailor made nanomaterials designed by electrodeposition methods, *Electrochimica Acta*, 49 (2003) pp. 51 – 61.
61. I. Corni, M. P. Ryan, A. R. Boccaccini, Electrophoretic Deposition (EPD): from traditional ceramics to nanotechnology, *J of Eur Cer Soc*, 28 (2008) pp. 1353 – 1362.
62. P. Sarkar, P. S. Nicholson, Electrophoretic deposition (EPD): Mechanisms, Kinetics and Applications to Ceramics, *J. Am. Cer. Soc*, 79 (8), (1996) pp. 1987–2002.
63. A. R. Boccaccini, I. Zhitomirsky, Application of electrophoretic and electrolytic deposition techniques in ceramics processing, *Current Opinion in Solid State and Materials Science*, 6, (2002) pp. 251 – 260.
64. Liang Yao, Chu Anzhong Chen, DiangangWang, Quanhe Bao, Jie Ma, Biao Qi, Application of PZT in the coating and porous materials fabrications, *Surface review and Lett*, 13 (2006) pp. 163 – 169.

65. J. Van Tassel, C. A. Randall, Mechanisms of Electrophoretic Deposition, *Key Engineering Materials*, 314 (2006) pp. 167–174.
66. C. Kaya, F. Kaya, B. Su, B. Thomas, A. R. B, Structural and functional thick ceramic coatings by electrophoretic deposition, *Surface Coatings Tech*, 191 (2005) pp. 303 – 310.
67. G. Anne, K. Vanmeensel, J. Vleugels, O. Van der Biest, Influence of the suspension composition on the electric field and deposition rate during electrophoretic deposition, *Colloids and Surfaces A: Physiochem Eng. Aspects*, 245 (2005) pp. 35 – 39.
68. I. Zhitomirsky, A. Petric, Electrophoretic deposition of ceramic materials for fuel cell applications, *J of Eur Cer Soc*, 20 (2000) pp. 2055 – 2061.
69. T. Sweeney, R. W. Whatmore, Electrophoretic deposition of PZT ceramic films, *Proceedings of the 10th IEEE International Symposium on Applications of Ferroelectrics*, IEEE, Piscataway, New Jersey, 1996.
70. B. Su, C. B. Ponton, T. W. Button, Hydrothermal and electrophoretic deposition of lead zirconate titanate (PZT) films, *J of Eur Cer Soc*, 21 (2001) pp. 1539 – 1542.
71. A. R. Boccacini, S. Y. Ng, Lead Zirconate Titanate films on metallic substrates by electrophoretic deposition, *J of Mat Sc & Engg, B* 116 (2005) pp. 208 – 214.
72. Jan Ma, R. Zhang, C. H. Liang, Colloidal characterization and electrophoretic deposition of PZT, *Material Letters*, 57 (2003) pp. 4648 – 4654.
73. Jan Ma, Wen Cheng, Deposition and packing study of sub-micron PZT ceramics using electrophoretic deposition, *Material Letters*, 56 (2002) pp. 721 – 727.
74. Y. Sakka, T. Uchikoshi, Forming and microstructure control of ceramics by electrophoretic deposition (EPD), *KONA powder & particle Journal*, 28 (2010) pp. 74 – 90.
75. A. P. Abellard, F. Levassort, D. Kuscer, J. Holc, J. M. Gregoeire, O. Noshchenko, M. Kosec, M. Lethiecq, Electrophoretic deposition (EPD) process of lead zirconate titanate (PZT) thick films, fabrication and high frequency medical imaging, *Proceedings of Acoustics 2012*, Nantes, France, 2012.
76. S. Doungdaw, T. Uchikoshi, Y. Noguchi, C. Eamchotchawalit, Y. Sakka, Electrophoretic deposition of PZT powder from ethanol suspension prepared with phosphate ester, *Science and Technology of Advanced Materials*, 6 (2005) pp. 927 – 932.

77. Danjela Kuscer, Tina Bakaric, Bojan Kozlevkar, Marija Kosec, Interactions between lead zirconate titanate, poly acrylic acid and poly vinyl butyral in ethanol and their influence on electrophoretic behaviour, *Journal of Physical chemistry B*, 117 (2013) pp. 1651 – 1659.
78. Danjela Kuscer, M. S. Bernardo, B. Malic, PZT-Based Thick Films Prepared by Electrophoretic Deposition from Suspensions with Different Alcohol-Based Solvents, *J. Electrochem Soc*, 162 (11) (2015) pp. D3040 – D3048.
79. J. Van.Tassel, C. A. Randall, Electrophoretic deposition and sintering of thin/thick PZT films, *J of Eur Cer Soc*, 19, 1999, pp. 955 – 958.
80. A. Wu, P. M. Vilarinho, S. Srinivasan, A. I. Kingon, I. M. Reaney, D. Woodard, A. R. Ramos, E. Alves, Microstructural studies of PZT thick films on Cu foils, *Acta Materialia*, 54 (2006) pp. 3211 – 3220.
81. B. D. Cullity, *Elements of X-Ray diffraction*, (Addison-Westy Pub Comp Inc, USA 1959).
82. Pavia, Lampman & Kriz, Vyvyan, Introduction to Spectroscopy, Fourth Edition, (Brooks/Cole, USA 2009).
83. Zhiyun Li, M. Jamal Deen, Shiva Kumar, P. Ravi Selvaganapathy, Raman spectroscopy for in-line water quality monitoring – instrumentation and potential, *Sensors*, 14 (2014), pp. 1725 – 1730.
84. Ryan Shaw, Dynamic Light Scattering Training: Achieving reliable nano particle sizing, *Malvern Instruments User's Manual*, ATA Scientific, www.atascientific.com.au.
85. Michael Thompson, CHNS Elemental Analysers, *amc technical briefs: Analytical Methods Committee*, AMTCB No. 29 (2008).
86. C. W. Oatley, W. C. Nixon, R. F. W. Pease, Scanning Electron Microscopy, *Advances in Electronics and Electron Physics*, 21 (1966) pp. 181 – 247.
87. David. B. Williams, C. Barry Carter, *Transmission Electron Microscopy, a textbook for Material Science*, (Springer Science 2009).
88. J. B. Reed, *Electron Microprobe Analysis 2nd Edition*, (Cambridge University Press 1993).
89. James Allen Christman, Piezoelectric measurement using an atomic force microscope, *PhD thesis*, Dept of Physics, Rayleigh, 1999.
90. Daniel Rugar, Paul Hansma, Atomic Force Microscopy, *Physics Today* (1990) pp. 23 – 30.

91. Surfix Easy X-series, *Technical Data Sheet*, PHYNIX GmbH.Co.KG, www.phynix.com.
92. IEEE Standard on *Piezoelectricity*, ANSI/IEEE Standard, pp. 176 – 1987
93. Damjanovic, *The Science of Hysteresis Vol 3*, by I. Mayergoyz and G. Bertotti (Elsevier 2005).
94. M. Stewart & M. G. Cain, Ferroelectric hysteresis measurement & analysis, *NPL Report* CMMT (A) 152, 1999.
95. Takaakitsurumi, S. M. Num, Y. B. Ki, S. Wada, High frequency measurement of P-E hysteresis curves of PZT thin films, *Ferroelectricity*, 259 (2001) pp. 43 – 48.
96. Jay. A. Switzer, Y. Zhou, Growth of Cerium (IV) oxide films by electrochemical generation of base method, *Journal of Alloys & Compounds*, 237 (1996) pp. 1 – 5.
97. G. Helen Annal Therese, P. Vishnu Kamath, Electrochemical synthesis of metal oxides and hydroxides, *Chem Mater*, 12 (2000) pp. 1195 – 1204.
98. R. Chaim, I. Silberman, L. Gal – Or, Electrolytic zirconia coatings, II. Microstructural aspects, *J. Electrochem Soc*, 138 (1991) pp. 1942 – 1946.
99. L. Gal – Or, I. Silberman, R. Chaim, Electrolytic zirconia coatings, I. Electrochemical aspects, *J. Electrochem Soc*, 138 (1991) pp. 1939 – 1942.
100. Shiow Kang Yen, Mechanism of electrolytic ZrO_2 coatings on commercial pure titanium, *Materials Chemistry and Physics*, 63 (2000) pp. 256 – 262.
101. E. Buixaderas, M. Berta, L. Kozielski, I. Gregora, Raman spectroscopy of $Pb(Zr_{1-x}Ti_x)O_2$ graded ceramics around the morphotropic phase boundary, *Phase Transitions*, 84 (2011) pp. 528 – 541.
102. M. Deluka, H. Fukumura, N. Tonari, C. Capiani, N. Hasuike, K. Kisoda, C. Galassi, H. Harima, Raman spectroscopic study of phase transtions in undoped morphotropic $PbZr_{1-x}Ti_xO_2$, *J of Raman Spectroscopy*, 42 (2011) pp. 488 – 495.
103. J. F. Meng, , R. S. Katiyar, G. T. Zou, X. H. Wang, Raman phonon modes and ferroelectric phase transitions in nanocrystalline lead zirconate titanate, *Phys Stat Sol*, 164 (1997) pp. 851 – 862.
104. J. Frantti, V.Lanto, Structural studies of Nd – modified lead zirconate titanate ceramics between 11 K and 680 K at morphotropic phase boundary, *Phycal Rev B*, 50 (1997) pp. 221 – 236.

105. Liang Ting, Li Junhong, Du Wenlong, Xue Chenyang, Zhang Wengdong, Raman scattering studies on PZT thin films for trigonal-tetragonal phase transitions, *J of Semiconductors*, 30 (2009) pp. 083001-1 – 083001-3.
106. Doron Aurbach, *Non Aqueous Electrochemistry*, (Marcel Dekker, USA 1999)
107. S. K. Pandey, A. R. Raju, R. Raman, S. N. Chatterjee, Structural, ferroelectric & characterisation of optical properties of PZT thin films, *Physica B*, 369 (2005) pp. 135 – 142.
108. Jang, Kuo, Fabrication & characterisation of PZT thick films for sensing & actuation, *Sensors*, 7 (2007) pp. 493 – 507.
109. Savastru, Tenciu, Lungu, Viespe, PZT films prepared by TVA and PLD from PbO_2:TiO_2:ZrO_2 (1:1:1) nanoceramic targets, *Digest Journal of Nanomaterials & Biostructures*, 6 (2011) pp. 207 – 212.
110. Takaki Tsurumi, Somg – Min – Num, Young bae Kii, Satoshi Wada, High frequency measurements of P – E Hysteresis curves of PZT thin films, *Ferroelectrics*, 259 (2001) pp. 43 – 48.
111. T. M. Kamel, Poling and switching of PZT ceramics, field and grain size effects, *Ph.D. thesis*, 2007
112. Zhu, Li, Zhou, Shi, Shung, Peizoelectric PZT thick films on $LaNiO_3$ buffered stainless steel foil for flexible device applications, *J Phys D Appl Phys*, 42 (2008) pp. 025504_1 – 025504_4.
113. M. Prabhu, Studies of pure and doped lead zirconate titanate ceramics and pulsed laser deposited lead zirconate titanate thin films, *Ph.D. thesis*, B. S. Abdul Rahman University, 2013.
114. Chandrasekar, Malathy Pushpavanam, Pulse and pulse reverse plating-Conceptual, advantages and applications. *Electrochimica* Acta, 53 (2008) pp. 3313–3322.
115. M. Aghazadeh and M. Hosseinifard, Electrochemical preparation of ZrO_2 nano powder: Impact of the pulse current on the crystal structure, composition and morphology. *Ceramics International*, 39 (2013) pp. 4427– 4435.
116. E. Setare, K. Raeissi, M. A. Golozar, M. H. Fathi, The structure and corrosion barrier performance of nanocrystalline zirconia electrodeposited coatings, *Corrosion Science*, 51 (2009) pp. 1802 – 1808.

117. N. R. de Tacconi, C. R. Chenthamarakshan, K. Rajeshwar, T. Pauport, D. Lincot, Pulsed electrodeposition of WO_3 – TiO_2 composite films, *Electrochemistry Communications*, 5 (2003) pp. 220 – 224.
118. M. S. Bernardo, B. Malic, D. Kuscer, PZT based thick films prepared by Electrophoretic Deposition from suspensions with different alcohol based solvents, *J of Electrochem Soc*, 162 (2015) pp. D3040 – D3048.
119. J. W. Kim, J. G. Heinrich, Influence of processing parameters on microstructure and ferroelectric properties of PZT coated SiC fibers, *J of Eur Cer Soc*, 25 (2005) pp. 1637 – 1645.
120. J. Van Tassel, Electrophoretic deposition: Fundamental mechanisms and examples with an in depth examination of ion depletion effect, *Ph.D. thesis*, The Graduate College, College of Earth and Mineral Sciences, The Pennsylvania State University, 2004.
121. S. R. Shannigrahi, S. Tripathy, Micro-Raman spectroscopic investigation of rare earth modified lead zirconate titanate ceramics, *Ceramics International*, 33 (2007) pp. 595 – 600.
122. R. F. Zhang, J. Ma, L. B. Kong, Lead Zirconate Titanate thick film prepared by Electrophoretic deposition from oxide mixture, *Journal of Materials Research*, 17 (2002) pp. 933 – 935.
123. Aiying Wu, P. M. Vilarinho, A. I. Kingon, Electrophoretic deposition of Lead Zirconate Titanate films on metal foils for embedded components, *J of Am Cer Soc*, 89 (2006) pp. 571 – 581.
124. T. M. Kamel, G. De With, Poling of hard ferroelectric PZT ceramics, *J of Eur Cer Soc*, 28 (2008) pp. 1827 – 1838.
125. T. M. Kamel, G. De With, Grain size effect on the poling of soft Pb(Zr, Ti)O_3 ferroelectric ceramics, *J of Eur Cer Soc*, 28 (2008), 851 – 861.
126. T. M. Kamel, F. X. N. M. Kools, G. De With, Poling of soft piezoceramic PZT, *J of Eur Cer Soc*, 27 (2007) pp. 2471 – 2479.
127. W. L. Zhong, Y. G. Wang, S. B. Yue, P. L. Zhang, Domain reorientation by poling of PZT ceramics in the morphotropic phase boundary region, *Solid State Communications*, 90 (1994) pp. 383 – 385.
128. Anderson. D. Prewitt, Effects of the poling process on dielectric, piezoelectric and ferroelectric properties of lead zirconate titanate, *Ph.D. thesis*, University of Florida, 2012.

129. H. Kim, F. Torres, Y. Wu, D. Villagran, Y. Lin, T. L. TSeng, Integrated 3D printing and Corona poling process of PVDF piezoelectric films for pressure sensor applications, *Smart Mat. Struct.* 26 (2017) pp. 080527_1 – 080527_9.

130. S. K. Mahadeva, J. Berring, K. Walus, B. Stoeber, Effect of poling time & grid voltage phase transition and piezoelectricity of poly (vinylidene fluoride) thin films using corona poling. *J Phys. D: Appl. Phys.* 46 (2013) pp. 1 – 7.

131. Y. Jiang, Y. Ye, J. Yu, Z. Wu, W. Li, J. Xu, G. Xie, Study of thermally poled & corona charged poly (vinylidene fluoride) films, *Polymn. Eng. Sc*, 47 (2007) pp. 1344 – 1350.

132. T. Kaura, R. Nath, M. M.Perlman, Simultaneous tretching & Corona poling of PVDF films, *J Phys. D: Appl. Phys.* 24 (1991) pp. 1848 – 1852.

133. A. Wu, P. M. Vlarinho, A. I. Kingon, Ceramic Processing strategies for thick films on Cu films, *Acta Materialia*, 58 (2010) pp. 2282 – 2290.

134. J. A. Brown, K. Dunphy, J. Leadbetter, R. B. Adamson, O. Beslin, A single-crystal hydrophone for increases sensitivity, *Proceedings of Meetings on Acoustics*, Montreal, Canada 2013.

135. J. C. Liu, Y. T. Cheng, S. Y. Ho, H. S. Hung, S. H. Chang, Fabrication and Characterisation of high sensitivity Underwater acoustic multimedia communication devices with thick composite PZT films, *J of Sensors*, 7326916 (2017) pp. 1 – 7.

136. W. W. L. Au, M. C. Hastings, *Principles of Marine Bioacoustics*, (Springer Science, LLC 2008).

137. H. Kara, R. Ramesh, R. Stevens, C. R. Bowen, Porous PZT ceramics for receiving transducers, *IEEE transactions on Ultrasonics, Ferroelectrics & Frequency Control*, 50 (2003) pp. 289 – 296.

PUBLICATIONS BASED ON WORK

Journal Papers

1. **Sherin Joseph**, A.V.Ramesh Kumar and Reji John, Electrophoretic deposition of lead zirconate titanate from a nanofluid medium for acoustic sensor applications, *Journal of Nanofluids,* 6 (2017) pp. 197 – 204.

2. **Sherin Joseph**, A.V.Ramesh Kumar and Reji John, Non-aqueous electrochemical deposition of PZT films for flexible sensor applications, *Journal of Modern Physical Letters B,* 31 (2017) pp. 1750287_1 – 1750287_14.

3. **Sherin Joseph**, A.V.Ramesh Kumar and Reji John, A novel approach to PZT coatings for conformal sensor applications, *Journal of Marine Biological Association of India*, 58 (2017) pp. 39 – 43.

Conference Proceedings

1. **Sherin Joseph,** A.V.Ramesh Kumar and Reji John, Electrochemical deposition of nanostructured lead zirconate titanate films using potentiostatic/galvanostatic techniques, *4th International conference on Nano science and Technology (COCHIN NANO 2016)*, CUSAT, February 2016, Kochi.

2. **Sherin Joseph**, A.V.Ramesh Kumar and Reji John, Development of flexible lead zirconate titanate material for acoustic conformal sensor applications and its characterisation by SEM and other techniques, *Proceedings of Microscopy In Materials Science And Biomimetic Technology*, DMSRDE, 2015, Kanpur, India.

ANNEXURE – 1

(BASED ON SUGGESTIONS OF THE EXAMINERS)

1. Was underwater studies performed for the PZT films prepared by ELD technique? If not, why?

For developing underwater acoustic sensors, lead zirconate titanate (PZT) films should have high d_{33} value after poling. The maximum d_{33} value, attained by the PZT film prepared by ELD method was found to be 1.3 pC/N which is very low when compared to the d_{33} value obtained for an EPD PZT film which is 71 pC/N. Further, it was found that ELD film when exposed to high voltage (1 – 3 kV/mm at a temperature of 100 ℃) for poling, which is a most essential process for a piezo material for developing an acoustic sensor, was showing dielectric breakdown. Many samples were tried in a similar way, however, could not make a sensor for getting the required performance.

2. How does the cost of the PZT films compare with that of polymeric materials?

The cost of the PZT film is relatively lower when compared to PVDF films. The raw material cost for preparing a 100 µm PZT film (area 2×2 cm^2) is around ₹60, whereas a 100 µm Goodfellow PVDF film (area 2×2 cm^2) costs around ₹1000.

3. How is time of deposition arrived at? How does time affect the film thickness and how is it measured?

The time of deposition of PZT films for both ELD and EPD methods have been extensively studied and optimised in the present work. The effect of time on deposit weight and faradaic efficiency of PZT films by ELD process have been given in detail in the section 3.2.2 and 3.3.2 of Chapter 4 in the thesis. It was observed that the film thickness increased with respect to time and found to vary from 15 to 160 µm. It was found that thickness of the PZT films reaches a saturation value of around 160 µm after a time of 5 minutes. Further it was found that thickness uniformity for the films was more for thin films obtained at lesser time periods than for thicker films. Based on the results, the optimum time required for deposition of uniform film was found to be 1 minute . The thickness of the PZT films were measured using an eddy current based coating thickness gauge.

4. What is the principle of electrodeposition? What is the main difference between EPD and ELD techniques?

Electrodeposition is the process of depositing a material on to a conducting surface from a solution containing ions or charged particles under the application of an electric field. This technique can be used to apply thin films on the surface of an object. The set up consists of two electrodes such as working electrode and counter electrode connected to a DC power supply where the working electrode is the surface on to which the material is to be deposited, the electrodes are kept dipped in an electrolyte solution which contains the material to be deposited.

ELD is a bottom up approach wherein a material is deposited as a thin or thick film/coating on to a substrate/electrode from the corresponding electrolyte (solution of metal salts), by an oxidation or reduction reaction. The constitution of an electrolyte bath decides the film composition. EPD on the other hand is a particulate technique in which the material to be deposited is dispersed in a suitable medium (For e.g. for PZT, it is dispersed in acetic acid). Electrophoretic deposition of materials is accomplished by the motion of charged particles dispersed in a suitable solvent towards an electrode/substrate under the action of an electric field. EPD process can be used to produce thin/thick films ranging from nanometre to centimetres whereas ELD is used to obtain films of limited thickness (micro or nano range). ELD does not require very high voltages but EPD requires very high voltages for deposition.

5. What are the other methods used for the deposition of PZT films?

Some of the other methods used for the deposition of PZT films are:

1. Sputtering – It is a physical vapour deposition (PVD) method of thin film deposition which involves ejecting material from a target that is a source on to a substrate.

2. Chemical vapour deposition (CVD) – In this method, the substrate is exposed to one or more volatile precursors, which react and decompose on the substrate surface to produce the desired deposit.

3. Sol-gel process – The sol-gel method involves the preparation of a sol with polymerizable oligomer species which polymerise during spin- or dip-coating deposition.

4. Hydrothermal growth – This technique involves the production of thick films from solution under the conditions of high temperature and pressure.

6. what is the principle of piezoelectric effect? Several polymers also show such effect. Name one such polymer and explain the reason for it to show piezoelectric effect.

Piezoelectric effect is the ability of certain materials to generate an electric charge in response to applied mechanical stress. This is known as direct piezoelectric effect. These materials also show a converse piezoelectric effect wherein mechanical stress is produced when an electric field is applied.

Polyvinylidene fluoride (PVDF) is one of the widely used piezoelectric polymers. Crystal structure plays an important role in the generation of piezoelectricity in a material. PVDF is a semi crystalline piezoelectric polymer and the polar crystalline phase imparts piezoelectricity to PVDF. There are four possible polymorphic phases α, β, γ and δ and PVDF depending on the conditions of crystallisation. The most highly polar phase of PVDF is the β phase, which has an all trans chain conformation in which all the hydrogen atoms are at one side of the polymer chain and all the fluorine atoms are at the other side of the polymer chain. In β phase unit cell, all the dipoles are aligned in the same direction in the same direction so that the polarity of chain is retained by the unit cell. So the piezoelectricity in PVDF is mainly due to the highly polar β phase.

7. Describe the principle of an acoustic sensor and how the material/process developed in this research will be useful for such an application.

Acoustic waves are used to detect and locate targets, quantify characteristics of marine environments, measure the location and velocity of moving targets and to transmit communication signals. Acoustic devices use the principle of electroacoustic transduction where electrical energy is converted to mechanical energy or vice versa. There are two types of acoustic systems: active and passive. Active devices generate sound using specially configured sensors/transducers called projectors. This sound travels through the underwater environment and get reflected from boundaries and targets, creating echoes that are recorded by a hydrophone. Passive devices do not project any sound but use only a hydrophone to listen to the sound radiated by targets. The major technology used for acoustic projection and reception is piezoelectric technology.

The PZT film developed in this work has been proposed to be used as sensing material in acoustic hydrophones which is used for the reception of acoustic signals underwater. Underwater acoustic measurements for the PZT films were carried out which indicated good sensitivity and can be used for high frequency underwater applications.